

Universidade Federal de Juiz de Fora  
Engenharia Elétrica  
Programa de Pós-Graduação em Engenharia Elétrica

**Thiago Rodrigues Oliveira**

**The Characterization of Hybrid PLC-wireless and PLC Channels in the  
Frequency Band Between 1.7 and 100 MHz for Data Communication**

Juiz de Fora

2015

**Thiago Rodrigues Oliveira**

**The Characterization of Hybrid PLC-wireless and PLC Channels in the  
Frequency Band Between 1.7 and 100 MHz for Data Communication**

Tese apresentada ao Programa de Pós-Graduação em Engenharia Elétrica da Universidade Federal de Juiz de Fora, na área de concentração em Sistemas Eletrônicos, como requisito parcial para obtenção do título de Doutor em Engenharia Elétrica.

Orientador: Moisés Vidal Ribeiro

Coorientador: Sérgio Lima Netto

Juiz de Fora

2015

Ficha catalográfica elaborada através do Modelo Latex do CDC da UFJF  
com os dados fornecidos pelo(a) autor(a)

Oliveira, Thiago.

The Characterization of Hybrid PLC-wireless and PLC Channels in the  
Frequency Band Between 1.7 and 100 MHz for Data Communication /  
Thiago Rodrigues Oliveira. – 2015.

131 f. : il.

Orientador: Moisés Vidal Ribeiro

Coorientador: Sérgio Lima Netto

Tese (Doutorado) – Universidade Federal de Juiz de Fora, Engenharia  
Elétrica. Programa de Pós-Graduação em Engenharia Elétrica, 2015.

1. PLC. 2. Hybrid PLC-wireless. 3. Estimation. 4. Frequency response.  
I. Ribeiro, Moises Vidal, orient. II. Netto, Sérgio Lima, coorient. III. Título.

**Thiago Rodrigues Oliveira**

**The Characterization of Hybrid PLC-wireless and PLC Channels in the  
Frequency Band Between 1.7 and 100 MHz for Data Communication**

Tese apresentada ao Programa de Pós-Graduação em Engenharia Elétrica da Universidade Federal de Juiz de Fora, na área de concentração em Sistemas Eletrônicos, como requisito parcial para obtenção do título de Doutor em Engenharia Elétrica.

Aprovada em: 24/03/2015

**BANCA EXAMINADORA**

---

Prof. Dr. Moisés Vidal Ribeiro - Orientador  
Universidade Federal de Juiz de Fora

---

Prof. Dr. Sérgio Lima Netto - Coorientador  
Universidade Federal do Rio de Janeiro

---

Prof. Ph.D Francisco Javier Cañete-Corripio  
Universidade de Málaga

---

Prof. Ph.D. Michel Daoud Yacoub  
Universidade Estadual de Campinas

---

Prof. Dr. Augusto Santiago Cerqueira  
Universidade Federal de Juiz de Fora

---

Prof. Dr. Rafael Antunes Nóbrega  
Universidade Federal de Juiz de Fora

## ACKNOWLEDGEMENTS

To my parents, Almir e Regina, for always encourage me to study and for teaching me important values.

To my beloved wife Amanda for all the fondness and love.

To my supervisor Moises, for believe in my potential and for the friendship.

To my co-supervisor Sergio and Prof. Camilla for important contributions in my work.

To all my friends that I made during my long walk in the University in which contributed directly or indirectly with my work.

*“Anyone who has never made a mistake  
has never tried anything new.”*

Albert Einstein

## RESUMO

Essa tese de doutorado apresenta, inicialmente, uma metodologia a ser empregada para a caracterização de redes de energia elétrica para fins de comunicação de dados. Esta metodologia engloba todos os procedimentos e ferramentas de processamento de sinais necessárias para a estimação de características importantes para a avaliação de canais de comunicação de dados. Em seguida, são apresentados resultados da aplicação de tal metodologia em dados provenientes de uma campanha de medição realizada em ambientes internos em residências brasileiras. Algumas características importantes desses canais, tais como ganho médio, banda de coerência, tempo de coerência, o valor quadrático médio do espalhamento de atraso, capacidade do canal e densidade espectral de potência do ruído, são analisadas considerando três bandas de frequência: de 1,7 até 30 MHz, de 1,7 até 50 MHz e de 1,7 até 100 MHz. Comparando os resultados de canais *power line communication* (PLC) em ambientes residenciais brasileiros com aqueles medidos em outros países, tais como Espanha, Estados Unidos, França e Itália, podemos notar que canais PLC brasileiros apresentam, em geral, menores atenuações, são menos seletivos em frequência e possuem menores espalhamentos de atraso. Por fim, um novo meio de comunicação baseada nas tecnologias PLC e sem fio é apresentada e definida como híbrido PLC-sem fio o qual permite a comunicação física e à distância com a rede de energia elétrica para fins de comunicação de dados. Tal canal de comunicação é avaliado em residências brasileiras e importantes características são extraídas e discutidas. Embora o canal híbrido PLC-sem fio tenha se mostrado mais adverso que o canal PLC para a comunicação de dados, a introdução da mobilidade, de uma forma que é impossível de se obter em sistemas puramente PLC, constitui sua principal vantagem. Essa mobilidade é um importante atrativo que coloca sistemas híbridos em uma posição privilegiada dentre os candidatos para compor a infraestrutura de telecomunicações em redes inteligentes (*smart grids*), ou para ser usada como uma ferramenta para promover a inclusão digital da população carente de países pobres ou em desenvolvimento.

Palavras-chave: PLC. Híbrido PLC-sem fio. Estimação. Resposta em frequência.

## ABSTRACT

This work outlines initially a methodology to be applied to the characterization of electric power grids for data communication purposes. This methodology englobes all the procedures and required signal processing tools for a reliable estimation of features that allow the suitability of a media for data communication. Next, PLC (power line communication) channel results provided by the use of such methodology in a data set obtained from a measurement campaign in in-home Brazilian places are presented. The analyzed channel features are the average channel gain, the coherence bandwidth, the coherence time, the root mean squared delay spread, the channel capacity and the noise power spectral density by considering the following frequency bands: from 1.7 up to 30 MHz, from 1.7 up to 50 MHz and from 1.7 up to 100 MHz. Comparisons among the results for in-home Brazilian PLC channels with other provided for other countries such as Spain, United States, France and Italy showed that, in general, in-home Brazilian PLC channels present smaller attenuation, are less frequency selective and showed smaller delay spread than these countries. Finally, a new medium to provide data communication is presented and defined as hybrid PLC-wireless, in which PLC and wireless technologies are combined. Such novel communication channel is characterized in in-home Brazilian places and important channel features are estimated and discussed. Though the hybrid PLC-wireless channel has been shown more adverse than the PLC channel, the introduction of mobility is its main advantage, something that is impossible in traditional PLC technologies. Thus, this mobility is an important issue that puts hybrid PLC-wireless technologies in a privileged position among the candidates to form the communication infrastructure for smart grids, or to be used as a tool to solve the digital divide problem that is more accentuated in poor and in developing countries.

Key-words: Power line communication. Hybrid wireline-wireless channel. Estimation. Frequency response.

## LIST OF FIGURES

Figure 1 – Measurement setup. . . . .	22
Figure 2 – PLC channel model. . . . .	23
Figure 3 – HS-OFDM transmission system. . . . .	24
Figure 4 – Transmitted signal. . . . .	26
Figure 5 – Region in which the synchronism is considered correct. . . . .	26
Figure 6 – Power line fundamental signal synchronization circuit. . . . .	30
Figure 7 – PLC channel frequency response estimation algorithm flowchart. . . . .	32
Figure 8 – Magnitude function. . . . .	34
Figure 9 – Impulse response. . . . .	34
Figure 10 – Coefficients of the vector $\mathbf{m}_t$ . . . . .	34
Figure 11 – Estimation of the correct synchronism point related to the number of HS-OFDM symbols. . . . .	35
Figure 12 – Evaluation of the synchronism technique. . . . .	35
Figure 13 – Comparison of estimates with and without the proposed enhancement procedure. . . . .	37
Figure 14 – CFR estimates of real PLC channel #1 with the presented methodology and by using a VNA. . . . .	38
Figure 15 – CFR estimates of real PLC channel #2 with the presented methodology and by using a VNA. . . . .	38
Figure 16 – Magnitude of the frequency response of seven measured PLC channels. . . . .	39
Figure 17 – Magnitude of CFR estimates of a periodically time-varying PLC channel. . . . .	39
Figure 18 – Magnitude of CFR estimates of a time invariant PLC channel. . . . .	40
Figure 19 – Comparison between magnitude of the frequency response estimate of a PLC coupler circuitry obtained by the presented methodology and by the VNA. . . . .	41
Figure 20 – Comparison between magnitude of the frequency response estimate of the transformer #1 obtained by the presented methodology and by the VNA. . . . .	41
Figure 21 – Comparison between magnitude of the frequency response estimate of the transformer #2 obtained by the presented methodology and by the VNA. . . . .	42
Figure 22 – General characterization of the measured in-home PLC channel magni- tude response. . . . .	51
Figure 23 – Cumulative distribution function of the estimated in-home PLC channel magnitude responses. . . . .	52
Figure 24 – Magnitude response statistics of one measured PLC channel. . . . .	52
Figure 25 – The histogram and distribution fitting of ACA feature for Band A. . . . .	55
Figure 26 – The histogram and distribution fitting of ACA feature for Band B. . . . .	55

Figure 27 – The histogram and distribution fitting of ACA feature for Band C. . . . .	56
Figure 28 – The histogram and distribution fitting of CB feature for Band A. . . . .	58
Figure 29 – The histogram and distribution fitting of CB feature for Band B. . . . .	58
Figure 30 – The histogram and distribution fitting of CB feature for Band C. . . . .	59
Figure 31 – The histogram and distribution fitting of RMS-DS feature for Band A. . . . .	60
Figure 32 – The histogram and distribution fitting of RMS-DS feature for Band B. . . . .	61
Figure 33 – The histogram and distribution fitting of RMS-DS feature for Band C. . . . .	61
Figure 34 – RMS-DS versus ACG for the measured in-home PLC channels in Brazil. . . . .	62
Figure 35 – Relation between the coherence bandwidth and the RMS-DS for the in-home PLC channels in Brazil. . . . .	62
Figure 36 – Coherence time of the measured in-home PLC channel. . . . .	63
Figure 37 – CDF of the coherence time for the three considered frequency bands. . . . .	64
Figure 38 – The histogram and distribution fitting of CT feature for Band A. . . . .	65
Figure 39 – The histogram and distribution fitting of CT feature for Band B. . . . .	65
Figure 40 – The histogram and distribution fitting of CT feature for Band C. . . . .	65
Figure 41 – Estimated noise PSD in the measured in-home PLC channel. . . . .	66
Figure 42 – Channel capacity of the measured in-home PLC channels. . . . .	67
Figure 43 – Complementary CDF of the channel capacity using the measured and colored noise. . . . .	67
Figure 44 – A hybrid PLC-wireless scenario. . . . .	71
Figure 45 – Block diagram of the measurement setup. . . . .	73
Figure 46 – Measured scenario. . . . .	75
Figure 47 – Magnitude responses of some measured channels. . . . .	75
Figure 48 – Magnitude responses of measured hybrid PLC-wireless channels for the transmission from wireless-PLC to PLC-wireless transceiver. . . . .	76
Figure 49 – Magnitude responses of measured hybrid PLC-wireless channels for the transmission from PLC-wireless to wireless-PLC transceiver. . . . .	77
Figure 50 – Magnitude responses of a single channel in both directions. . . . .	77
Figure 51 – Magnitude responses of some measured hybrid PLC-wireless for different locations of the wireless-PLC transceiver. . . . .	78
Figure 52 – Statistical parameters extracted from estimated magnitude responses of the <i>short-path</i> hybrid PLC-wireless channels. . . . .	78
Figure 53 – Statistical parameters extracted from estimated magnitude responses of the <i>long-path</i> hybrid PLC-wireless channels. . . . .	79
Figure 54 – The histogram and distribution fitting of ACA for <i>short-path channels</i> . . . . .	80
Figure 55 – The histogram and distribution fitting of ACA for <i>long-path channels</i> . . . . .	81
Figure 56 – The histogram and distribution fitting of CB for <i>short-path channels</i> . . . . .	83
Figure 57 – The histogram and distribution fitting of CB for <i>long-path channels</i> . . . . .	83
Figure 58 – The histogram and distribution fitting of RMS-DS for <i>short-path channels</i> . . . . .	85

Figure 59 – The histogram and distribution fitting of RMS-DS for <i>long-path channels</i> .	85
Figure 60 – Scatter plot of CB versus RMS-DS. . . . .	86
Figure 61 – Correlation evolution for the <i>short-path channel</i> . . . . .	87
Figure 62 – CT CDF of the <i>short-path channel</i> for distinct correlation levels. . . . .	87
Figure 63 – Correlation evolution for <i>long-path channel</i> . . . . .	88
Figure 64 – CDF of CT for <i>short-path channel</i> by considering distinct values of correlation levels. . . . .	88
Figure 65 – The histogram and distribution fitting of CT for <i>short-path channels</i> . . . . .	89
Figure 66 – The histogram and distribution fitting of CT for <i>long-path channels</i> . . . . .	89
Figure 67 – Statistical parameters of PSD of the additive noise at the input of the hybrid-wireless transceiver. . . . .	90
Figure 68 – Statistical parameters of PSD of the additive noise at the input of the hybrid-PLC transceiver. . . . .	90
Figure 69 – Mean values of channel capacity for the <i>short-path</i> and <i>long-path channels</i> .	91
Figure 70 – CCDF of channel capacity for <i>short-path channel</i> and <i>long-path channel</i> .	92

## LIST OF TABLES

Table 1 – Transmitted signal features and values of the parameters used by the PLC frequency response estimation algorithm. . . . .	33
Table 2 – Parameters of an outdoor PLC channel model [41]. . . . .	33
Table 3 – MSE between the simulated and estimated CFR. . . . .	36
Table 4 – Main features of the measured places. . . . .	45
Table 5 – Penalty term $c_n$ of different information-based model evaluation criteria: AIC, BIC and EDC. . . . .	50
Table 6 – PLC channel average channel attenuation for Band A, Band B and Band C. . . . .	54
Table 7 – Coherence bandwidth estimated for the measured PLC channels. . . . .	57
Table 8 – RMS-DS for the measured in-home PLC channels in Band A, Band B and Band C. . . . .	59
Table 9 – Parameters of (3.7) estimated for the measured PLC channels. . . . .	61
Table 10 – Values of the parameters that are adopted to calculate the coherence time [36]. . . . .	63
Table 11 – Chosen Subbands for Analysis. . . . .	74
Table 12 – ACA for the Measured Hybrid PLC-Wireless Channels. . . . .	79
Table 13 – CB for the Measured Hybrid PLC-Wireless Channels. . . . .	82
Table 14 – RMS-DS of the Measured Hybrid PLC-Wireless Channels. . . . .	84
Table 15 – MLE results of the statistical distribution fitting of the ACA (dB) for Band A (SE is the estimated standard error). . . . .	111
Table 16 – MLE results of the statistical distribution fitting of the ACA (dB) for Band B (SE is the estimated standard error). . . . .	112
Table 17 – MLE results of the statistical distribution fitting of the ACA (dB) for Band C (SE is the estimated standard error). . . . .	113
Table 18 – MLE results of the statistical distribution fitting of the RMS-DS ( $\mu s$ ) for Band A (SE is the estimated standard error). . . . .	114
Table 19 – MLE results of the statistical distribution fitting of the RMS-DS ( $\mu s$ ) for Band B (SE is the estimated standard error). . . . .	115
Table 20 – MLE results of the statistical distribution fitting of the RMS-DS ( $\mu s$ ) for Band C (SE is the estimated standard error). . . . .	116
Table 21 – MLE results of the statistical distribution fitting of the CB (MHz) for Band A (SE is the estimated standard error). . . . .	117
Table 22 – MLE results of the statistical distribution fitting of the CB (MHz) for Band B (SE is the estimated standard error). . . . .	118
Table 23 – MLE results of the statistical distribution fitting of the CB (MHz) for Band C (SE is the estimated standard error). . . . .	119
Table 24 – MLE results of the statistical distribution fitting of the CT (ms) for Band A (SE is the estimated standard error). . . . .	120

Table 25 – MLE results of the statistical distribution fitting of the CT (ms) for Band B (SE is the estimated standard error). . . . .	121
Table 26 – MLE results of the statistical distribution fitting of the CT (ms) for Band C (SE is the estimated standard error). . . . .	122
Table 27 – MLE results of the statistical distribution fitting of the ACA (dB) for <i>short path</i> channel (SE is the estimated standard error). . . . .	124
Table 28 – MLE results of the statistical distribution fitting of the ACA (dB) for <i>long-path channel</i> (SE is the estimated standard error). . . . .	125
Table 29 – MLE results of the statistical distribution fitting of the CB (MHz) for <i>short-path channel</i> (SE is the estimated standard error). . . . .	126
Table 30 – MLE results of the statistical distribution fitting of the CB (MHz) for <i>long-path channel</i> (SE is the estimated standard error). . . . .	127
Table 31 – MLE results of the statistical distribution fitting of the RMS-DS ( $\mu s$ ) for <i>short-path channel</i> (SE is the estimated standard error). . . . .	128
Table 32 – MLE results of the statistical distribution fitting of the RMS-DS ( $\mu s$ ) for <i>long-path channel</i> (SE is the estimated standard error). . . . .	129
Table 33 – MLE results of the statistical distribution fitting of the CT (ms) for <i>short-path channel</i> (SE is the estimated standard error). . . . .	130
Table 34 – MLE results of the statistical distribution fitting of the CT (ms) for <i>long-path channel</i> (SE is the estimated standard error). . . . .	131

## ACRONYMS

**ACA** average channel attenuation

**ACG** average channel gain

**AGC** automatic gain control

**AIC** Akaike information criterion

**BIC** Bayesian information criterion

**CB** coherence bandwidth

**CCDF** complementary cumulative distribution function

**CDF** cumulative distribution function

**CFR** channel frequency response

**CIR** channel impulse response

**CP** cyclic prefix

**CT** coherence time

**DAC** digital-to-analog converter

**DFT** discrete Fourier transform

**EDC** efficient determination criterion

**FIR** finite impulse response

**GDP** gross domestic product

**HS-OFDM** Hermitian symmetric orthogonally frequency division multiplexing

**IBI** interblock interference

**IDFT** inverse discrete Fourier transform

**ISI** inter symbol interference

**LPF** low pass filter

**ML** maximum likelihood

**MLE** maximum likelihood estimate

**MMSE** minimum mean squared error

**OFDM** orthogonally frequency division multiplexing

**PDF** probability density function

**PLC** power line communication

**PSD** power spectrum density

**RMS-DS** root mean squared delay spread

**SFO** sampling frequency offset

**US** United States

**VNA** vectorial network analyzer

# CONTENTS

<b>1</b>	<b>INTRODUCTION . . . . .</b>	<b>17</b>
1.1	THESIS OBJECTIVES . . . . .	18
1.2	THESIS OUTLINE . . . . .	19
1.3	SUMMARY . . . . .	19
<b>2</b>	<b>A METHODOLOGY FOR ESTIMATING FREQUENCY RES- PONSES OF ELECTRIC POWER GRIDS . . . . .</b>	<b>20</b>
2.1	PROBLEM FORMULATION . . . . .	22
2.2	THE METHODOLOGY FOR CHANNEL FREQUENCY RESPONSE ESTIMATION . . . . .	24
2.2.1	<b>Signal generation . . . . .</b>	24
2.2.2	<b>Synchronization . . . . .</b>	25
2.2.3	<b>Channel estimation . . . . .</b>	27
2.2.4	<b>Channel estimation enhancement . . . . .</b>	28
2.2.5	<b>Sampling frequency offset error estimation and correction . . .</b>	28
2.2.6	<b>Trigger source circuit . . . . .</b>	29
2.2.7	<b>General overview of the algorithm . . . . .</b>	30
2.3	EXPERIMENTAL RESULTS . . . . .	30
2.3.1	<b>Performance analysis: PLC channel model . . . . .</b>	31
2.3.2	<b>Performance analysis: real PLC scenario . . . . .</b>	36
2.3.2.1	<i>Comparison between the methodology and the VNA . . . . .</i>	37
2.3.2.2	<i>Estimation of real CFR . . . . .</i>	37
2.3.3	<b>Performance analysis: application on electrical devices . . . . .</b>	40
2.4	SUMMARY . . . . .	40
<b>3</b>	<b>THE CHARACTERIZATION OF BRAZILIAN IN-HOME PLC CHANNELS . . . . .</b>	<b>43</b>
3.1	MEASUREMENT SETUP AND CAMPAIGN . . . . .	44
3.2	PLC CHANNEL FEATURES . . . . .	45
3.2.1	<b>Average channel gain (ACG) . . . . .</b>	45
3.2.2	<b>Coherence bandwidth (CB) . . . . .</b>	46
3.2.3	<b>Root mean squared delay spread (RMS-DS) . . . . .</b>	46
3.2.4	<b>Relation between RMS-DS and ACG . . . . .</b>	47
3.2.5	<b>Relation between CB and RMS-DS . . . . .</b>	47
3.2.6	<b>Coherence time (CT) . . . . .</b>	47
3.2.7	<b>PSD of the additive noise . . . . .</b>	48

3.2.8	<b>Channel capacity</b>	48
3.3	<b>FIT EVALUATION</b>	48
3.3.1	<b>Maximum Likelihood Estimation</b>	49
3.3.2	<b>Information criteria</b>	49
3.4	<b>NUMERICAL ANALYSIS</b>	50
3.4.1	<b>Channel Magnitude Function</b>	50
3.4.2	<b>Average channel attenuation (ACA)</b>	53
3.4.2.1	<i>Statistical modeling</i>	53
3.4.3	<b>Coherence bandwidth (CB)</b>	55
3.4.3.1	<i>Statistical modeling</i>	58
3.4.4	<b>Root mean squared delay spread (RMS-DS)</b>	59
3.4.4.1	<i>Statistical modeling</i>	59
3.4.5	<b>RMS-DS versus ACG</b>	60
3.4.6	<b>CB versus RMS-DS</b>	62
3.4.7	<b>Coherence time (CT)</b>	63
3.4.7.1	<i>Statistical modeling</i>	64
3.4.8	<b>PSD of the additive noise</b>	64
3.4.9	<b>Channel capacity</b>	66
3.5	<b>SUMMARY</b>	68
4	<b>THE CHARACTERIZATION OF THE IN-HOME BRAZILIAN HYBRID PLC-WIRELESS CHANNELS</b>	<b>69</b>
4.1	<b>THE HYBRID PLC-WIRELESS CHANNEL: PROBLEM FORMULATION</b>	70
4.2	<b>MEASUREMENT SETUP AND CAMPAIGN</b>	73
4.3	<b>RESULTS AND ANALYSIS</b>	74
4.3.1	<b>Channel frequency response analyses</b>	74
4.3.1.1	<i>Comparison between PLC-PLC, PLC-wireless, Wireless-PLC and Wireless-wireless transmission</i>	74
4.3.1.2	<i>Magnitude Response Symmetry</i>	75
4.3.1.3	<i>Influence of small distance variations on the magnitude response</i>	76
4.3.1.4	<i>Statistics</i>	76
4.3.2	<b>Average channel attenuation (ACA)</b>	78
4.3.2.1	<i>Statistical modeling</i>	80
4.3.3	<b>Coherence bandwidth (CB)</b>	80
4.3.3.1	<i>Statistical modeling</i>	83
4.3.4	<b>Root mean squared delay spread (RMS-DS)</b>	84
4.3.4.1	<i>Statistical modeling</i>	84
4.3.5	<b>CB versus RMS-DS</b>	85
4.3.6	<b>Coherence time (CT)</b>	85

4.3.6.1	<i>Statistical modeling</i> . . . . .	86
4.3.7	<b>Additive noise</b> . . . . .	89
4.3.8	Channel capacity . . . . .	91
4.4	SUMMARY . . . . .	92
<b>5</b>	<b>CONCLUSIONS</b> . . . . .	<b>93</b>
5.1	FUTURE WORKS . . . . .	95
	 <b>REFERENCES</b> . . . . .	 <b>97</b>
	 <b>APPENDIX A – List of Contributions</b> . . . . .	 <b>105</b>
A.1	Related with Chap. 2 . . . . .	105
A.2	Related with Chap. 3 . . . . .	105
A.3	Related with Chap. 4 . . . . .	106
	 <b>APPENDIX B – Statistical Distributions</b> . . . . .	 <b>107</b>
	 <b>APPENDIX C – MLE Results for PLC Channel Features</b> . .	 <b>110</b>
	 <b>APPENDIX D – MLE Results for Hybrid PLC-wireless Channel Features</b> . . . . .	 <b>123</b>

## 1 INTRODUCTION

Power line communication (PLC) is the technology that makes use of the existing and ubiquitous infrastructure of electrical power systems to provide data communication. This technology has received considerable attention due to its low installation costs, as most needed infrastructure (electric power systems) is ubiquitous and is already installed [1].

On the other hand, since electric power grids were not specified and designed for data communications purposes (e.g., power cables are unshielded, show attenuation exponentially increasing with frequency and distance, present high power impulsive noise presence and time-varying behavior, etc), they constitute a challenging transmission medium to be pursued [2]. Therefore, some regulatory rules imposing constraints on the use of PLC technology have been established to avoid interferences of PLC systems (secondary user) in other existing communication services (primary user) operating in the same frequency band, such as military applications and amateur radio [3, 4, 5, 6]. Therefore, the success of PLC systems requires a thorough study of the main features of electric power grids to support the design of PLC systems that maximize the resources of this challenging communication medium. Thus, the use of an appropriate measurement methodology capable of estimating all the relevant features of the electric power grids that affect data communication is of primary importance.

The use of electric power grids for data transmission is not recent. Indeed, several power utilities have been making use of high voltage power cables to send signals – transmitted with low data rates – to control and monitor the electric power system [7, 1]. On the other hand, the use of electric power grids for broadband communications is fairly recent and demands considerable efforts to make such technology practicable and of value for emerging telecommunication applications.

Due to the high number of consumers (potential subscribers of broadband services) connected to the medium and low voltage electric power, power cables become a very attractive alternative to receive broadband PLC systems and, thus, there is a growing demand for the characterization of other kind of electric power grids. On the other hand, whereas there have been a lot of works that evaluate PLC channels in general, a complete and detailed study of in-home scenario in developing and underdeveloped countries are missing. Indeed, the majority of the reported results are focused on the characterization of in-home PLC channels in developed countries, such as France, Italy, Spain and United States (US). This is an important gap to be overcome, since PLC systems can significantly contribute to mitigate the digital divide that affects a large number of people worldwide, mainly concentrated in developing and underdeveloped countries.

Furthermore, there is a growing demand for the characterization of other kind

of electric power grids, besides the efforts addressed to the characterization of outdoor (medium and low voltage) and indoor (residential, commercial and industrial environments) power grids. Indeed, the idea of providing data communication through power cables can be exploited in several contexts. In this sense, the application of the PLC technology in automotive vehicles [8, 9, 10, 11, 12, 13] has been drawing attention, since the amount of data due to the growing number of sensors justifies the implementation of PLC for data transmission in order to reduce manufacturing and maintenance costs. Furthermore, other possible candidates that have been evaluated somehow to receive the PLC technology are ships [14, 15, 16, 17], aircrafts [18, 19, 20], train [21], mine facilities [22] and offshore oil platforms [23]. More recently, some works are aiming at a combination of PLC and wireless systems to provide a cooperative communication [24, 25, 26, 27], by using both communication strategies in parallel to improve channel diversity. On the other hand, other data communication possibilities have not been addressed in the literature, considering the combination of PLC and wireless technologies.

## 1.1 THESIS OBJECTIVES

In the context of the characterization of PLC channels for data communication purposes, this thesis has the following objectives:

- To present of a complete methodology that can be applied to provide estimates of the channel frequency response. The methodology is based on a sounding technique and is suitable for characterizing time-varying PLC channels, since one channel estimate is obtained in a short period of time. All the needed procedures and signal processing tools are discussed and evaluated with synthetic and real data;
- To fill a gap regarding the characterization of in-home PLC channels in developing countries, through the analysis of a set of key PLC channel features extracted from in-home PLC channels, which were measured in Brazil, considering three frequency bands: from 1.7 up to 30 MHz, from 1.7 up to 50 MHz and from 1.7 up to 100 MHz. Also, statistical models of some important channel features and a comparison with some other reported results are presented;
- To introduce and characterize a new communication medium made from a combination between PLC and wireless channels, with all transceivers (PLC and wireless) operating at the same frequency band. Such communication medium is here referred as hybrid PLC-wireless channel and constitutes an interesting solution to introduce mobility that is impossible in traditional PLC systems.

## 1.2 THESIS OUTLINE

This thesis is organized as follows: Chap. 2 details an appropriate methodology to be applied for the characterization of frequency responses of PLC channels as well as electrical devices in general. In Chap. 3, the characterization of Brazilian in-home PLC channels and statistical models for main channel features is presented. The so called hybrid PLC-wireless channel is stated and important results and discussions about this kind of communication medium for Brazilian in-home scenarios are presented in Chap. 4. The conclusions of this work are summarized in Chap. 5.

## 1.3 SUMMARY

This chapter presented a brief introduction of this thesis. Also, the main objectives and the organization of this work were summarized. The next chapter will propose a complete methodology to be used to characterize PLC channels.

## 2 A METHODOLOGY FOR ESTIMATING FREQUENCY RESPONSES OF ELECTRIC POWER GRIDS

The knowledge and understanding of the electric power grids as communication medium are of utmost importance to design reliable and efficient PLC technologies that deal with the hardness and limitations of media that were developed to transmit a huge amount of energy at very low frequency (50 Hz or 60 Hz). In this regards, it is well known that the channel frequency response (CFR) of a data communication media is one of the most relevant information because it defines the strategy to deal with the impairments in such data communication medium. Based on the CFR, several features can be extracted, such as average channel gain (ACG), coherence bandwidth (CB), coherence time (CT), theoretical channel capacity and root mean squared delay spread (RMS-DS).

The CFR estimation methodologies for data communication purposes (in which the considered frequency bandwidth is much broader than the mains frequency) can be grouped into two approaches:

- vectorial network analyzer (VNA): where the frequency response is estimated from the S-parameters [28];
- Sounding: where the frequency response is estimated by using signal generation and acquisition equipments together with signal processing tools [29].

The first class, related with the use of the VNA, due to its simplicity, has been widely applied to estimate CFR in homes [28, 30, 31, 32, 33] and vehicles [34, 10, 13] because the distances from the injecting and extracting points are short. However, the use of VNA-based approach can result in wrong estimates of the CFR because it demands a time interval (sweep time) higher than 100 ms to yield one estimate of the CFR while the coherence time  $T_c$ , the time interval in which the channel impulse response is considered time invariant, of electric power grids is lower than 2 ms [35, 36].

On the other hand, the sounding approach is more suitable for estimating CFRs. This is because the time interval required to provide one measure of the CFR can be made lower than the coherence time by choosing data generation and acquisition equipment and changing some parameters of the signal processing tools considered in the sounding approach. Also, this approach can offer improved performance if the distances are long (more than 10 meters), such as in outdoor low-, medium-, and high-voltage electric power grids.

Regarding the sounding approach, a technique that only estimates the amplitude spectrum of a CFR, which is based on spectrum analyzer, was discussed in [38, 39, 40]. A brief description of a channel estimation technique was addressed in [35]. The use of signal generation and acquisition equipment together with sounding technique based on an

orthogonally frequency division multiplexing (OFDM) for estimation CFR was addressed in [41, 15]. The limitation of these contributions is the fact that few attentions is driven to the following issues altogether: (i) the choice of channel estimation technique; (ii) the choice of timing synchronization technique; (iii) the design of sampling frequency offset (SFO) correction technique; and (iv) channel estimation enhancement technique. In fact, the majority of contributions pays more attention to the characterization of communication media than to the applied methodologies, such as [32, 33]. Thus, a contribution that presents a reliable and easy to use methodology for estimating CFR by addressing the four aforementioned issues is missing in the literature. As a result, fair comparisons among measurements carried out in different parts of the world can not be correctly analyzed. Also, some contradictory information regarding the characterization of electric power grids as communication media have appeared (e.g., lognormality discussion about the average channel gain [32, 42]). Therefore, it is of utmost importance to introduce a CFR estimation methodology that could be worldwide used.

To deal with this issue, this chapter discusses a complete sounding-based methodology for estimating CFR of electric power grids for data communication purposes. The presented methodology discusses a comprehensive description of an OFDM-based sounding approach by addressing SFO error estimation and correction, timing synchronization, channel estimation and channel estimation enhancement techniques. The effectiveness of this methodology is validated by using well-known power line channel models as well as measured ones, covering the frequency band from 1.7 up to 50 MHz. Measurement results show that the presented methodology is capable of offering one estimate of PLC channels per time interval as low as  $T_f = 23.4 \mu\text{s}$  for the chosen set of parameters (as detailed discussed in 2.3). As a result, it is possible to characterize periodically and time-varying behaviors of electric power grids because  $T_f < T_c$  ( $T_c$  is the coherence time), something that is impossible to be achieved by using a VNA-based approach. In fact, depending on the adopted frequency resolution and bandwidth, the sweep time of a VNA can be in the order of some hundreds of milliseconds (see for instance the datasheet in [43]). Additionally, it is shown that the methodology can be successfully applied to characterize frequency responses of electric equipment and, as a consequence, it is very useful for both power line communication and power system applications.

To introduce all these technical contributions, this chapter is organized as follows: Sec. 2.1 describes the problems related to the PLC-channel frequency response estimation. Sec. 2.2 gives a detailed description of the proposed methodology. The frequency-estimation results are shown in Sec. 2.3.

## 2.1 PROBLEM FORMULATION

For illustration purposes, the measurement setup used for PLC channel measurement [44] is depicted in Fig. 1. In this scenario, the received signal  $y(t)$  can be modeled by

$$y(t) = \tilde{y}(t) + v(t) = \int_{-\infty}^{\infty} x(\tau)h_{\text{eq}}(t, \tau)d\tau + v(t), \quad (2.1)$$

in which  $h_{\text{eq}}(t, \tau)$  is the linear and time-varying channel impulse response and  $v(t)$  is the additive noise. The function  $h_{\text{eq}}(t, \tau)$  accounts for all the linear filtering to which the signal  $x(t)$  is subject and the noise term  $v(t)$  includes all the perturbations that affect the communication channel. We assume that  $y[n] = y(t)|_{t=nT_s} = \tilde{y}[n] + v[n]$ , where  $T_s \geq \frac{1}{2B}$  and  $B$  is the frequency bandwidth.

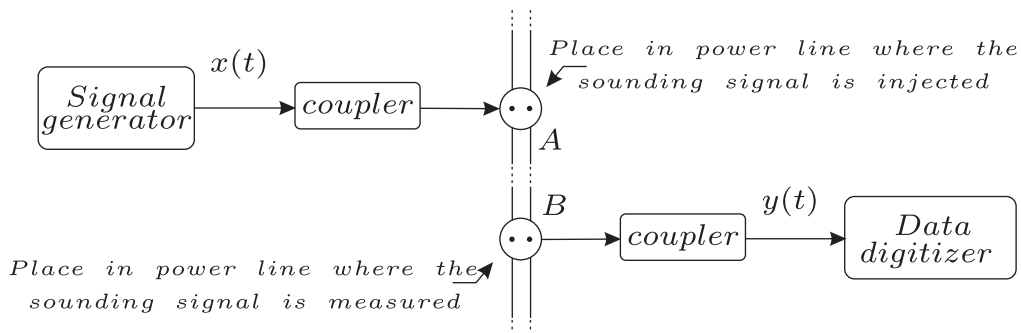


Figure 1: Measurement setup.

Note that  $h_{\text{eq}}(t, \tau)$  addresses the time-varying channel model that is composed of the front/end of the transceiver and the communication medium, as depicted in Fig. 2. In Fig. 2, the boxes are labeled with  $h_A(t)$ ,  $h_{F,T_x}(t)$ ,  $h_{F,R_x}(t)$ ,  $h_{C,T_x}(t)$ ,  $h_{C,R_x}(t)$ ,  $h_{AGC}(t)$  and  $h(t, \tau)$ , which correspond to the impulse-response functions of the amplifier, transmitter and receiver low pass filter (LPF), transmitter and receiver couplers, automatic gain control (AGC) and the PLC channel, respectively. It is important to notice the bandwidth limiting role of both LPFs which are intended to limit the signal bandwidth to  $B$  Hz. For a compact notation, we consider  $h_T(t) = h_A(t) \star h_{F,T_x}(t) \star h_{C,T_x}(t)$  and  $h_R(t) = h_{C,R_x}(t) \star h_{F,R_x}(t) \star h_{AGC}(t)$ , where  $\star$  denotes the linear-convolution operation and we assume that  $h_{\text{eq}}(t, \tau) = h_{\text{eq}}(t - \tau)$  because the CFR estimation is carried out in a time interval lower than  $T_c$ . The analog signal  $y(t) = \tilde{y}(t) + v(t)$ , where  $\tilde{y}(t) = x(t + T_d) \star h_T(t + T_d) \star h(t)$  and  $v(t) = v_r(t) \star h_R(t)$ . Also is worth emphasizing that the delay  $T_d$ , which the channel adds to the transmitted signal, is unknown to the receiver and, for this reason, has to be estimated *a priori* to any processing (timing synchronization).

Now, suppose that, at the receiver side, a perfect timing synchronization has been achieved, and that after the cyclic prefix (it is assumed that the OFDM with cyclic prefix signal is used as sounding signal, as detailed in Subsection 2.2.1) has been

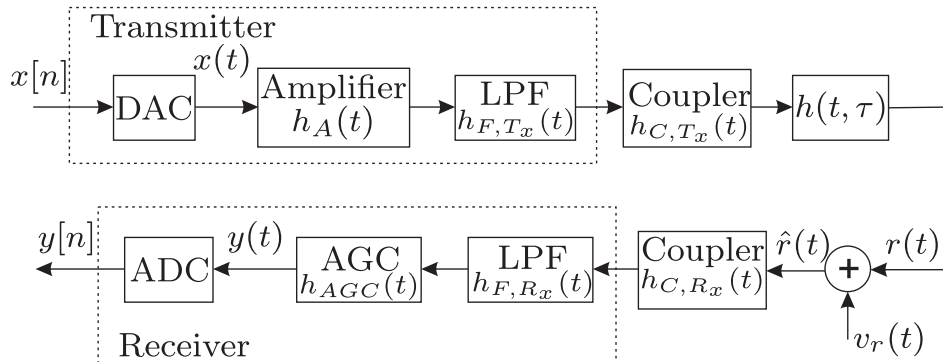


Figure 2: PLC channel model.

removed, we are left with the vectors of samples of the form  $\mathbf{y}_i \in \mathbb{R}^{2N \times 1}$ . By considering  $h_{eq}[n] = h_T(t) \star h(t) \star h_R(t)|_{t=nT_s}$  and using the notation  $\mathbf{h}_{eq} = \{h_{eq}[0] \ h_{eq}[1] \ \dots \ h_{eq}[L_{eq}-1]\}^T$ , it can be written  $\mathbf{H}_{eq} = (1/\sqrt{2N})\mathbf{W}\{\mathbf{h}_{eq}^T \ \mathbf{0}_{2N-L_{eq}}^T\}^T$ , where the superscript  $T$  denotes the transpose operation and  $\mathbf{W}$  denotes the matrix that performs the discrete Fourier transform (DFT). Similarly, by considering  $h_R[n] = h_R(t)|_{t=nT_s}$  and using the notation  $\mathbf{h}_R = [h_R[0] \ h_R[1] \ \dots \ h_R[L_R-1]]^T$ , we can write  $\mathbf{H}_R = (1/\sqrt{2N})\mathbf{W}\{\mathbf{h}_R^T \ \mathbf{0}_{2N-L_R}^T\}^T$ . Thus, by defining the matrix  $\mathcal{H}_{eq} = \mathbf{diag}\{H_{eq}[0], \dots, H_{eq}[2N-1]\}$  and  $\mathcal{H}_R = \mathbf{diag}\{H_R[0], \dots, H_R[2N-1]\}$ , one can write that

$$\mathbf{Y}_i = \frac{1}{\sqrt{N}}\mathbf{W}\mathbf{y}_i = \mathcal{H}_{eq}\mathbf{X}_i + \mathcal{H}_R\mathbf{V}_r. \quad (2.2)$$

Considering that the zero-forcing criterion is used and with  $\mathbf{X}_i = \{X_i[0], X_i[1], \dots, X_i[2N-1]\}^T$ , the OFDM input symbol, known *a priori* by the receiver, the following channel estimate is obtained:

$$\hat{\mathbf{H}}_{eq} = [\mathbf{diag}(\mathbf{X}_i)]^{-1} \mathbf{Y}_i = \mathbf{H}_{eq} + [\mathbf{diag}(\mathbf{X}_i)]^{-1} \mathcal{H}_R \mathbf{V}_r. \quad (2.3)$$

At this point, a few comments related to the estimation problem must be emphasized:

- A careful choice of  $\mathbf{X}_i$  is fundamental to render a useful estimation of the PLC CFR, a reduced peak to average power ratio and an improved timing synchronization.
- A proper estimation of  $T_d$  must be achieved to avoid interblock interference.
- A proper SFO error estimation and correction is needed to avoid the degradation of the estimates.
- A signal enhancement technique is demanded to reduce the hardness of additive noise (disturbances) in the electric power grids.

## 2.2 THE METHODOLOGY FOR CHANNEL FREQUENCY RESPONSE ESTIMATION

The CFR estimation methodology involves the following issues, to be detailed in the subsequent subsections:

- Signal generation;
- Timing synchronization;
- Sampling frequency offset error estimation and correction;
- Channel estimation;
- Channel estimation enhancement.

### 2.2.1 Signal generation

The modulated signal  $x(t)$  chosen to be transmitted is an OFDM signal, occupying a bandwidth of  $B$  Hz. The OFDM variation that exploit the hermitian symmetry property and referred in this work as Hermitian symmetric orthogonally frequency division multiplexing (HS-OFDM) [45, 46] is adopted here as the baseband transmission modulation scheme, as represented in Fig. 3. In this scheme, the modulated data are submitted to a serial-to-parallel converter that outputs the vector  $\mathbf{X}_i \in \mathbb{C}^{N \times 1}$  next mapped into a vector, denoted by  $\mathbf{X}_{map,i} = \{X_{map,i}[0], X_{map,i}[1], \dots, X_{map,i}[2N-1]\}^T$ , according to the following rule

$$X_{map,i}[k] = \begin{cases} \Re\{X_i[N-1]\}, & k = 0 \\ X_i[k], & k = 1, \dots, N-2 \\ \Im\{X_i[N-1]\}, & k = N-1 \\ X_i^*[2N-2-k], & k = N, N+1, \dots, 2N-1 \end{cases}, \quad (2.4)$$

in which  $\Re\{\cdot\}$  and  $\Im\{\cdot\}$  denote the real and imaginary parts, respectively, of a given number, and  $*$  denotes the complex-conjugation operation.

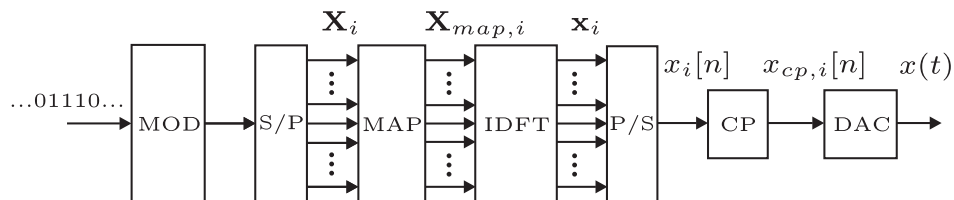


Figure 3: HS-OFDM transmission system.

To complete the HS-OFDM generation process, a  $L_{cp}$ -length cyclic prefix (CP) is inserted in each OFDM symbol. To this end, let us consider  $\mathbf{x}_i = \frac{1}{\sqrt{2N}} \mathbf{W}^\dagger \mathbf{X}_{map,i}$ , where  $\mathbf{X}_{map,i} \in \mathbb{R}^{2N \times 1}$  is the frequency domain representation of the  $i^{th}$  HS-OFDM symbol,

the matrix  $\mathbf{W}$  is the  $2N \times 2N$  DFT matrix and  $(\dagger)$  the Hermitian operator. We have then, by pre-appending the CP, the vector with the last  $L_{cp}$  coefficients of  $\mathbf{x}_i$ , we get  $\mathbf{x}_{cp,i} = \{x_i[2N - L_{cp}] \ x_i[2N - L_{cp} + 1] \ \dots \ x_i[2N - 1] \ \mathbf{x}_i^T\}^T$ .

Following this framework, the input signal to the channel is the infinite succession of HS-OFDM symbols represented in the discrete time-domain by

$$x_{cp}[n] = \sum_{i=-\infty}^{\infty} \sum_{j=0}^{N+L_{cp}-1} x_{cp,i}[j] \delta[n - i(N + L_{cp}) - j], \quad (2.5)$$

in which  $\delta[\ell]$  is the Kronecker delta function, with unitary value for  $\ell = 0$  and null for all other values of  $\ell$ .  $T_f = (N + L_{cp})T_s$  is the period of the HS-OFDM symbol ( $T_f < T_c$ ). Also,  $x_{cp,i}[j]$  is the  $j^{th}$  coefficient of the vector  $\mathbf{x}_{cp,i}$ .

### 2.2.2 Synchronization

In possession of the sequence  $\{y[n]\}$ , of length  $L_y$ , that represents the discrete signal measured at the PLC channel output, the timing synchronization process is performed. It is applied to each portion of the auxiliary sequence defined as  $\{y_j[n]\} = \{y[n + \Delta]\}_{n=0}^{L_j-1}$ , where  $\Delta$  is varied until all the sequence  $\{y[n]\}$  is analyzed, and  $L_j$  denotes the length of the sequence  $\{y_j[n]\}$  which must be properly chosen to include an entire HS-OFDM symbol. The aim of this step is to identify the initial sample of each HS-OFDM transmitted symbol (timing synchronization).

There are in the literature several strategies for timing synchronization in OFDM-based systems, which can be classified into two main groups: based on training information [47] and based on the redundance of the cyclic prefix [48]. The algorithms of the first group can achieve some performance improvement if compared with those of the second group [49]. On the other hand, the latter are less complex and can reach good performance if applied as a coarse estimate followed by a fine tuning strategy [50].

In this work, the synchronization task is based on the cyclic prefix redundancy incorporated to the HS-OFDM symbol [51], which can be detected through the correlation between the vectors  $\mathbf{y}_{1,l} = \{y_j[l] \ y_j[l + 1] \ \dots \ y_j[l + L_{cp} - 1]\}^T$  and  $\mathbf{y}_{2,l} = \{y_j[l + 2N] \ y_j[l + 2N + 1] \ \dots \ y_j[l + 2N + L_{cp} - 1]\}^T$ . Thus, by defining the correlation vector as  $\mathbf{y}_{corr} = [y_{corr}(0) \ y_{corr}(1) \ \dots \ y_{corr}(L_j - (2N + L_{cp} + 1))]^T$ , one has that

$$y_{corr}[l] = \langle \mathbf{y}_{1,l}, \mathbf{y}_{2,l} \rangle = \mathbf{y}_{1,l}^T \mathbf{y}_{2,l}, \quad (2.6)$$

where the symbol  $\langle \cdot, \cdot \rangle$  denotes the inner product operator and  $l$  is the  $l^{th}$  shift of the vectors  $\mathbf{y}_{1,l}$  and  $\mathbf{y}_{2,l}$ .

To ensure that the synchronization step works properly, it is suggested that the transmitted frame assume the profile indicated in Fig. 4. In that case, the transmitted signal is composed of two different HS-OFDM symbols, periodically transmitted. This

configuration provides a delay and a channel estimation for each HS-OFDM symbol, with the receiver requiring only the two HS-OFDM originally sent symbols.



Figure 4: Transmitted signal.

Consider that the initial (coarse) estimation of the synchronism point, which indicates the initial sample of an HS-OFDM symbol within the sequence  $\{y_j[n]\}$  (the samples that comprise the CP are exuded) is given by

$$l_{sync} = l_{max} + L_{cp} = \arg \max_l (y_{corr}[l]) + L_{cp}. \quad (2.7)$$

The signal transmitted over the channel suffers a time scattering that is related to the channel impulse response spread. This phenomenon introduces interblock interference (IBI) and affects the synchronization process. If  $L_{cp} \geq L_{eq}$  there is a region that can be considered as the beginning of the HS-OFDM symbol. In other words, the synchronization is correct if  $l_{sync}$  is within the interval depicted in Fig. 5.

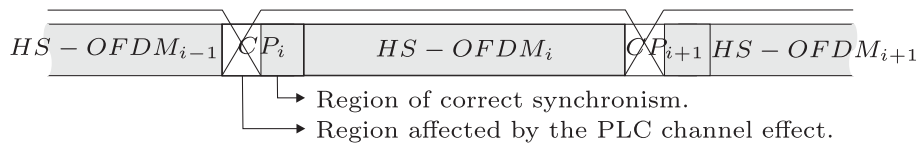


Figure 5: Region in which the synchronism is considered correct.

In practice, it is observed that the synchronism estimate, as derived in (2.7), is highly affected by channel noise and scattering effect. To circumvent this weakness, we propose the use of the metric defined as

$$m_t[r] = \frac{1}{K_d} \sum_{p=1}^{K_d} \left[ y_j \left( l_{sync} - \frac{R}{2} + r - p \right) - y_j \left( l_{sync} - \frac{R}{2} + 2N + r - p \right) \right]^2, \quad (2.8)$$

where  $r = 0, 1, \dots, R - 1$ . Actually, (2.8) evaluates the mean square error of  $K_d$  samples that precede the  $l_{sync}^{th}$  sample with its correspondent samples displaced by  $2N$  samples, similar to the metric introduced in [52]. This calculation is taken over the interval  $l_{sync} - R/2 \leq l_{sync} \leq l_{sync} + R/2$ , where  $R \in \mathbb{Z}$ . Therefore, it can be observed that low-valued coefficients within  $\mathbf{m}_t = \{m[0] \ m[1] \ \dots \ m[R-1]\}^T$ , where  $l_{sync}$  is found, are in the region of the correct synchronism. These values tend to increase when  $l_{sync}$  moves into the signal HS-OFDM from the boundary defined by the CP. Thus, a new synchronization point can be defined as  $l'_{sync} = l_{sync} - \arg \min_r \{m_t[r]\}$ , where the term  $\arg \min_r \{m_t[r]\}$  corresponds to the lowest coefficient of the vector  $\mathbf{m}_t$ .

After the starting point of a HS-OFDM symbol is estimated, within the current sequence  $\{y_j[n]\}$ , a shift of  $\Delta$  samples is performed in order to get the forthcoming sequence  $\{y_{j+1}[n]\}$ . The initial sample of the  $i^{\text{th}}$  HS-OFDM symbol in the sequence  $\{y[n]\}$  can be represented by  $n'_{sync,i} = l'_{sync} + \Delta$ , where  $i = 0, 1, \dots, K - 1$  and  $K$  is the number of obtained estimates.

As a final step in the synchronization process, we average all starting points  $n'_{sync,i}$ ,  $i = 0, 1, \dots, K - 1$ , of the  $K$  HS-OFDM symbols to mitigate the effect of the noise, and the final synchronism point is determined as

$$\hat{n}_{sync} = \frac{1}{K} \sum_{i=0}^{K-1} n'_{sync,i} - (i(2N + L_{cp})). \quad (2.9)$$

This simple averaging procedure, combined with the correlation-based estimate, effectively substitutes a more elaborated estimation procedure, such as the ones based on the maximum likelihood (ML) algorithm [53] or the minimum mean squared error (MMSE) algorithm [54].

### 2.2.3 Channel estimation

Once  $\hat{n}_{sync}$  is defined, we obtain the vectors  $\mathbf{y}_{med,i} = \{y_{med,i}[0], y_{med,i}[1], \dots, y_{med,i}[2N - 1]\}^T$ , in which  $y_{med,i}(j) = y[\hat{n}_{sync} + i(2N + L_{cp}) + j]$ ,  $i = 0, 1, \dots, K - 1$  and  $j = 0, 1, \dots, 2N - 1$ , comprising the samples of the  $i^{\text{th}}$  HS-OFDM symbol not including the CP samples.

The problem remaining is to select which HS-OFDM symbol, either  $A$  or  $B$ , the vector  $\mathbf{y}_{med,i}$  belongs to. Let the vectors  $\mathbf{x}_i \in \mathbb{R}^{2N \times 1}$  be the distinct HS-OFDM transmitted symbols. As the transmitted signal has two different HS-OFDM symbols in it, we can now calculate the correlations operations  $corr_{A,i} = \langle \mathbf{x}_A, \mathbf{y}_{med,i} \rangle$  and  $corr_{B,i} = \langle \mathbf{x}_B, \mathbf{y}_{med,i} \rangle$  and state the following decision rule:

If  $corr_{A,i} > corr_{B,i}$ , then the vector  $\mathbf{y}_{med,i}$  corresponds to the symbol HS-OFDM $_A$ ;

Else if  $corr_{A,i} < corr_{B,i}$ , then the vector  $\mathbf{y}_{med,i}$  corresponds to the symbol HS-OFDM $_B$ ;

Else if  $corr_{A,i} = corr_{B,i}$ , then the vector  $\mathbf{y}_{med,i}$  is discarded.

Let the  $i^{\text{th}}$  CFR estimate designated by  $\hat{\mathbf{H}}_{eq,i} = \{\hat{H}_{eq,i}[0], \hat{H}_{eq,i}[1], \dots, \hat{H}_{eq,i}[2N - 1]\}^T$ . With the notation  $\mathbf{Y}_{med,i} = (1/\sqrt{2N}) \mathbf{W} \mathbf{y}_{med,i}$  and  $\mathbf{X}_{map,i} = (1/\sqrt{N}) \mathbf{W} \mathbf{x}_i$ , by applying the zero-forcing criterion, we thus have that

$$\hat{\mathbf{H}}_{eq,i} = [\text{diag}(\mathbf{X}_{map,i})]^{-1} \mathbf{Y}_{med,i}. \quad (2.10)$$

### 2.2.4 Channel estimation enhancement

The effects of additive channel noise on the frequency-response estimates given by (2.10) can be significantly reduced by deploying the procedure described as follows.

The estimate of the CFR can be rewritten as  $\mathcal{H}_{eq} = \sqrt{2N} \mathbf{diag}\{\mathbf{F}_{2N,2N} \mathbf{h}_{eq,ext}\}$ , where  $\mathbf{F}_{2N,2N}$  is the  $2N \times 2N$  matrix with  $2N > L_{eq}$ , that is applied to the inverse discrete Fourier transform (IDFT), and  $\mathbf{h}_{eq,ext} = \{h[0], h[1], \dots, h[L_{eq} - 1], 0, \dots, 0\}^T$  is the extended version of the channel impulse response with  $2N - L_{eq}$  zeros appended.

If the received signal is corrupted by the additive noise, the last coefficients in the channel impulse response, derived from the IDFT of (2.10), should be different from zero. Assuming that the length of the impulse response is such that  $L_{eq} < L_{cp} \ll 2N$ , then it becomes clear that the last samples of the estimated channel impulse response are just noisy coefficients that can be disregarded [55] to attain a more reliable estimate. Since, in practice, the true value of  $L_{eq}$  is unknown, a reasonable assumption here is to consider  $L_{eq} = L_{cp}$ . The matrix  $\mathbf{W}_o$  that projects a given  $2N$ -length vector onto this  $L_{cp}$ -dimension subspace is given by  $\mathbf{W}_o = \mathbf{F}_{2N,L_{cp}} (\mathbf{F}_{2N,L_{cp}}^\dagger \mathbf{F}_{2N,L_{cp}})^{-1} \mathbf{F}_{2N,L_{cp}}^\dagger$ , where  $\mathbf{F}_{2N,L_{cp}}$  is a  $2N \times L_{cp}$  matrix containing the first  $L_{cp}$  columns of the  $2N$ -point DFT matrix. Thus, an improved channel estimate for the  $i^{th}$  CFR is given by

$$\hat{\mathbf{H}}_{eq,i}^w = \mathbf{W}_o \hat{\mathbf{H}}_{eq,i}. \quad (2.11)$$

### 2.2.5 Sampling frequency offset error estimation and correction

When the frequency of the clock in the signal generator and the acquisition equipment are different, then sampling frequency offset (SFO) error occur. The SFO can result in severe degradation of CFR estimates, as discussed in [50]. When the distances between the injecting and extracting points are short, a cable can be used in order to guarantee the same clock in both transmitter and receiver equipment. On the other hand, for large distances some signal processing tools must be applied to estimate the SFO and provide its correction.

The SFO can be estimated from two consecutive received OFDM symbols by using

$$\text{SFO}_{error} = \frac{1}{2N + L_{cp}} \left( \arg \max_s \{|\hat{h}_{eq,i+1}^w[s]|\} - \arg \max_s \{|\hat{h}_{eq,i}^w[s]|\} \right), \quad (2.12)$$

where  $s = 0, 1, \dots, 2N - 1$  and  $\hat{h}_{eq,i}^w[s]$  is the  $i^{th}$  enhanced channel impulse response estimate. Also, the  $\text{SFO}_{error}$  estimate can be enhanced and result in  $\mu_{\text{SFO}_{error}}$ , by averaging the values in a vector  $\epsilon$  where each coefficient corresponds to the error from each pair of consecutive channel impulse response (CIR).

Based on the  $\mu_{\text{SFO}_{error}}$  value, a new sequence  $\{z[n]\}$  can be obtained through a

interpolation technique by using [56]

$$z[n] = \sum_{\lambda=0}^{L_p} \mu_n^\lambda \sum_{\varrho=0}^{I-1} b_\lambda[\varrho] y[m_n - \varrho], \quad (2.13)$$

where  $I$  is the number of taps if the interpolating filter is of finite impulse response (FIR),  $L_p$  is the polynomial's degree,  $b_\lambda[\varrho]$  are independent coefficients,  $\mu_n = (1 - \mu_{SFO_{error}}) - m_n$ , and  $m_n = \lfloor n(1 - \mu_{SFO_{error}}) \rfloor$ , in which  $\lfloor x \rfloor = \max\{m \in \mathbb{Z} | m \leq x\}$  denotes the largest integer not exceeding  $x$ . The values of the coefficients  $b_\lambda[\varrho]$ , the quantities  $L_p$  and  $I$  can be obtained according with [57]. The procedure for SFO estimation and correction is summarized in **Algorithm 1**.

Note that the correction of the SFO error will be performed using the enhanced CIR estimates,  $\hat{\mathbf{h}}_{eq,i}^w$ , and will result in the signal  $\{z[n]\}$ . Then, the methodology is applied again, but the signal  $\{y[n]\}$  is replaced by  $\{z[n]\}$ .

---

**Algorithm 1:** SFO error estimation and correction algorithm.

---

**Data:**  $\{y[n]\}, \hat{\mathbf{h}}_{eq}^w$

**Result:**  $\{z[n]\}$

Initialization:  $i = 0, n = 0$ ;

**while**  $i \leq K - 2$  **do**

$$\left| \begin{array}{l} \epsilon[i] = \frac{1}{2N+L_{cp}} \left( \arg \max_s \{ |\hat{h}_{eq,i+1}^w[s]| \} - \arg \max_s \{ |\hat{h}_{eq,i}^w[s]| \} \right); \\ i = i + 1; \end{array} \right.$$

**end**

$$\mu_{SFO_{error}} = \frac{1}{K-1} \sum_{i=0}^{K-2} \epsilon[i];$$

**while**  $n \leq L_y - I$  **do**

$$\left| \begin{array}{l} z[n] = \sum_{\lambda=0}^{L_p} ((1 - \mu_{SFO_{error}}) - \text{int}[n(1 - \mu_{SFO_{error}})])^\lambda \sum_{\varrho=0}^{I-1} b_\lambda[\varrho] y[m_n - \varrho]; \\ n = n + 1; \end{array} \right.$$

**end**

---

### 2.2.6 Trigger source circuit

The circuit shown in Fig. 6 can be used in cases when the channel variability with respect to the zero crossing of the power fundamental signal is analyzed. The component  $U1$  is an opto-transistor that works as a switch that is closed every time that its polarization condition is satisfied. The signal  $v_{out}(t)$  can be used as a trigger that starts the measurements performed by the data acquisition equipment. With this triggering device, the first estimation corresponds to the HS-OFDM symbol received immediately after the detection of a zero crossing fundamental signal. As a result, it is possible to correlate the CFR estimates of the PLC channel with the periodicity of the main voltage signal (50 or 60 Hz) of electric power grids.

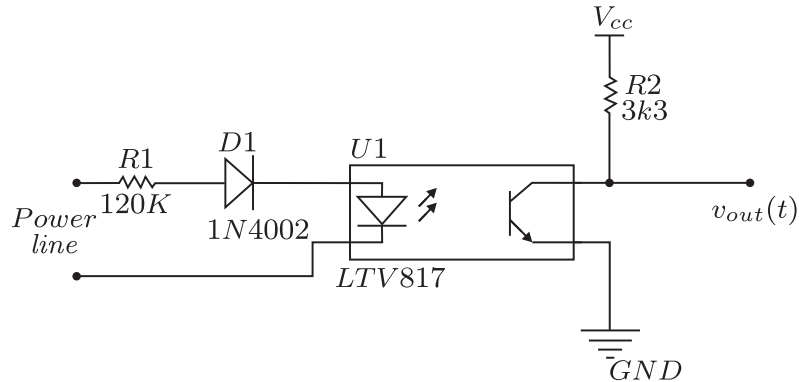


Figure 6: Power line fundamental signal synchronization circuit.

### 2.2.7 General overview of the algorithm

The general structure of the algorithm for channel estimation, following all stages detailed above, is summarized in **Algorithm 2**. The structure of the algorithm is also depicted in Fig. 7.

## 2.3 EXPERIMENTAL RESULTS

The results obtained using the presented methodology will be discussed in three parts. In the first part, the performance of the presented methodology is evaluated using a well-known PLC channel model. In the second part, the methodology is analyzed on the measured data taken in real electric power grids. Finally, in the third part some results will be illustrated when considering the frequency response estimation of some electrical devices. In all cases, the adopted sampling frequency is 200 MHz and the analysis covers a frequency bandwidth from 1.7 up to 50 MHz to agree with the telecommunication regulation for PLC technology in Brazil [58]. The transmitted signal features and adopted parameters are listed in Tab. 1. The number of symbols and the value  $L_j$  match with the requirement mentioned in Section 2.2.2, in order to ensure that the synchronization process works properly. The binary phase shift keying (BPSK) modulation was chosen due to its simple implementation and because it results in a very low peak to average power ratio (PAPR) [59], which significantly reduces the errors introduced by the conversion process performed for the digital-to-analog converter (DAC). The number of sub-carriers gives a frequency resolution of, approximately, 48.8 kHz, lower than the coherence bandwidth of indoor PLC channels. Furthermore, the symbol duration ( $T = 23.04 \mu s$ ) is made much less than  $600 \mu s$ , which is the shortest coherence time of indoor PLC channels, according to [35]. The length of the CP was chosen based on [60] in which the influence of this parameter was evaluated in more than 160 types of indoor PLC channels, measured in 20 different places. Finally, the last three parameters in Tab. 1 were heuristically chosen.

---

**Algorithm 2:** PLC channel estimation algorithm.

---

**Data:**  $\{x[n]\}, \{y[n]\}$   
**Result:**  $\hat{\mathbf{H}}_i^w$   
 Initialization:  $\Delta = 0, i = 0$  ;  
**while**  $\Delta \leq L - L_j$  **do**  
      $\{y_j[n]\} = \{y[n + \Delta]\}_{n=0}^{L_j-1}$ ;  
     **for**  $l = 1, 2, \dots, L_j - (2N + L_{cp} + 1)$  **do**  
          $y_{corr}[l] = \langle \mathbf{y}_{1,l}, \mathbf{y}_{2,l} \rangle = \mathbf{y}_{1,l}^T \mathbf{y}_{2,l}$ ;  
     **end**  
      $l_{\max} = \arg \max_l (y_{corr}[l])$ ;  
      $l_{sync} = l_{\max} + L_{cp}$ ;  
     **for**  $r = 0, 1, \dots, R - 1$  **do**  
          $m_t[r] = \frac{1}{K_d} \sum_{p=1}^{K_d} \left[ y_j \left( l_{sync} - \frac{R}{2} + r - p \right) - y_j \left( l_{sync} - \frac{R}{2} + 2N + r - p \right) \right]^2$ ;  
     **end**  
      $l'_{sync} = l_{sync} - \arg \min_n m_t[n]$ ;  
      $n'_{sync,i} = l'_{sync} + \Delta$ ;  
      $i = i + 1$ ;  
      $\Delta = n'_{sync,i} + L_{cp}$   
**end**  
 $\hat{n}_{sync} = \frac{1}{K} \sum_{i=0}^{K-1} n'_{sync,i} - (i(2N + L_{cp}))$ ;  
 $i = 0$ ;  
**while**  $i \leq K - 1$  **do**  
      $\mathbf{y}_{med,i} = \left\{ y \left[ \hat{n}_{sync} + (i \times (2N + L_{cp})) \right], y \left[ \hat{n}_{sync} + (i \times (2N + L_{cp})) + 1 \right], \dots \right.$   
      $\left. \dots, y \left[ \hat{n}_{sync} + (i \times (2N + L_{cp})) + 2N - 1 \right] \right\}^T$  ;  
      $corr_{A,i} = \langle \mathbf{x}_A, \mathbf{y}_{med,i} \rangle$ ;  
      $corr_{B,i} = \langle \mathbf{x}_B, \mathbf{y}_{med,i} \rangle$ ;  
     **if**  $corr_{A,i} > corr_{B,i}$  **then**  $\hat{\mathbf{H}}_{eq,i} = [\text{diag}(\mathbf{X}_{map,A})]^{-1} \mathbf{Y}_{med,i}$ ;  
     **if**  $corr_{B,i} > corr_{A,i}$  **then**  $\hat{\mathbf{H}}_{eq,i} = [\text{diag}(\mathbf{X}_{map,B})]^{-1} \mathbf{Y}_{med,i}$ ;  
     **else** the vector  $\mathbf{y}_{med,i}$  is discarded;  
      $\hat{\mathbf{H}}_{eq,i}^w = \mathbf{W}_o \hat{\mathbf{H}}_{eq,i}$ ;  
      $i = i + 1$ ;  
**end**

---

### 2.3.1 Performance analysis: PLC channel model

A simulated environment was used to evaluate the performance of the presented methodology. Initially the PLC model proposed by [41], applied to describe the channel

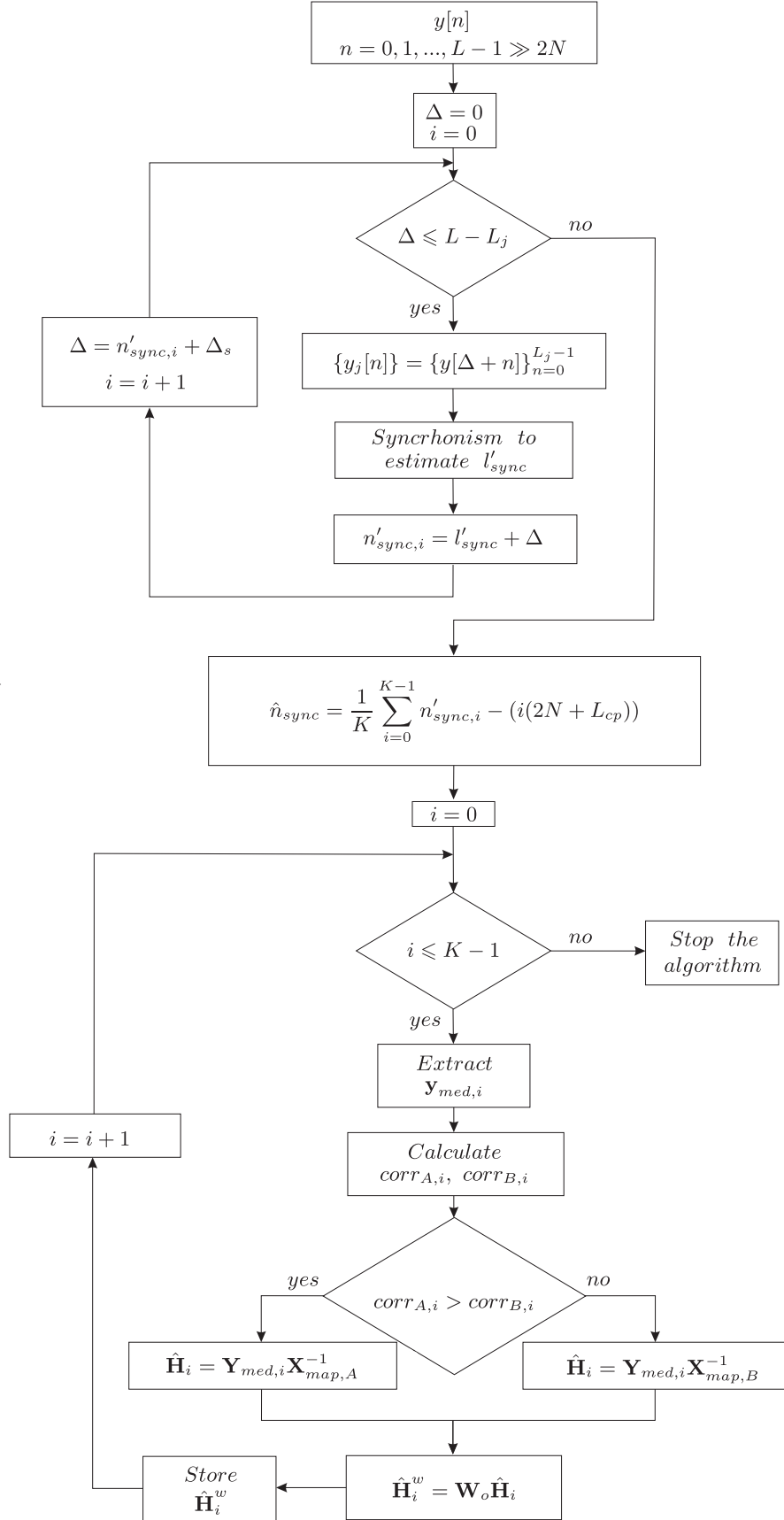


Figure 7: PLC channel frequency response estimation algorithm flowchart.

Table 1: Transmitted signal features and values of the parameters used by the PLC frequency response estimation algorithm.

Number of HS-OFDM symbols	2
Modulation	BPSK
Number of sub-carriers	$N = 2048$
CP length	$L_{cp} = 512$
Frequency resolution	48.8 kHz
Symbol duration	$T_f = 23.04\mu s$
Length of the sequence $\{y_j[n]\}$	$L_j = 9216$
Number of samples used to compute $\mathbf{m}_t$	$K_d = 8$
Number of shift in the vector $\mathbf{m}_t$ calculus	$R = 128$
Number of symbols in the synchronism step	$K = 36$

frequency response, given by

$$H(f) = \sum_{i=1}^N \underbrace{g_i}_{\text{gain}} \cdot \underbrace{e^{-(a_0+a_1f^k)d_i}}_{\text{attenuation coefficient}} \cdot \underbrace{e^{-j2\pi f\tau_i}}_{\text{delay coefficient}}, \quad f \geq 0, \quad (2.14)$$

where  $N$  is the number of considered paths,  $i$  is the path index,  $g_i$  is the gain of the  $i^{th}$  path,  $a_0$  and  $a_1$  are attenuation coefficients,  $k$  is the exponent of the attenuation coefficients,  $d_i$  is the length of the  $i^{th}$  path and  $\tau_i$  is its associated delay.

Table 2 presents the parameters of a well know PLC channel that was applied in the performance tests. Applying these parameters in (2.14), results in the frequency response magnitude depicted in Fig. 8 and in the impulse response shown in Fig. 9.

Table 2: Parameters of an outdoor PLC channel model [41].

$i$	1	2	3	4
$g_i$	0.64	0.38	-0.15	0.05
$d_i(m)$	200.00	222.40	224.80	267.50
$k = 1$	$a_0 = 0$	$a_1 = 7.8 \cdot 10^{-10}$		

Figure 10 shows the values of the coefficients of the vector  $\mathbf{m}_t$  that are used in the synchronization process. Notice that the position 80 refers to the initial estimation of the synchronization point ( $l_{sync}$ ). Moreover, in Fig. 10, the region of correct synchronism, as discussed in Section 2.2.2 (see Fig. 5), can be easily observed as the one with smaller values for the coefficients of the vector  $\mathbf{m}_t$ .

Figure 11 shows how the average value of the synchronism point ( $\hat{n}_{sync}$ ) varies with the number of considered HS-OFDM symbols. The vertical axis refers to the displacement of the estimated synchronism point with respect to the boundary defined by the CP. The positive values refer to the number of samples in that the synchronism point advances into the HS-OFDM symbol. On the other hand, negative values refer to the distance of the synchronism point to the ideal point (with value 0) into the CP. Notice that this last

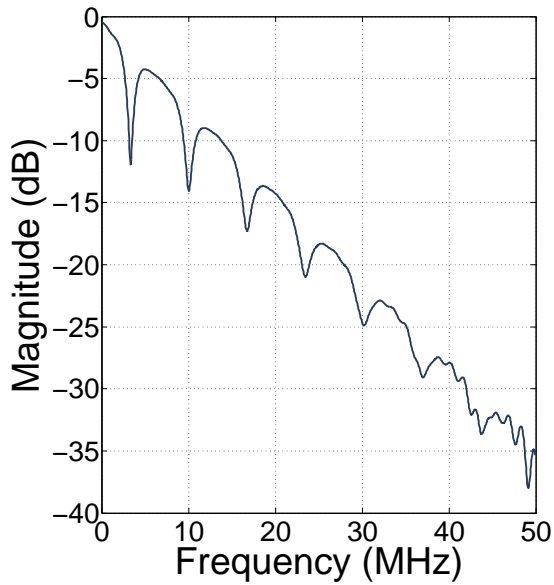


Figure 8: Magnitude function.

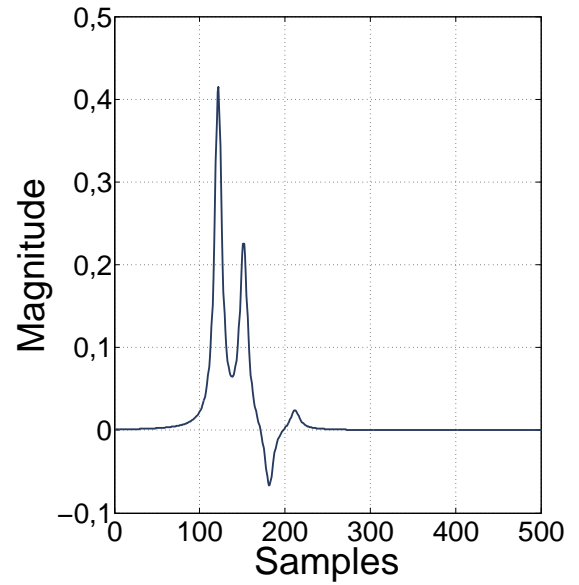
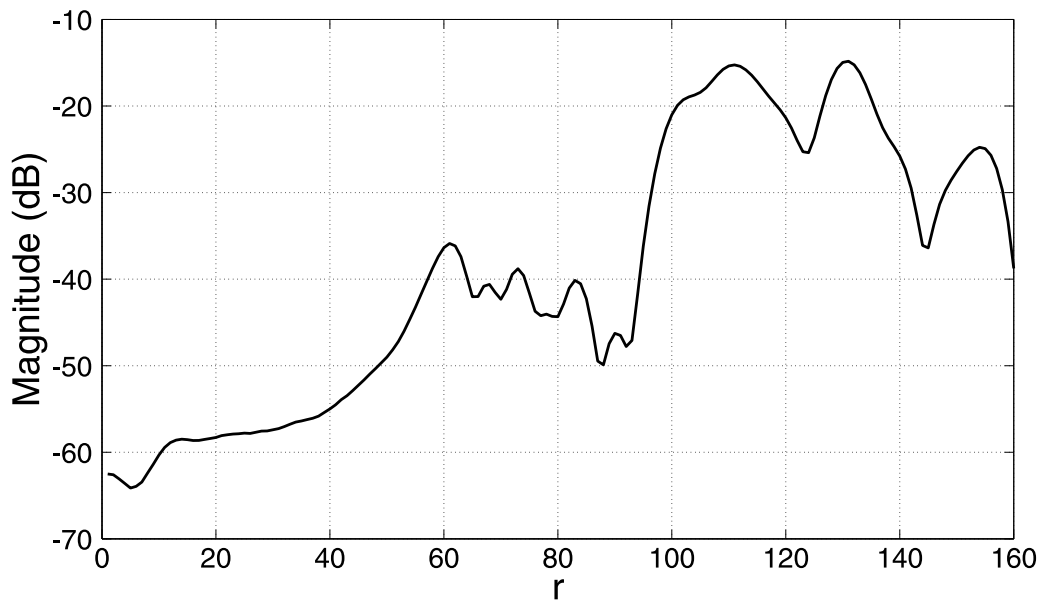


Figure 9: Impulse response.

Figure 10: Coefficients of the vector  $\mathbf{m}_t$ .

procedure plays a key role in the synchronization step, since individual estimates of the synchronism point can present a high error ratio (see Fig. 12).

The performance of the synchronism process is depicted in Fig. 12. In this case, the analysis was made with the signal transmitted through the PLC channel model and with additive white Gaussian noise (AWGN) by considering a signal-to-noise ratio (SNR) from 0 up to 30 dB, in steps of 5 dB. The simulation was taken over 1024 symbols for

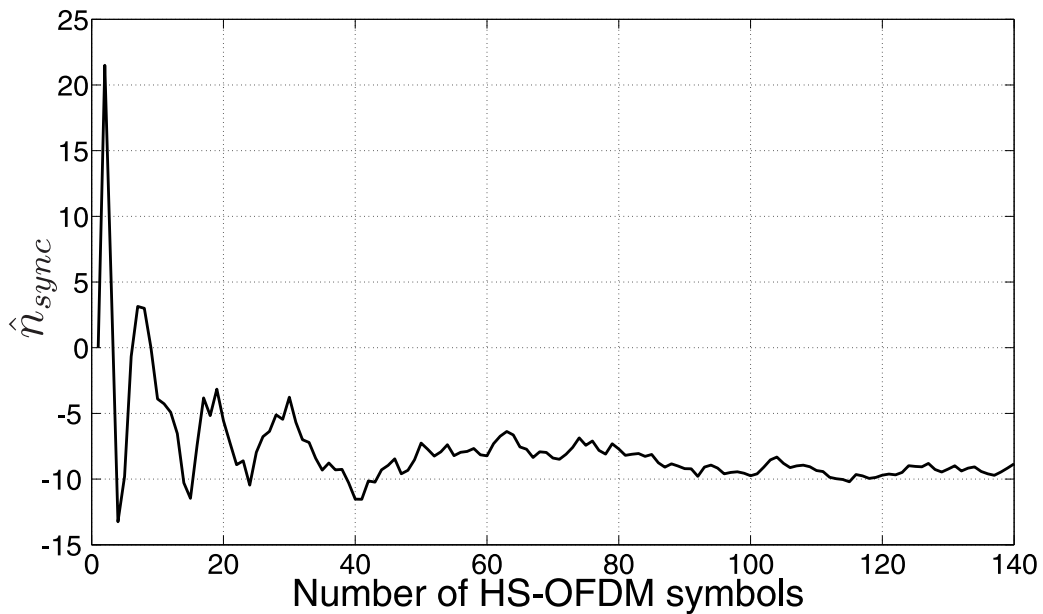


Figure 11: Estimation of the correct synchronism point related to the number of HS-OFDM symbols.

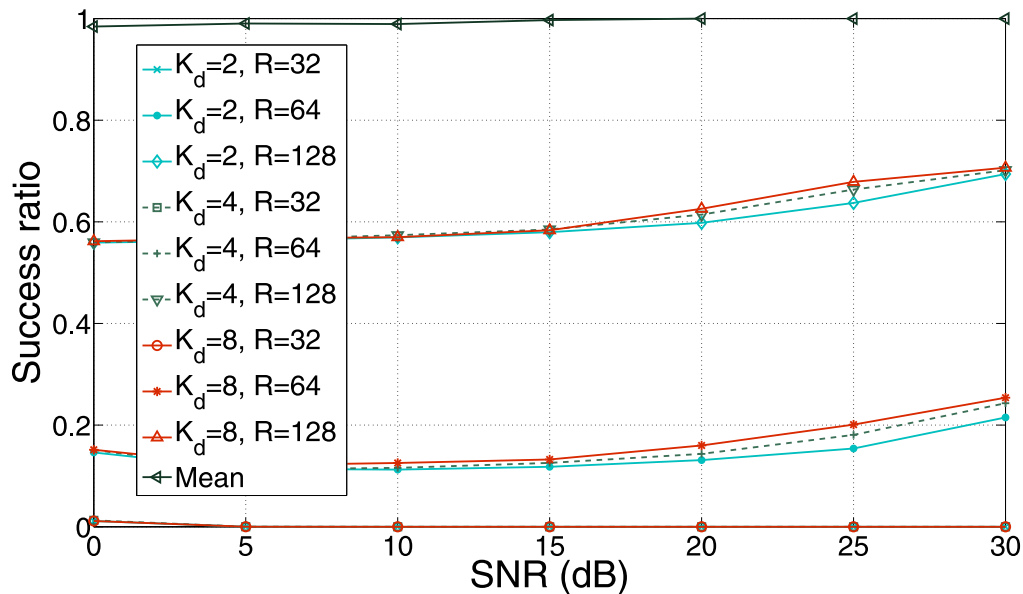


Figure 12: Evaluation of the synchronism technique.

each SNR. The first number of the legend in the graphic is related to the  $K_d$  samples used when determining  $\mathbf{m}_t$  and the second number refers to the shift  $R$  performed in the vector  $\mathbf{m}_t$ . As can be seen in this figure, for  $R = 32$  the synchronism point is erroneously estimated within the symbol HS-OFDM almost all the time. For  $R = 128$  the synchronism is correctly estimated more than 55% of the cases, reaching more than 70% for  $K_d = 8$  and  $\text{SNR} = 30$  dB. The best result in Fig. 12, referred to as ‘average’ in the legend, is related to the last procedure of the synchronization step, given by Eq. (2.9), considering  $K = 140$ ,  $K_d = 2$  and  $R = 128$ .

The improvement obtained with the use of the enhancement procedure was evaluated by considering the mean square error (MSE) metric. On that sense, the MSE between the simulated and estimated (with enhancement procedure) CFRs can be compared to the MSE between the simulated frequency response and the CFR estimated without the enhancement procedure. Furthermore, the comparison was made with respect to the MSE between the simulated frequency response and those from average of estimations (largely applied for noise interference mitigation, see [35]). This comparison was made considering ideal synchronism condition. Results for several scenarios varying the SNR from 0 up to 30 dB, in steps of 5 dB, were examined (1024 channel estimations were taken for each scenario and the noise is the AWGN) and considering the average of 2, 4, 8 and 16 channel estimations – for the MSE computation 1024 averaged estimations were taken for each SNR. Results for SNR equal to 20 dB are summarized in Tab. 3. It is important to notice that each time the amount of channel estimates used in the average is folded, the MSE is reduced by approximately 3 dB. On the other hand, the proposed enhancement procedure improves the estimation in almost 10 dB in all frequencies, which is very similar with the performance obtained to the average of 8 estimations. It is important to keep in mind that the larger the number of estimates the greater the time interval from which it represents. Also, it is important to mention that similar improvements were observed in all tested SNRs and, furthermore, that the enhancement procedure has an important impact in the estimated frequency response of PLC channels. In fact, the enhanced estimate makes use of only one coarse estimate of the PLC CFR and results in a smooth and enhanced curve, as can be seen in Fig. 13 for the SNR equal to 20 dB.

Table 3: MSE between the simulated and estimated CFR.

Type of estimate	MSE (dB)
Single	-39.42
Mean of 2	-42.56
Mean of 4	-45.73
Mean of 8	-48.84
Mean of 16	-52.01
Single enhanced	-48.84

### 2.3.2 Performance analysis: real PLC scenario

In this section the presented results were obtained from measurements taken in typical apartments in Brazil. The transmitted signal was generated offline and loaded into an arbitrary waveform generator system of 14 bits resolution, and the receiver was a 16-bit digitizer, both equipments operating with the same clock frequency of 200 MHz. The clock signal in both equipments was the same.

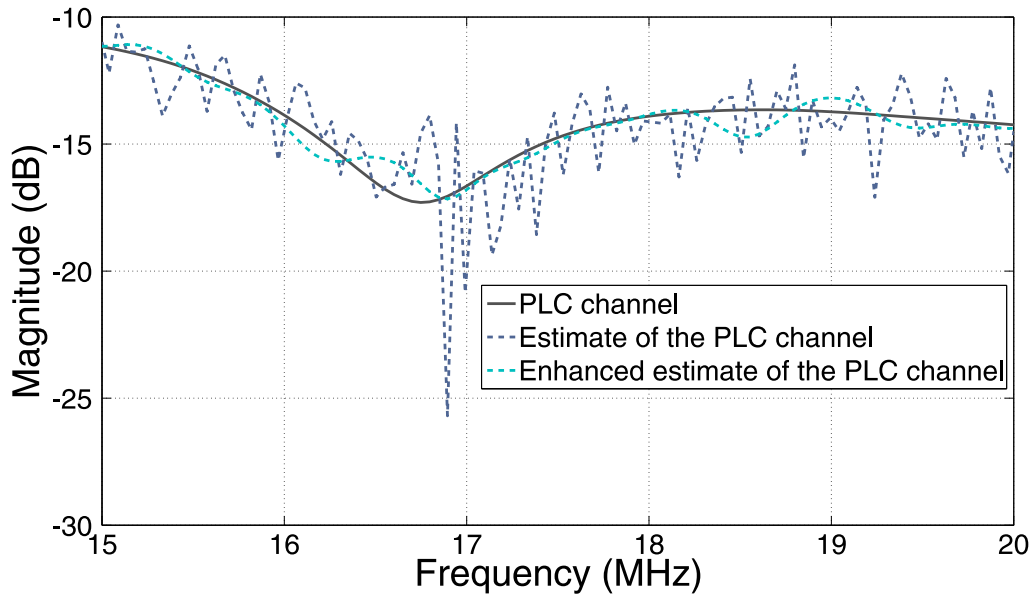


Figure 13: Comparison of estimates with and without the proposed enhancement procedure.

### 2.3.2.1 Comparison between the methodology and the VNA

In Figs. 14 and 15 the magnitude of two measured PLC channels are depicted. On both graphics the measures obtained by the presented methodology and the VNA (E5061B from Agilent) are plotted. It is very important to highlight the differences between the measures. While the presented methodology gives an estimate each  $23 \mu\text{s}$ , approximately, the VNA demands a time interval more than  $300 \text{ ms}$ , for a frequency resolution close to the presented by the methodology. So, one estimate of the PLC channel given by the VNA can represent distinct PLC channels in different frequency intervals. This must be the main reason for some discrepancies presented in Figs. 14 and 15 between the estimates from the presented methodology and that one obtained with the VNA. Based on CFR estimates of real PLC channels it indicate that the presented methodology can offer good results in comparison with the VNA.

### 2.3.2.2 Estimation of real CFR

Figure 16 shows a single magnitude response of seven different PLC channels in a typical apartment in Juiz de Fora, Brazil, as an example of the application of the presented methodology. This figure shows how the CFRs can be different in an indoor electric power grid.

In order to verify the performance of the presented methodology to estimate a periodically and time-varying PLC channel, a drill fed by a source based on silicon controlled rectifier (SCR's) was connected to the power line under investigation. The estimate of the CFR can be seen in Fig. 17, where the color bar denotes the channel gain in decibel and the measurement was triggered by the circuit of Fig. 6. As the main frequency

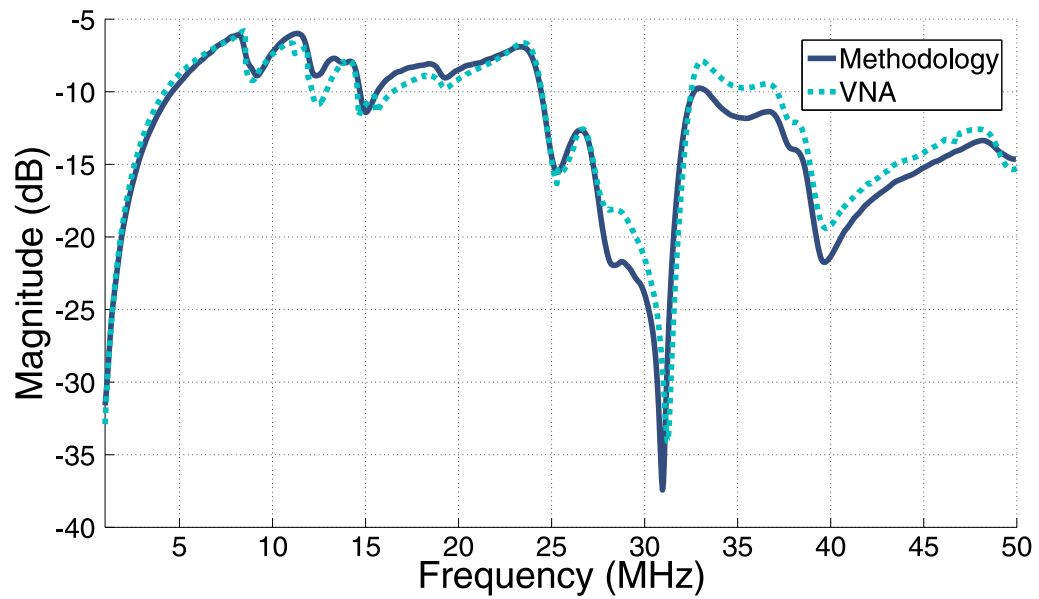


Figure 14: CFR estimates of real PLC channel #1 with the presented methodology and by using a VNA.

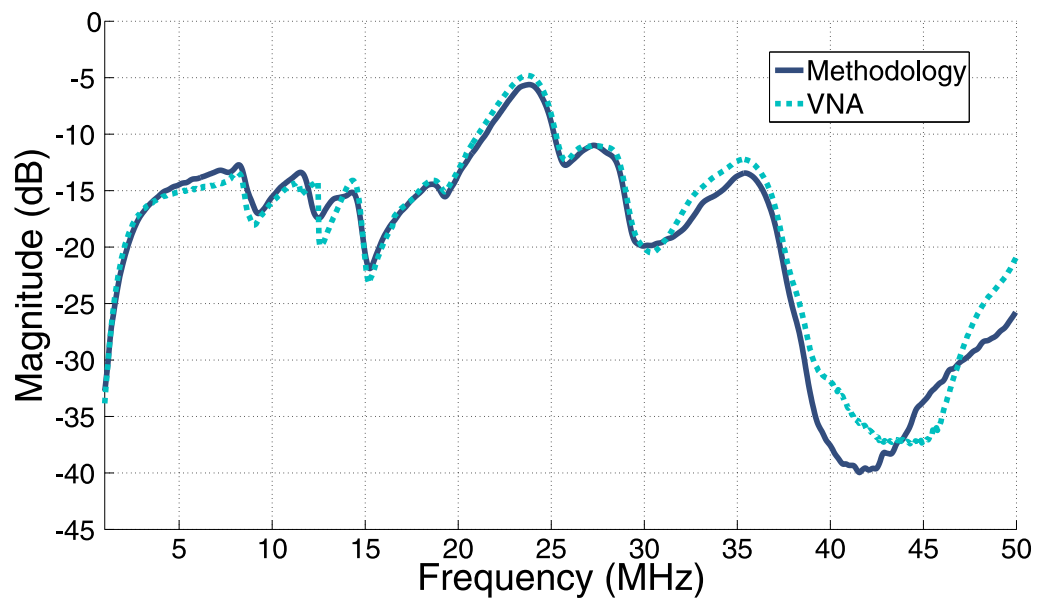


Figure 15: CFR estimates of real PLC channel #2 with the presented methodology and by using a VNA.

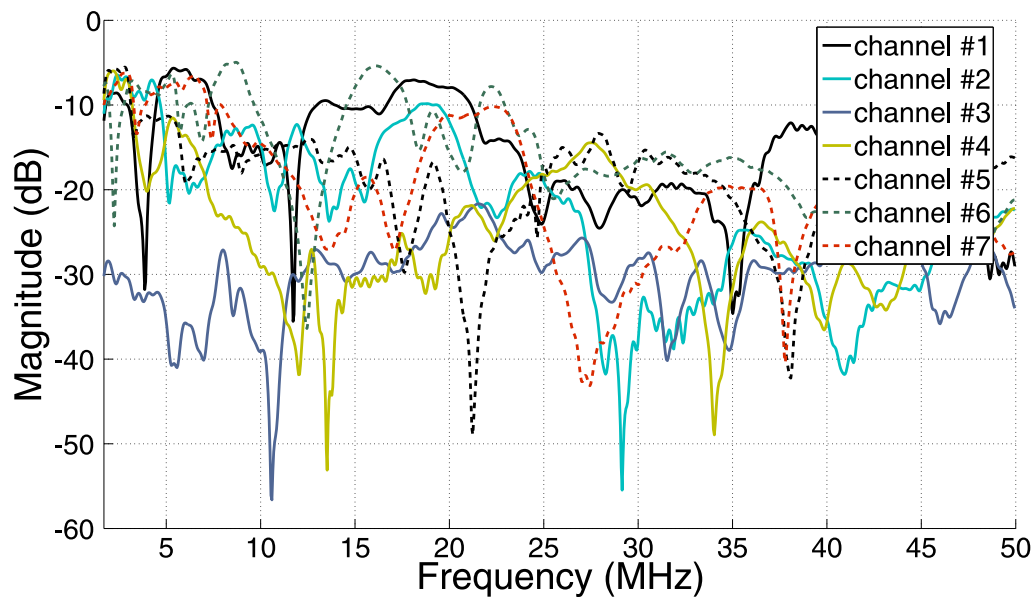


Figure 16: Magnitude of the frequency response of seven measured PLC channels.

in Brazil is 60 Hz, the changes occur approximately around every 8.33 ms (a half cycle of the main frequency). In the analyzed case, this behavior can be clearly verified in some frequencies around 6 and 27 MHz. Figure 18 shows the CFR of successive measures of time invariant PLC channels. These figures are composed of more than 2,000 consecutive CFR. This is a kind of result that is impossible to be obtained with the VNA because its sweep time is higher than 300 ms.

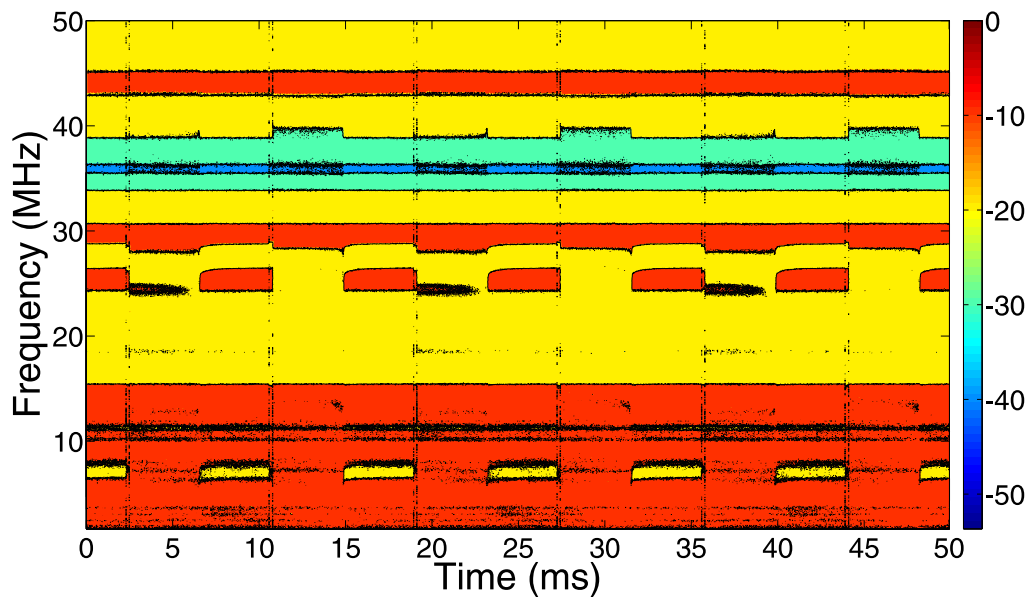


Figure 17: Magnitude of CFR estimates of a periodically time-varying PLC channel.

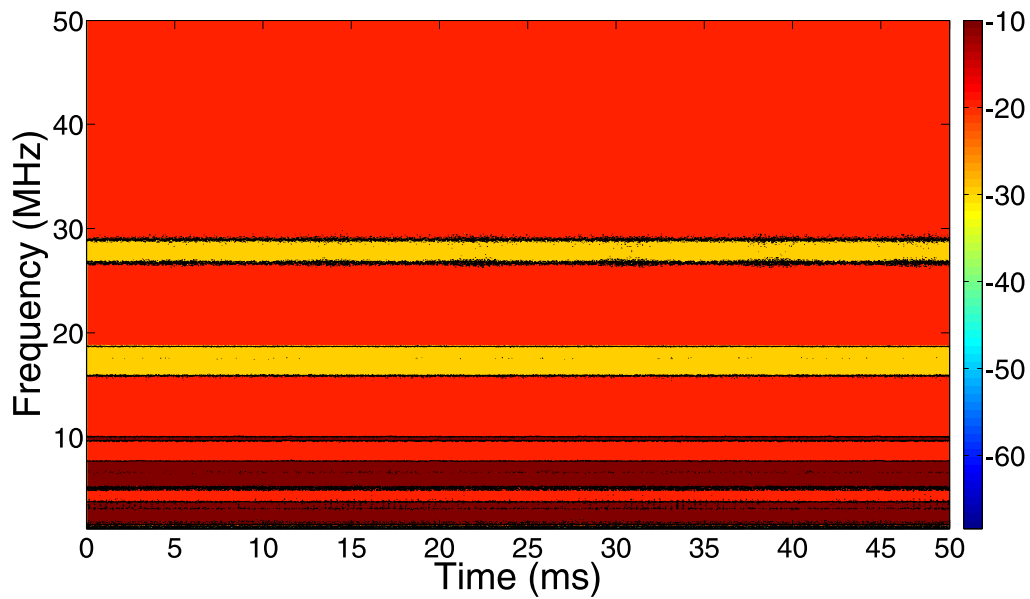


Figure 18: Magnitude of CFR estimates of a time invariant PLC channel.

### 2.3.3 Performance analysis: application on electrical devices

The applicability of the frequency response of electrical devices to support several analysis [61, 62, 63, 64, 65, 66, 67] is well known. In order to illustrate the flexibility of the presented methodology, Figs. 19, 20 and 21 portray the magnitude estimates of the CFR of some electrical devices. Again, the CFR estimates obtained through the methodology are compared with those from the VNA. In Fig. 19 the comparison is performed with the coupler circuitry used to avoid damages in the equipments involved on the PLC channel measurements. The coupler behavior as a high pass filter, blocking the main voltage signal (50 or 60 Hz) of the power lines is clear. Figures 20 and 21 show the CFR of two monophasic transformers. The transformer #1 is of 18 VA while transformer #2 is of 1 kVA.

These plots show the effectiveness of the presented methodology as the estimate of the magnitude function present low differences in comparison with the VNA. This and several other comparisons confirm that the proposed methodology is useful for estimating the CFR of the electric power grids and electrical devices.

## 2.4 SUMMARY

This chapter presented a methodology to be applied to estimate the channel frequency response of electric power grid and electrical devices. The next chapter will present and discuss the results related with the characterization of in-home PLC channels in Brazilian places.

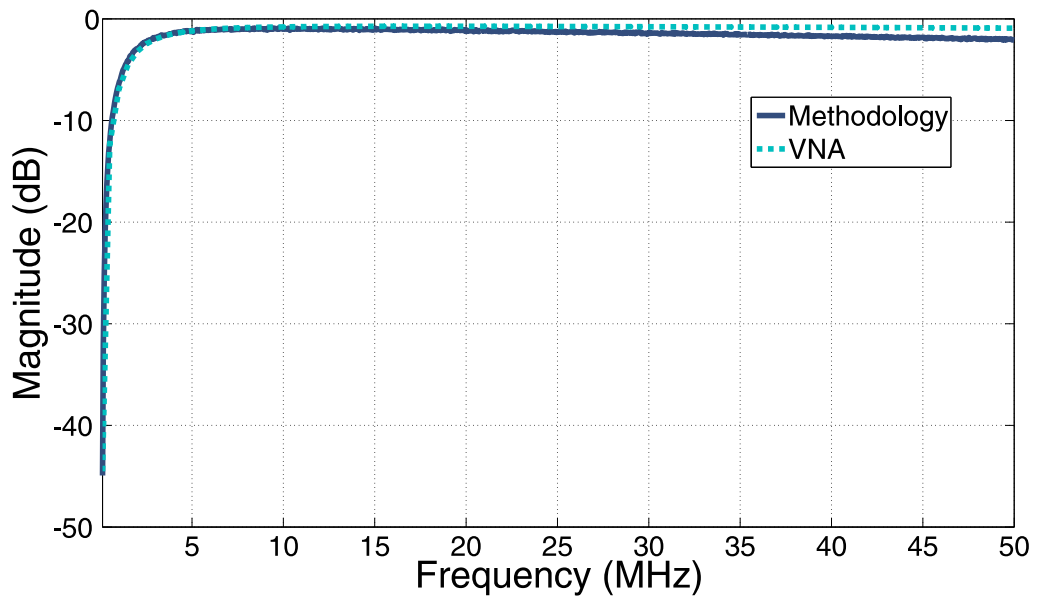


Figure 19: Comparison between magnitude of the frequency response estimate of a PLC coupler circuitry obtained by the presented methodology and by the VNA.

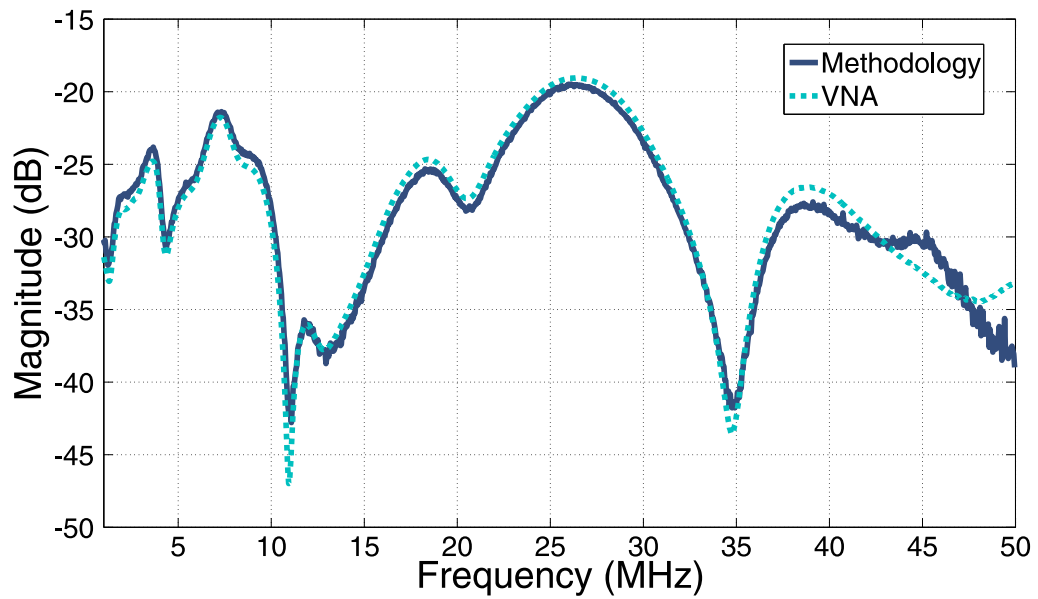


Figure 20: Comparison between magnitude of the frequency response estimate of the transformer #1 obtained by the presented methodology and by the VNA.

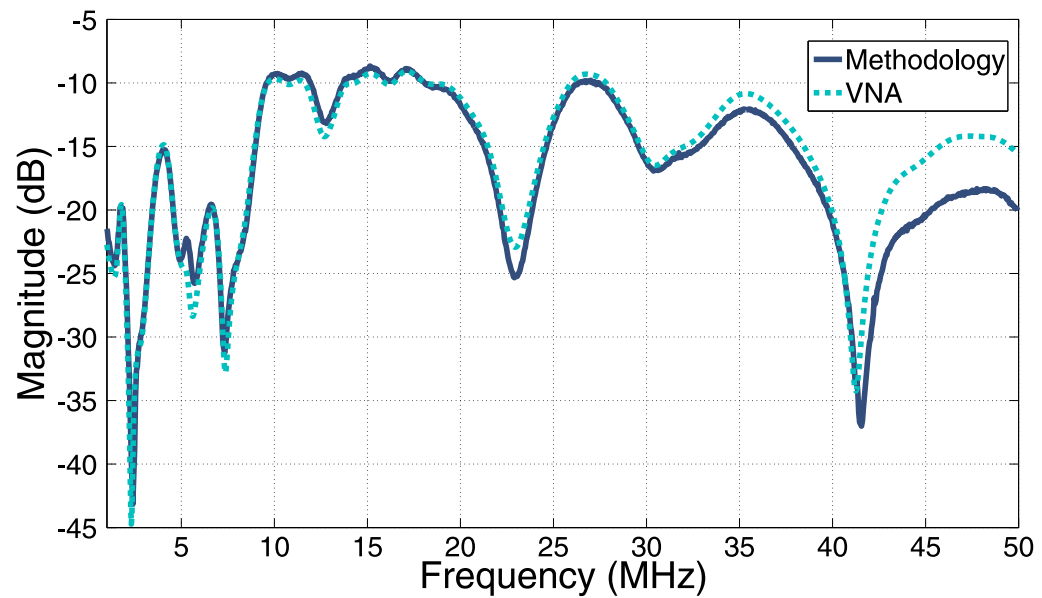


Figure 21: Comparison between magnitude of the frequency response estimate of the transformer #2 obtained by the presented methodology and by the VNA.

### 3 THE CHARACTERIZATION OF BRAZILIAN IN-HOME PLC CHANNELS

A growing interest in the use of electric power grids for communications purposes is notorious. In fact, power line communication (PLC) systems and their applications have been investigated by academic and business sectors. As electric power grids were not originally designed for communication purposes, they constitute a challenging data communication medium, in which the transmitted signals suffer severe attenuations and are strongly corrupted by colored and impulsive noise. The diversity of topologies of electric power grids and the dynamic operation of the connected devices (loads) make these grids hard to characterize and model. Furthermore, some regulatory rules that imposing some constraints on the use of PLC technology were established in order to avoid interferences of PLC systems (secondary user) in other existing communication services operating in the same frequency band such (primary user) as for military applications and amateur radio [3, 4, 5, 6].

In this sense, an expressive effort for the characterization of PLC channels is needed in order to allow a better exploitation of such challenging and opportunistic communication medium. Indeed, there are few contributions in the literature focused on this issue that can be classified according to the voltage level and frequency bandwidth. For instance, the outdoor PLC channel can be evaluated for low-voltage [68], medium-voltage [69] and high-voltage [70]. Also, underground medium-voltage PLC channels are evaluated in [71]. For the indoor-PLC case, there is the following subdivision: residential and commercial buildings (usually referenced as in-home) [72], in cars [11], ships [15] and aircrafts [73]. Finally, the PLC channel characterization can be performed by considering distinct bandwidths, usually classified as narrowband and broadband. The narrowband PLC comprises the frequencies up to a few hundreds kHz [33] and are used for low data rate applications, such as those in smart grids [74, 75]. On the other hand, for broadband PLC systems the analyzed bandwidths are those limited to the frequency of 30 MHz [76, 77], which is regulated in some European countries, and to the frequency of 100 MHz [72], where channel capacities in the order of 1-2 Gbps can be achieved. In Brazil, the regulation allows that the broadband PLC systems operate in the frequency band from 1.7 up to 50 MHz which is a frequency band that lacks a characterization. There are also few works that provide analysis covering the frequency band of up to 300 MHz [32, 76].

Focusing on the in-home PLC scenario, some few contributions related to developed countries can be highlighted. For PLC channels in Spain, [78] presented results of channel attenuation and noise, for frequencies up to 30 MHz, [79] considered other features, such as the ACG, the delay spread and CB, while [80] discussed the normality/lognormality natures of the ACG and delay spread. More recently, [32] analyzed the ACG, CB and RMS-DS considering the bandwidth from 1.8 up to 100 MHz and also expanding the

limit frequency to 300 MHz. In [81, 76], the in-home PLC channels in some urban and suburban US residences are characterized in terms of ACG and RMS-DS, considering the bandwidth ranging from 2 up to 30 MHz. The results reported for in-home PLC channels in France are found in [72, 82], where the PLC channel is evaluated in terms of ACG, CB and RMS-DS, for frequencies up to 100 MHz. The analysis related to the time varying behavior of PLC channel is addressed in only a few works, such as [35], and lacks a more thorough statistical analysis.

Also, in most of the previously cited works the characterization of electric power grids for data communication purposes is performed over measurements obtained with a VNA. This practice reduces the fidelity of the analysis with the reality of the electric power grids, since the sweep time spent to achieve one measure with the VNA may be higher than the CT – period of time in which the PLC channel can be considered time invariant – of the PLC channels. In fact, although the VNA sweep time depends on the equipment model and on the chosen frequency bandwidth and resolution, modern VNAs require a few hundreds milliseconds to perform one measurement, which is much more than a typical CT of in-home PLC channel, reported as not less than  $600 \mu\text{s}$  by [35]. As a consequence, a proper characterization of the coherence time is missing in the literature.

This chapter aims to offer a complete characterization of in-home PLC channels in Brazil by addressing the following frequency bands are: from 1.7 up to 30 MHz, from 1.7 up to 50 MHz and from 1.7 up to 100 MHz. Thus, this contribution constitutes an important reference to support future efforts in modeling and designing in-home broadband PLC systems that can be suitable for both in developing and developed countries. Also, a statistical modeling for ACA, RMS-DS, CB and CT is performed and discussed.

### 3.1 MEASUREMENT SETUP AND CAMPAIGN

The characterization of the Brazilian in-home PLC channels was supported, for the most part, by estimates of the CFR. Complementary characterization were performed through measurements of the noise power spectrum density (PSD). The CFR measurement setup is depicted in Fig. 1. As we can see, the setup consists of three main components:

- Signal generator: Device composed of an arbitrary signal generator board mounted in a rugged computer. A pre-designed sounding sequence is loaded into it and converted to an analog signal to be submitted to the PLC channel under analysis;
- Data digitizer: Acts as a receiver, measuring the transmitted sounding signal after propagating through the PLC channel, and converts it into a digital representation for the subsequent analysis.
- Coupler: Circuitry used to connect both the signal generator and the data digitizer

to the PLC channel under analysis. The coupler is essentially a high pass filter, blocking the main voltage signal (60 Hz in Brazil) that can damage both, the signal generator and the data digitizer, presenting very low attenuations in the bandwidth of interest.

With the possession of the discrete-time version of both the generated and measured signals, the channel-estimation methodology described in Chap. 2 is performed, encompassing the following stages: (i) input-output timing synchronization; (ii) initial channel estimation; (iii) SFO correction; (iv) channel estimation; (v) channel estimation enhancement, which mitigates noise effects. The chosen parameters for the channel estimation setup is summarized in Tab. 1. In this framework, the transmitted signal is composed of HS-OFDM symbols, using a 200-MHz sampling frequency, and the frequency resolution is around 48.83 kHz. For the measurement of the noise PSD the data digitizer was used when no sounding signal was being transmitted.

The measurement campaign of the Brazilian in-home PLC channels was performed in seven different typical sites in a urban area of Juiz de Fora city, as detailed in Tab. 4.

Table 4: Main features of the measured places.

Construction type	Age (years)	Constructed area ( $m^2$ )
House #1	30	78
House #2	10	69
Apartment #1	9	54
Apartment #2	9	42
Apartment #3	18	65
Apartment #4	3	62
Apartment #5	2	54

From the entire campaign, 245 different combinations of pairs of outlets were measured, providing a total of 148,037 different CFR estimates, with an average of 604 consecutive CFR estimates for each PLC channel configuration. Furthermore, for each outlet, a measurement of the noise was taken.

## 3.2 PLC CHANNEL FEATURES

The well known features that are used for characterizing the in-home PLC channels are described as follows.

### 3.2.1 Average channel gain (ACG)

The ACG is expressed by

$$\bar{G} = \frac{1}{B} \int_B |H(f)| df, \quad (3.1)$$

where  $H(f)$  is the channel frequency response at the frequency  $f$  and  $B$  is the frequency bandwidth, usually presented in decibel (dB) as  $\overline{G}_{dB} = 10 \log_{10} \overline{G}$ . The average channel attenuation (ACA), given by  $\overline{A}_{dB} = -\overline{G}_{dB}$ , takes the place of ACG in some performed analyses.

The ACA values can give an indication of the level of attenuation presented in a given communication channel, and as a consequence, an estimate of the channel capacity that can be expected on average.

### 3.2.2 Coherence bandwidth (CB)

The CB reflects the maximum bandwidth in which the CFR magnitude can be considered flat. Thus, the CB indicates how selective the channel is and can be estimated through [83]

$$\rho_H(\delta f) = \frac{E\{(H(f) - \mu_H)(H(f + \delta f) - \mu_H)^*\}}{\sigma_H^2}, \quad 0 \leq |\rho_H(\delta f)| \leq 1, \quad (3.2)$$

where  $\delta f$  is the frequency spacing and  $\mu_H = E\{H(f)\}$ , in which  $E\{\cdot\}$  denotes the expectation operator.

In this way, the CB ( $B_c$ ) of a communication channel can be estimated when

$$|\rho_H(B_c)| \geq \varphi, \quad (3.3)$$

where  $\{\varphi \in \mathbb{R} \mid \varphi \in (0, 1)\}$  refers to the lowest correlation level on which it was observed a CB of  $B_c$ . In this contribution, the correlation levels of 0.9, 0.7 and 0.5 were considered and are denoted by  $B_{09}$ ,  $B_{07}$  and  $B_{05}$ , respectively.

The CB is a key parameter used to evaluate the need for equalization and/or coding to deal with dispersive multipath effects.

### 3.2.3 Root mean squared delay spread (RMS-DS)

The RMS-DS represents the distribution of the transmitted power over the various paths in a multipath environment, and can be defined as the square root of the second central moment of a power delay profile. For a CIR  $h(t)$ , the power delay profile can be calculated with

$$P(t) = \frac{|h(t)|^2}{\int_{-\infty}^{\infty} |h(t)|^2 dt}. \quad (3.4)$$

The resulting RMS-DS is given by

$$\sigma_\tau = \int (\sigma - \sigma_e - \sigma_A)^2 P(\sigma) d\sigma, \quad (3.5)$$

where  $\sigma_A$  corresponds to the time delay of the first transmitted signal at the receiver and  $\sigma_e$  is the mean excess delay given by

$$\sigma_e = \int (\sigma - \sigma_A) P(\sigma) d\sigma. \quad (3.6)$$

Such channel feature indicates how dispersive the communication channel is. This information is usually used to support the specification of the guard interval duration, in a multi-carrier modulation (i.e., HS-OFDM and OFDM) in order to avoid inter symbol interference (ISI).

### 3.2.4 Relation between RMS-DS and ACG

According to [76], the relation between the RMS-DS and the ACG can be approximated by

$$\sigma_\tau (\mu s) = \alpha \cdot \overline{G}_{dB} + \beta. \quad (3.7)$$

This negative correlation indicates that PLC channels with high values of RMS-DS exhibits high attenuations (or low channel gain).

### 3.2.5 Relation between CB and RMS-DS

The relation between the CB and the RMS-DS is generally expressed (in units of microseconds) by

$$\sigma_\tau \approx \frac{\gamma}{B_{09}}, \quad (3.8)$$

where  $\gamma$  depends on the channel type and  $B_{09}$  (in kHz) is the CB at a correlation level equal to 0.9.

### 3.2.6 Coherence time (CT)

The CT, denoted by  $T_c^\beta$ , is the time duration in which the CIR can be considered time invariant. The CT can be evaluated as [36]

$$T_c^\beta = M_c(2N + L_{cp})T_s, \quad (3.9)$$

where  $M_c$  is the number of channel measurements needed to reach a correlation equal to  $\beta$ ,  $T_s$  denotes the sampling period,  $N$  is the number of subcarrier in a HS-OFDM symbol and  $L_{cp}$  is the length of the CP.

This channel feature is crucial, for instance, to indicate the periodicity in which the channel state information must be estimated in order to perform an effective equalization as well a resource allocation.

### 3.2.7 PSD of the additive noise

The PSD of the additive noise is obtained by using a well-known Welch procedure [37] which is briefly described as follows: Let the vector  $\mathbf{v} = [v(0) \ v(1) \ \dots \ v(L_v - 1)]^T$  be constituted by the samples of the measured additive noise in a PLC channel. We can extract  $K_s$  segments defined as  $\{v_K[n]\} = \{v[n + KD]\}$ , with  $n = 0, 1, \dots, L_{v,s} - 1$ ;  $K = 0, 1, \dots, K_s - 1$ ; composed of overlapping samples, when  $D < L_s$ .

Then, the PSD of the additive noise can be estimated through

$$S[k] = \frac{1}{K_s} \sum_{K=0}^{K_s-1} P_K[k], \quad k = 0, 1, \dots, L_s - 1, \quad (3.10)$$

where

$$P_K[k] = \frac{L_s}{U} |V_K[k]|^2, \quad (3.11)$$

in which  $U$  is a normalization factor given by

$$U = \frac{1}{L_s} \sum_{n=0}^{L_s-1} |w[n]|^2, \quad (3.12)$$

$$V_K[k] = \frac{1}{L_s} \sum_{n=0}^{L_s-1} v_K[n] w[n] e^{-j2\pi kn/L_s}, \quad k = 0, 1, \dots, L_s - 1, \quad (3.13)$$

and  $\{w[n]\}_{n=0}^{L_s-1}$  is a window.

### 3.2.8 Channel capacity

Due to the fact that PLC channels are frequency selective and the additive noise is a colored Gaussian random process, their theoretical channel capacity can be evaluated as [84]

$$C = \max_{S_x(f)} \int_B \log_2 \left( 1 + \frac{S_x(f) |H(f)|^2}{S_N(f)} \right) df, \quad (3.14)$$

where  $B$  is the frequency bandwidth;  $S_x(f)$  and  $S_N(f)$  denotes the power spectral densities of the transmitted signal and the additive noise, respectively,  $H(f)$  is the frequency response of the PLC channel and  $\int_B S_x(f) df = P_x$ , where  $P_x$  is the transmission power. A discrete version of (3.14) was used to evaluate the channel capacity.

## 3.3 FIT EVALUATION

Statistical models of some key features constitute an important and valuable information to be taken into account for the development and evaluation of any communication system. Indeed, the Nakagami, Rician, Rayleigh and Weibull statistical distributions have

been widely applied to model the fading behavior of wireless channels [85, 86]. More recently, the Gamma [87] and Inverse Gaussian [88] distributions are been considered to model fading effects for frequencies above 60 GHz in free-space optical communications.

The suitability of the fitting between the dataset that represents each considered channel feature (ACA, RMS-DS, CB and CT) and the statistical distributions considered in this work, in which the corresponding probability density function (pdf) can be accessed in B, were evaluated in terms of the following metrics.

### 3.3.1 Maximum Likelihood Estimation

Let  $X_1, X_2, \dots, X_n$  be a random sample of pdf  $f(x|\boldsymbol{\theta})$ , where  $\boldsymbol{\theta} = [\theta_1, \dots, \theta_K]^T$  represents the set of  $k$  unknown parameters. Thus, the likelihood function can be defined as [89]

$$L(\boldsymbol{\theta}) = \prod_{i=1}^n f(x_i|\theta_1, \dots, \theta_K), \quad (3.15)$$

which is commonly replaced by its logarithmic version, referred to as the log-likelihood function, given by

$$l(\boldsymbol{\theta}) = \sum_{i=1}^n \log(f(x_i|\theta_1, \dots, \theta_K)). \quad (3.16)$$

The maximum likelihood estimate (MLE), represented by the vector  $\hat{\boldsymbol{\theta}}$ , is obtained through

$$\hat{\boldsymbol{\theta}} = \arg \max_{\boldsymbol{\theta}} l(\boldsymbol{\theta}). \quad (3.17)$$

Such maximization problem is easily performed for some distributions with explicit solutions, as the Normal distribution. Other statistical distributions, however, such as the Skew-normal and the Gamma distributions, for instance, do not allow an analytical solution for this problem which is then solved by a numerical procedure [90].

### 3.3.2 Information criteria

The Akaike information criterion (AIC), the Bayesian information criterion (BIC) and the efficient determination criterion (EDC) [91] were also applied to verify the suitability of the fit between the datasets and each considered statistical distribution. The three aforementioned information criteria can be calculated by [91]

$$-2l(\hat{\boldsymbol{\theta}}) + Kc_n, \quad (3.18)$$

where  $K$  is the number of model parameters and  $c_n$  is the penalty term, which varies according to Tab. 5, where  $n$  is the dataset length. As can be noted in (3.18), there is an introduction of the term ( $Kc_n$ ) to the log-likelihood value in order to penalize the number

of distribution parameters, allowing a fair comparison between the fit given by statistical distributions with different number of parameters, which in our case assume the values  $K = 1, 2, 3$ . Contrary to the log-likelihood function, a lower value for the information criterion (see (3.18)) indicates a better fitting between the dataset and the considered distribution.

Table 5: Penalty term  $c_n$  of different information-based model evaluation criteria: AIC, BIC and EDC.

Criterion	$c_n$
AIC	2
BIC	$\log(n)$
EDC	$0.2\sqrt{n}$

### 3.4 NUMERICAL ANALYSIS

In this work, the in-home PLC channel estimation and characterization were performed by addressing the three distinct frequency bands:

- Band A, from 1.7 up to 30 MHz.
- Band B, from 1.7 up to 50 MHz.
- Band C, from 1.7 up to 100 MHz.

The measured in-home PLC channels were analyzed in terms of the features defined in Sec. 3.2. Also, an exploratory analysis was performed in the datasets associated with ACA, RMS-DS, CB and CT features for measured in-home PLC channels. In this case, a statistical modeling for the ACA, RMS-DS, CB and CT features was performed considering several symmetric and asymmetric continuous statistical distributions, chosen according to the general behavior observed in each dataset. In fact, the dataset for the CB and the CT show values with a limited resolution due to the estimation procedure, but these features are originally continuous random variables. Therefore, the considered symmetric distributions are the Logistic, the Normal and the t-Student, while the asymmetric ones are the Exponential, Gamma, Inverse Gaussian, Log-logistic, Log-normal, Nakagami, Rayleigh, Rician, Skew-normal and Weibull. All the results and corresponding analysis are presented as follows.

#### 3.4.1 Channel Magnitude Function

By considering the Band C, which comprises Band A and Band B as well, some interesting features of the in-home PLC channel magnitude response are depicted in Fig. 22. The parameters are the maximum, the minimum, the mean and the 50<sup>th</sup> and 90<sup>th</sup>

percentiles. The percentile reflects a value below which a given percentage of observations fall. As we can observe, the channel magnitude function slightly decreases as the frequency increases, which configures a well-know behavior of PLC channels. Also, the minimum attenuation is lower than 10 dB for the frequencies below 50 MHz and between 10 and 18 dB in the remaining frequencies. On the other hand, attenuations as high as 100 dB can be observed in some channel responses. The mean values of magnitude attenuation per frequency component is in between 20 and 40 dB, and such values are very close to the 50<sup>th</sup> percentile profile.

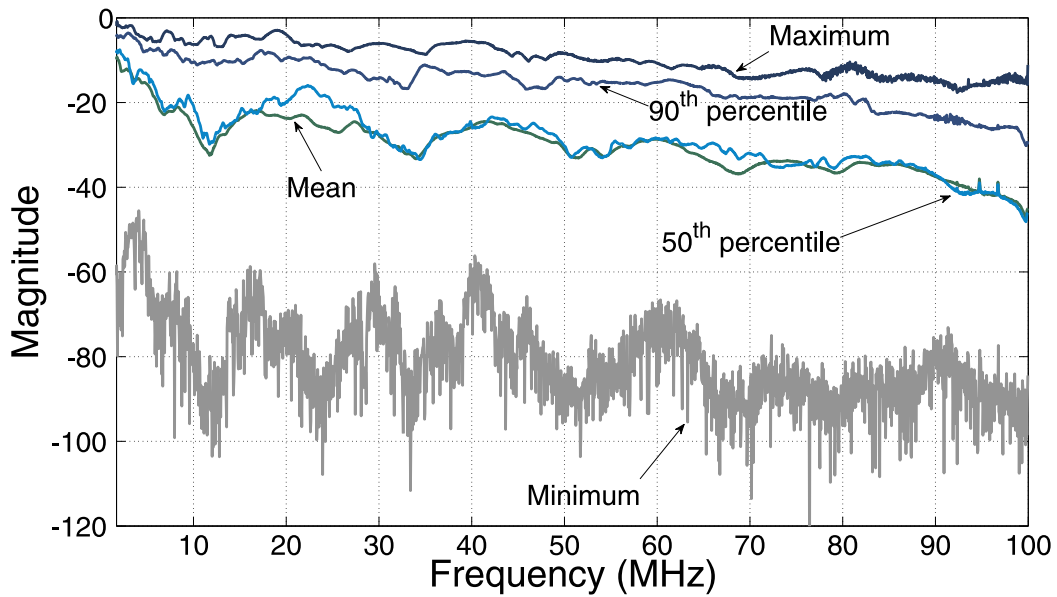


Figure 22: General characterization of the measured in-home PLC channel magnitude response.

The empirical cumulative distribution function (CDF) of the magnitude responses for Band A, Band B and Band C are shown separately in Fig. 23. As we can note, the distance of the curves for Band B and Band C are, approximately, 6 dB, for the probabilities values between 0.2 and 0.8. In the same interval of probabilities, the distances between the curves for Band A and Band B reach almost 15 dB. Also, higher attenuations are found in Band C than in Band A and Band B, what agrees with the theory of signal propagation through a non-ideal conductor. For instance, the probabilities that the attenuation is lower than 20 dB is 0.5, 0.7 and 0.9, approximately, for Band A, Band B and Band C, respectively. Additionally, this plot confirms that the in-home PLC channels are frequency selective.

Figure 24 shows the maximum, mean e minimum value of the magnitude response for 645 consecutive CFR estimates related with one measured PLC channel. As can be seen, in this case, the magnitude response can vary, for some frequencies, up to almost 45 dB.

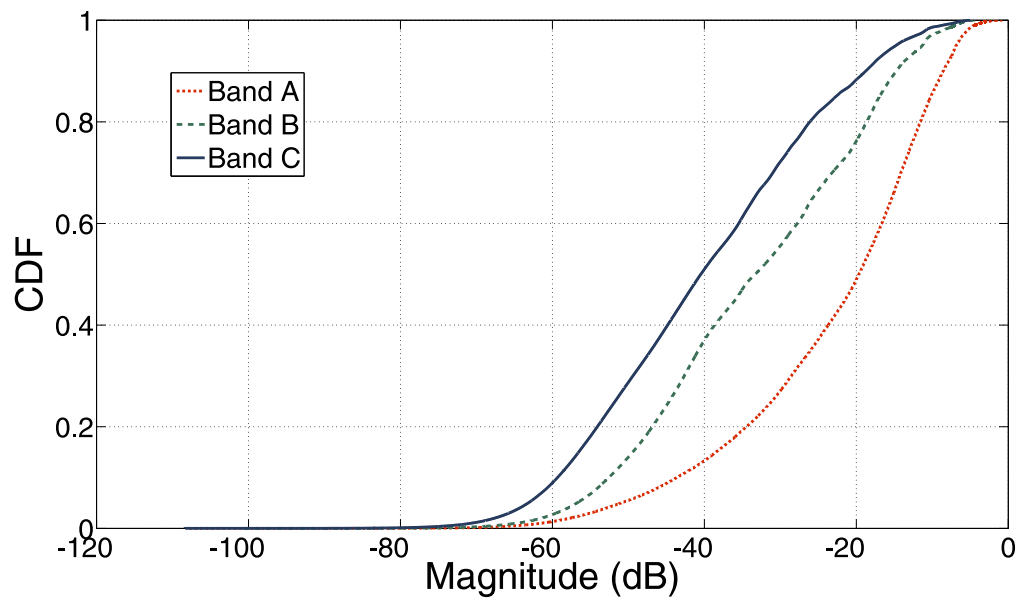


Figure 23: Cumulative distribution function of the estimated in-home PLC channel magnitude responses.

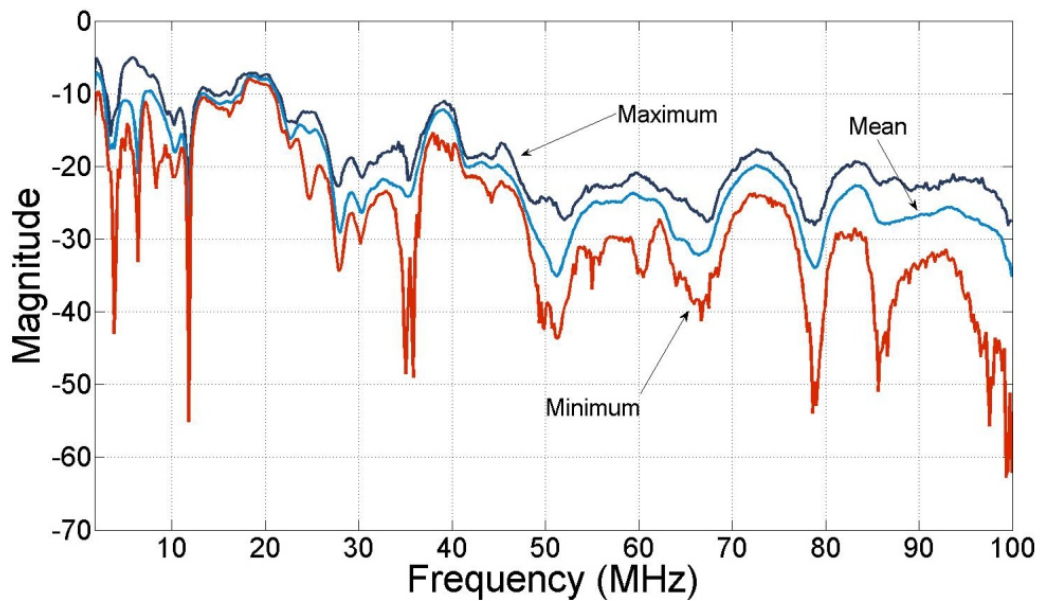


Figure 24: Magnitude response statistics of one measured PLC channel.

### 3.4.2 Average channel attenuation (ACA)

The ACA results are summarized in Tab. 6. Considering the Band A, the obtained results can be compared to those ones presented in [81] for in-home PLC systems in US. While the maximum, mean and minimum ACA values reported for US residences were around 68, 48.9 and 19 dB, respectively, for the Brazilian case they were around 51, 23.3 and 9 dB, indicating much lower attenuation levels in the Brazilian residences. From the author's point of view, the main reasons for that distinct behavior are as follows:

- The sizes of typical apartments and residences in Brazil are smaller than in US (see Tab. II in [92]) and, as a result, the distances for data communication as well as the number of branches tend to be lower in the Brazilian scenarios;
- The US gross domestic product (GDP) is almost five times the Brazilian one. That indicates a more intensive use of electrical and electronic equipments, leading to higher levels of unwanted electromagnetic radiation and induction, impedance mismatching and increasing attenuations due to multipath signal propagation.

From the results presented in [80], for in-home PLC channels measured in Spain, the maximum magnitude values are similar to those ones measured in US [81], whereas the minimum values are close to the Brazilian values, corroborating with what was aforementioned. In average, the Spanish ACA values are approximately 9 dB lower than the US ones but almost 20 dB higher than what was measured in Brazil, what reflects the fact that Spain has a GDP value in between that ones from Brazil and US.

The results for Band B revealed that the mean ACA value expected in in-home Brazilian PLC channels is around 25 dB. Also, this value can reach a maximum of more than 52 dB. In the best scenario, the ACA value was less than 10 dB. Results for ACA in this frequency band in other countries are not found in the literature and the same occurs to all analyzed PLC channel features.

Considering the Band C, a minimum ACA of 13 dB and a maximum of 55 dB were observed. The mean ACA value for Band C is almost 8 dB and 5 dB higher than that one for Band A and Band B, respectively. In Italy, the minimum ACA value is lower than in Brazil (7.6 dB) but the ACA can reach higher values of up to 57 dB. The mean ACA value observed in Italy of 35 dB, approximately, is almost 5 dB higher than in the Brazilian case.

#### 3.4.2.1 *Statistical modeling*

The parameters of the statistical distribution that provides the best fit and the fit to the Normal distribution for the ACA are summarized in Tab. 15, 16 and 17, in Appendix C, for Band A, Band B and Band C, respectively. As we can observe, the Skew-normal is

Table 6: PLC channel average channel attenuation for Band A, Band B and Band C.

Average channel attenuation (dB)			
	Band A	Band B	Band C
Maximum	51.089	52.623	55.269
Minimum	9.145	9.977	13.557
Mean	23.281	25.244	30.211
Standard Deviation	8.609	8.283	9.158
50-th percentile	22.767	25.673	30.822
90-th percentile	34.693	33.758	39.649

the statistical distribution that better fits the ACA of the measured Brazilian in-home PLC channels, when considering Band A. Regarding Band B and Band C, the best fits are offered by the Nakagami distribution.

Furthermore, the results of the fit to the Normal distribution are analyzed. As we can see in Tab. 15, the values of the Log-likelihood function and of the AIC, BIC and EDC evaluation criteria are too close if a comparison between the Skew-normal and the Normal distributions, for the Band A (let for instance the EDC value of  $4.6768 \times 10^4$  and  $4.7244 \times 10^4$  for the Skew-normal and Normal distributions, respectively) is carried out. This result is confirmed by Fig. 25 where it can be seen that the Normal distribution also offers a good approximation to the histogram that represents the dataset of the ACA feature. For the same frequency band, the ACA in in-home PLC channels in US are considered normally distributed, as detailed in [46], through the application of some normality tests. These tests were performed in in-home PLC channels in Spain [56] and the null hypothesis in which the ACA is considered normally distributed was rejected. In this contribution, the Jarque-Bera, Lilliefors, and Kolmogorov- Smirnov tests [93], performed at a 5% and 1% of correlation level, were applied and the normality assumption with respect to the ACA feature was strongly rejected. This result is contrary of what can be inferred by inspecting Fig. 25 and Tab. 15, from which it seems that the Normal distribution provides a good fit to the dataset. Thus, these contradictory results lead us to the conclusion that such normality tests, widely used in the PLC field, are not suitable for providing a reliable statistical inference when dealing with large sample size [94, 95]. Similar conclusions concerning the suitability of the Normal distribution to fit the ACA can be appointed for Band B and Band C, as we can see in Fig. 26 and Fig. 27, respectively.

Regarding Band C, for comparison purposes, in [32] the best normal distribution fit for the ACA related to in-home PLC channels in Italy resulting in mean and standard deviation,  $(\mu, \sigma)$ , equal to  $(35.412, 10.521)$  dB, against  $(30.211, 9.158)$  dB for Brazilian scenario. These results reinforce the fact that in-home PLC channels in Italy suffer, on average, additional attenuation, in order of 5 dB, in comparison to their Brazilian

counterparts.

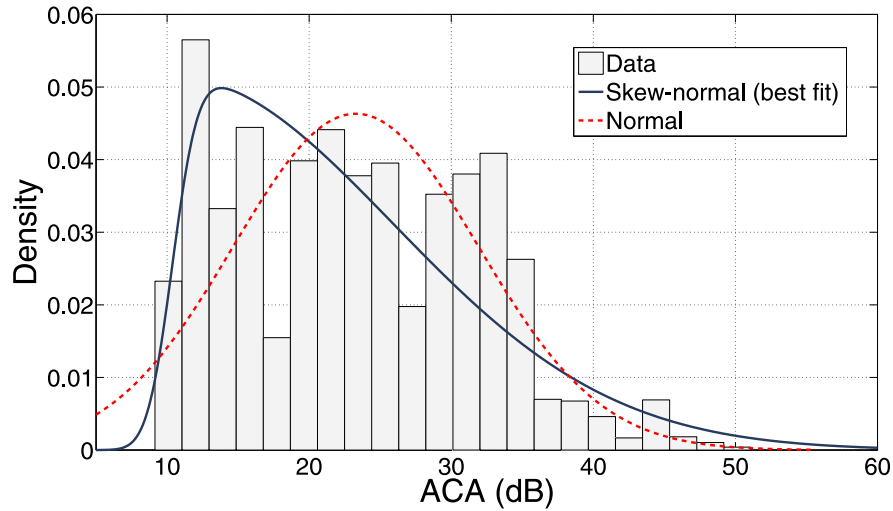


Figure 25: The histogram and distribution fitting of ACA feature for Band A.

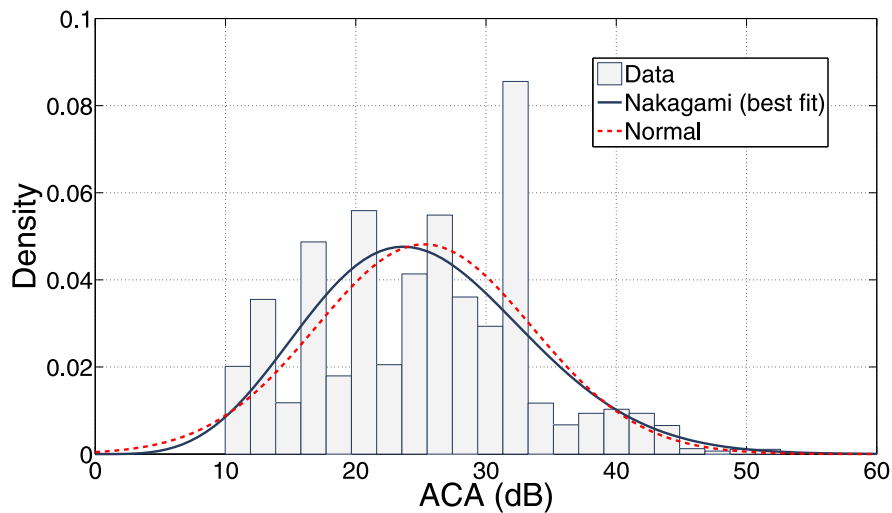


Figure 26: The histogram and distribution fitting of ACA feature for Band B.

### 3.4.3 Coherence bandwidth (CB)

The obtained results for the CB are summarized in Tab. 7, where  $B_{0.5}$ ,  $B_{0.7}$  and  $B_{0.9}$  refer to the correlation levels equal to 0.5, 0.7 and 0.9, respectively. Obtained results reveal that differences between the CB minimum, maximum and mean values for the Band A, Band B and Band C reduce if the correlation level increases. In fact, if we focus on  $B_{0.9}$ , the CB are very similar to all chosen frequency bands, meaning that the frequency selectivity is independent of the frequency bandwidth.

Regarding Band A, the mean value of 4.19 MHz for  $B_{0.5}$  can be noted. This mean value decreases to 3.77 MHz and 644.29 kHz for  $B_{0.7}$  and  $B_{0.9}$ , respectively. Comparing the  $B_{0.9}$  value with its Spanish [79] (for Band A) and French [72] (for Band C) counterparts,

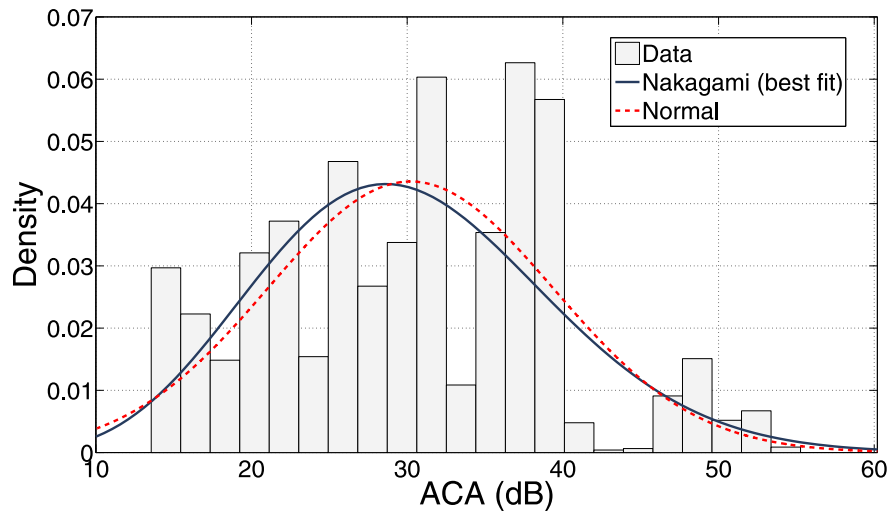


Figure 27: The histogram and distribution fitting of ACA feature for Band C.

we notice a wider CB for Brazilian in-home PLC channels. Thus, Brazilian in-home PLC channels are flatter than in these countries. In fact, the maximum CB value observed in Brazil is approximately 2.5 and 1.6 times its Spanish and French counterparts, respectively. In addition, while in 50% of Brazilian in-home PLC channels the CB is above 537 kHz, only about 10% of the Spanish in-home PLC channels present a CB above this value (see Fig. 4b in [79]).

For Band B, the mean value for the  $B_{09}$  is lower than those observed for Band A and higher than to se observed for Band C. Also, while in 90% of the observed cases the  $B_{09}$  is below 1.61 MHz and 1.12 MHz for Band C and Band A, respectively, this value is below 1.22 MHz for Band B.

Table 7: Coherence bandwidth estimated for the measured PLC channels.

		Coherence bandwidth (kHz)						
		Maximum	Minimum	Mean	Standard deviation	50% below	90% below	
Band A	$B_{05}$	$28.27 \times 10^3$	341.79	$4.19 \times 10^3$	$4.88 \times 10^3$	$2.78 \times 10^3$	$7.18 \times 10^3$	
	$B_{07}$	$7.47 \times 10^3$	195.31	$1.77 \times 10^3$	$1.21 \times 10^3$	$1.37 \times 10^3$	$3.27 \times 10^3$	
	$B_{09}$	$2.78 \times 10^3$	97.66	644.29	387.70	537.11	$1.12 \times 10^3$	
Band B	$B_{05}$	$48.29 \times 10^3$	390.62	$3.99 \times 10^3$	$4.02 \times 10^3$	$2.73 \times 10^3$	$7.18 \times 10^3$	
	$B_{07}$	$10.64 \times 10^3$	244.14	$1.90 \times 10^3$	$1.42 \times 10^3$	$1.42 \times 10^3$	$3.71 \times 10^3$	
	$B_{09}$	$3.71 \times 10^3$	146.48	720.55	488.65	585.94	$1.22 \times 10^3$	
Band C	$B_{05}$	$95.22 \times 10^3$	439.45	$7.99 \times 10^3$	$15.21 \times 10^3$	$2.93 \times 10^3$	$12.94 \times 10^3$	
	$B_{07}$	$38.04 \times 10^3$	97.66	$2.67 \times 10^3$	$4.49 \times 10^3$	$1.66 \times 10^3$	$3.61 \times 10^3$	
	$B_{09}$	$3.08 \times 10^3$	97.66	780.27	528.63	585.94	$1.61 \times 10^3$	

### 3.4.3.1 Statistical modeling

The statistical modeling of the CB, considering the correlation level of 90%, for the best knowledge of the author, is analyzed at the first time. The results revealed that the CB is better fitted by the Inverse Gaussian for Band A, Band B and Band C, as depicted in Figs. 28, 29 and 30, respectively. For comparison purposes the fit for the Log-normal distribution is performed and it is also depicted in the aforementioned graphics, since the histograms suggest that the dataset of the CB presents positive asymmetry. It is important to state that the fit to the Log-normal distribution achieved very close performance in terms of log-likelihood and all evaluated criteria if compared to those results provided by the best fitted distributions. The parameters of the best fitted statistical distribution (Inverse Gaussian) and for the Log-normal distribution, together with the information criteria results, are summarized in Tabs. 21, 22 and 23, in Appendix C.

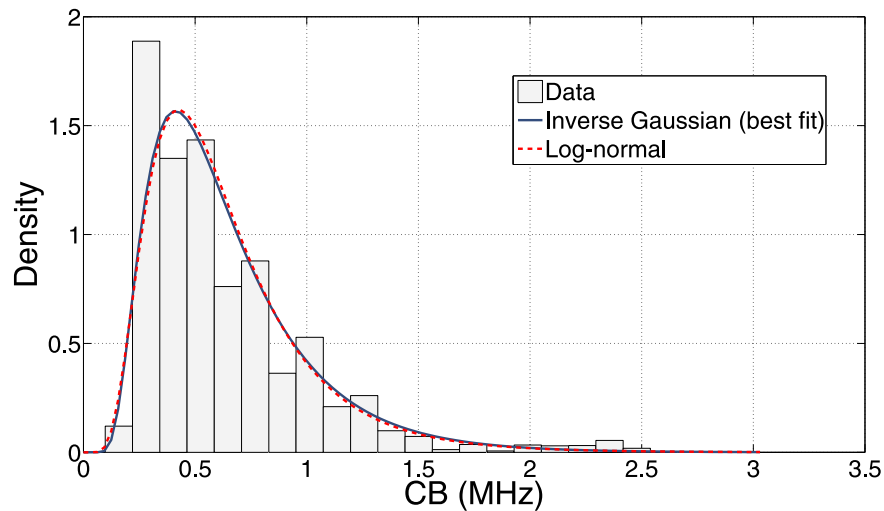


Figure 28: The histogram and distribution fitting of CB feature for Band A.

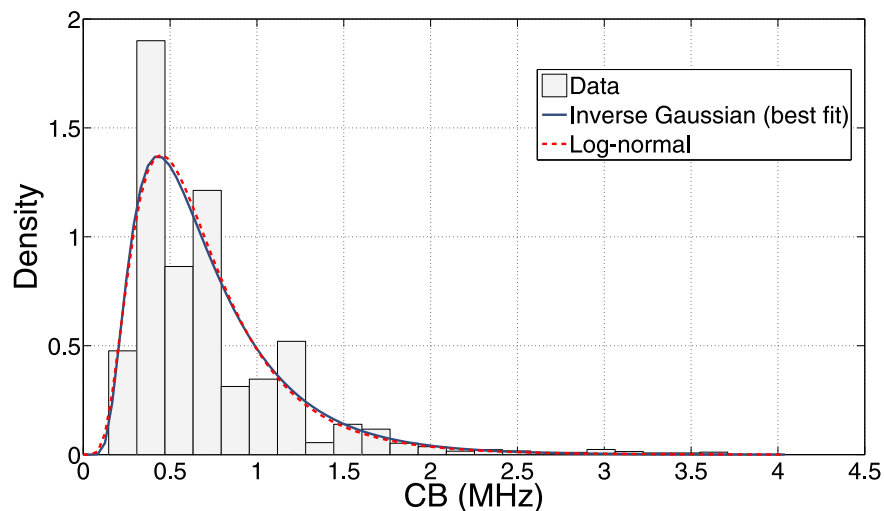


Figure 29: The histogram and distribution fitting of CB feature for Band B.

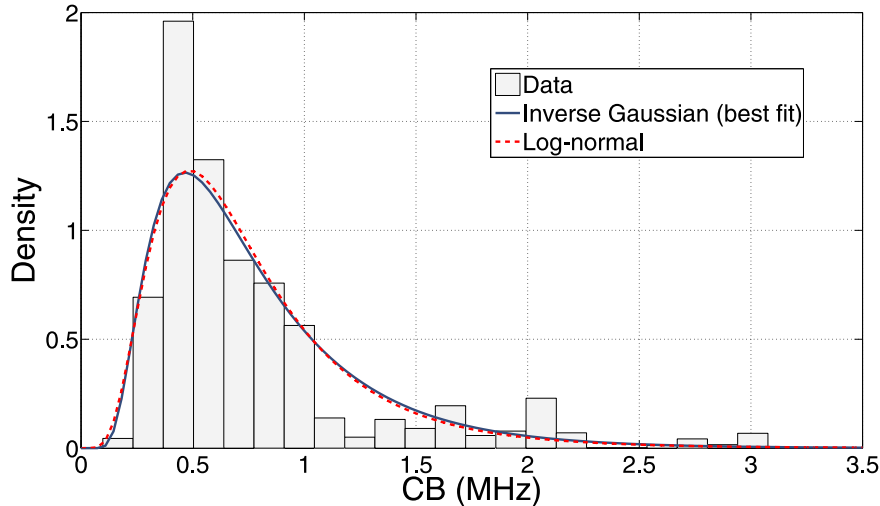


Figure 30: The histogram and distribution fitting of CB feature for Band C.

#### 3.4.4 Root mean squared delay spread (RMS-DS)

The obtained results for RMS-DS are summarized in Tab. 8. Regarding Band A, Brazilian in-home PLC channels show the smallest RMS-DS values ( $0.15 \mu s$ ) in comparison to their US counterpart ( $0.53 \mu s$ ) [81]. Also, the RMS-DS is above  $0.47 \mu s$  in 50% of in-home PLC channels in US, against  $0.14 \mu s$  for the same percentage in Brazil. For Band B the mean value observed for the RMS-DS was of  $0.138 \mu s$  and for 90% of the observed cases this value was below  $0.214 \mu s$ . Now considering Band C, a comparison with the results presented in [72] (French scenario) shows that Brazilian in-home PLC channels present the smallest values for RMS-DS. While in France, the RMS-DS has mean value equal to  $0.309 \mu s$  and can reach  $0.601 \mu s$  in 90% of the cases, these values are  $0.133 \mu s$  and  $0.204 \mu s$ , respectively, in Brazil. From the author's point of view, the reasons for that are those appointed before for the ACG.

Table 8: RMS-DS for the measured in-home PLC channels in Band A, Band B and Band C.

RMS-DS ( $\mu s$ )			
	Band A	Band B	Band C
Maximum	0.493	0.471	0.465
Minimum	0.039	0.031	0.029
Mean	0.148	0.138	0.133
Std	0.064	0.064	0.064
50-th percentile	0.140	0.134	0.127
90-th percentile	0.227	0.214	0.204

##### 3.4.4.1 Statistical modeling

With respect to the statistical modeling of the RMS-DS feature, the histograms depicted in Figs. 31, 32 and 33 show a clear positive asymmetry. In fact, the analysis

of the RMS-DS for Brazilian in-home PLC channels revealed that this feature is better modeled by a Gamma distribution, for all considered frequency bands. This result is different from those reported in [96, 77], for US in-home PLC channels, and in [80] for PLC channels in Spain, regarding the frequency Band A, and the one presented in [32], for in-home PLC channels in Italy for frequency Band C, in which the RMS-DS was considered log-normally distributed. On the other hand, the results achieved by fitting the RMS-DS of Brazilian in-home PLC channels with the Log-normal distribution are not so distant to those obtained for the Gamma distribution, as we can see in Tabs. 18, 19 and 20, in Appendix C. For instance, regarding Band A, a relative difference of 0.02 (very low) is observed between the EDC value for the Gamma and Log-normal distributions. The suitability of the Log-normal distribution to fit the RMS-DS can be visually verified in Fig. 31. The same behavior is observed for both Band B and Band C, as depicted in Fig. 32 and Fig. 33, respectively.

As reported for ACA, results of lognormality tests performed to the RMS-DS datasets from Brazilian in-home PLC channels were contrary to the aforementioned discussion. Indeed, lognormality assumption of the RMS-DS can be accepted and, thus, somehow the results agree with what were reported in US [77], Spain [56] and Italy [32].

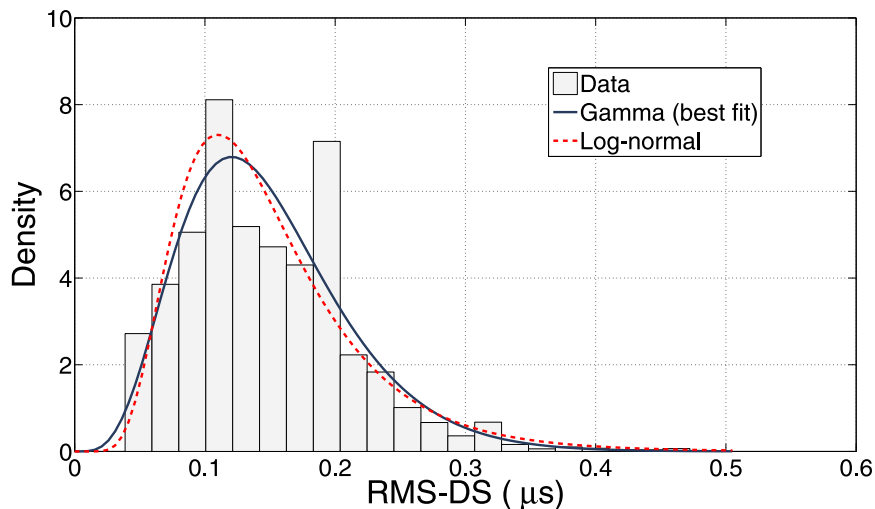


Figure 31: The histogram and distribution fitting of RMS-DS feature for Band A.

### 3.4.5 RMS-DS versus ACG

A linear relation between RMS-DS and ACG, which is usually expressed by (3.7), can be drawn as seen in Fig. 34. The parameters of (3.7) for the Brazilian in-home PLC channels are listed in Tab. 9. They are represented by the solid and straight lines in Fig. 34 for the three frequency bands considered in the current work. Surprisingly, the linear relationships between RMS-DS and ACG for Band A, Band B and Band C result into three almost parallel straight lines ( $\alpha$  values are almost the same). Also, the dispersion around

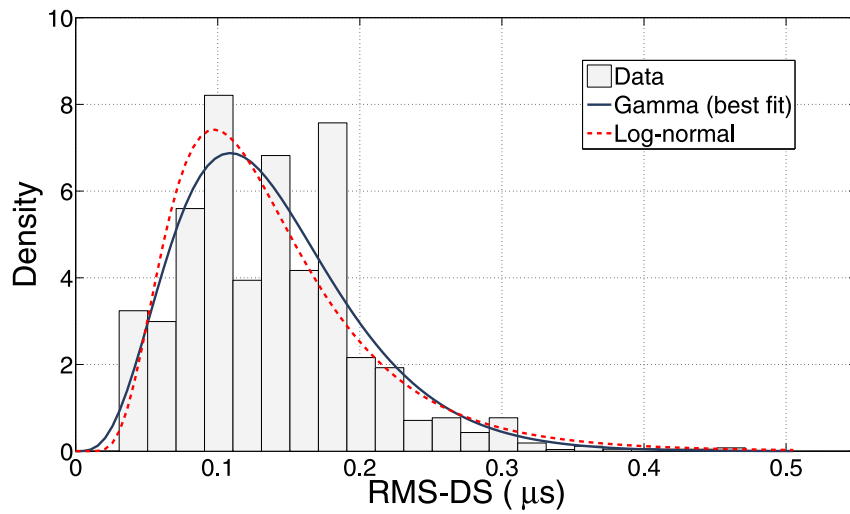


Figure 32: The histogram and distribution fitting of RMS-DS feature for Band B.

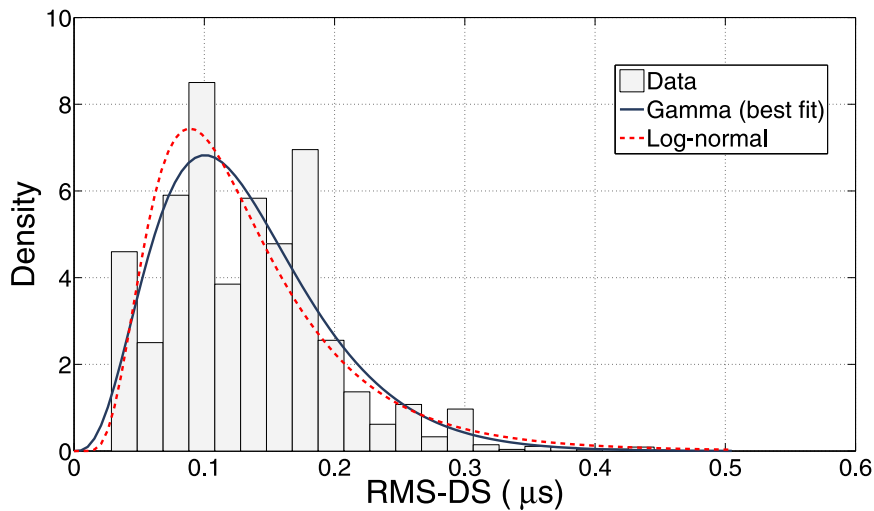


Figure 33: The histogram and distribution fitting of RMS-DS feature for Band C.

the trend line for the lowest values of ACG is more accentuated for the values less than, approximately,  $-40$  dB. Regarding Band A, a comparison among in-home PLC channels in US [76] and in Brazil shows that Brazilian counterparts present similar behavior to those channels from urban and suburban areas in US.

Table 9: Parameters of (3.7) estimated for the measured PLC channels.

	$\alpha$ ( $\mu s/dB$ )	$\beta$ ( $\mu s$ )
Band A	$-0.0054$	$0.0219$
Band B	$-0.0058$	$-0.0079$
Band C	$-0.0056$	$-0.0379$

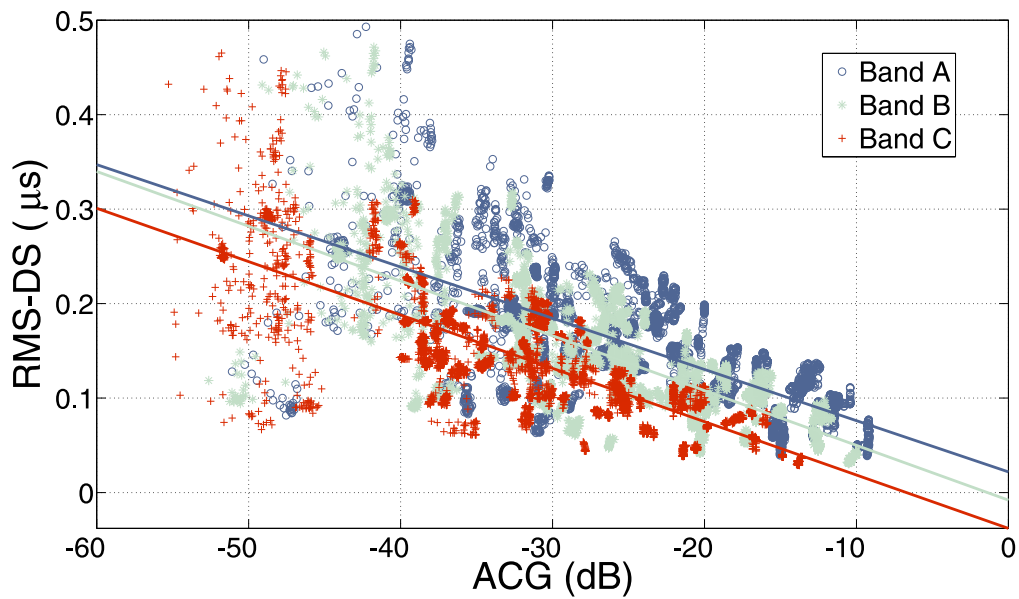


Figure 34: RMS-DS versus ACG for the measured in-home PLC channels in Brazil.

### 3.4.6 CB versus RMS-DS

Figure 35 shows the inverse relation between RMS-DS and CB observed in Brazilian in-home PLC channels for all considered frequency bands. The best curve fitting for (3.8), which are represented by the dotted lines in the plot (only for the Band C), is based on the minimum mean square error (MMSE) criterium. The least-square curve fitting yielded  $\gamma = 77$ ,  $\gamma = 77$  and  $\gamma = 78$  for Band A, Band B and Band C, respectively. For comparison purposes,  $\gamma = 55$  was attained with French in-home PLC channels [72], while  $\gamma = 57$  is presented for the cases in Italy [32], both for Band C.

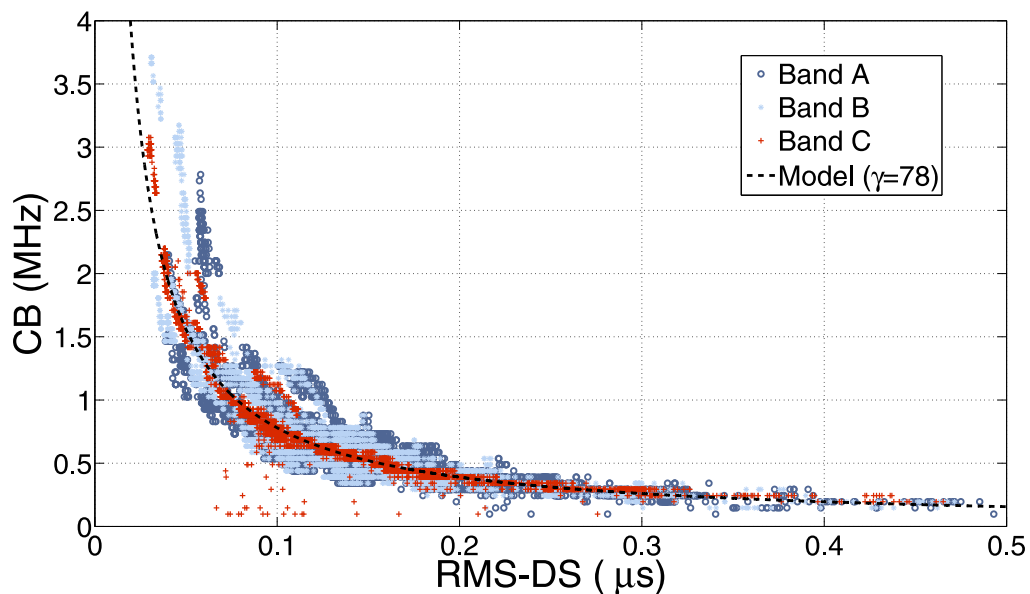


Figure 35: Relation between the coherence bandwidth and the RMS-DS for the in-home PLC channels in Brazil.

### 3.4.7 Coherence time (CT)

In order to calculate the coherence time from the CIR, the methodology described in [36] is applied with the parameters of the setup listed in Tab. 10. Figure 36 shows how the measured Brazilian in-home PLC channels vary with time. For the sake of simplicity, in this plot only Band C is considered. Each horizontal line in the graph reflects a set of consecutive estimates of Brazilian in-home PLC channels, and the colors are used to differentiate the correlation level (used to reveal the time-varying behavior) with respect to the first estimate.

Table 10: Values of the parameters that are adopted to calculate the coherence time [36].

Description	Variable	Value
Measured CIR energy % (truncated CIR)	$K_t$	0.9
Coefficients amplitude % (sparse CIR)	$K_s$	-40 dB
Selecting the most relevant factors	$K_c$	-20 dB

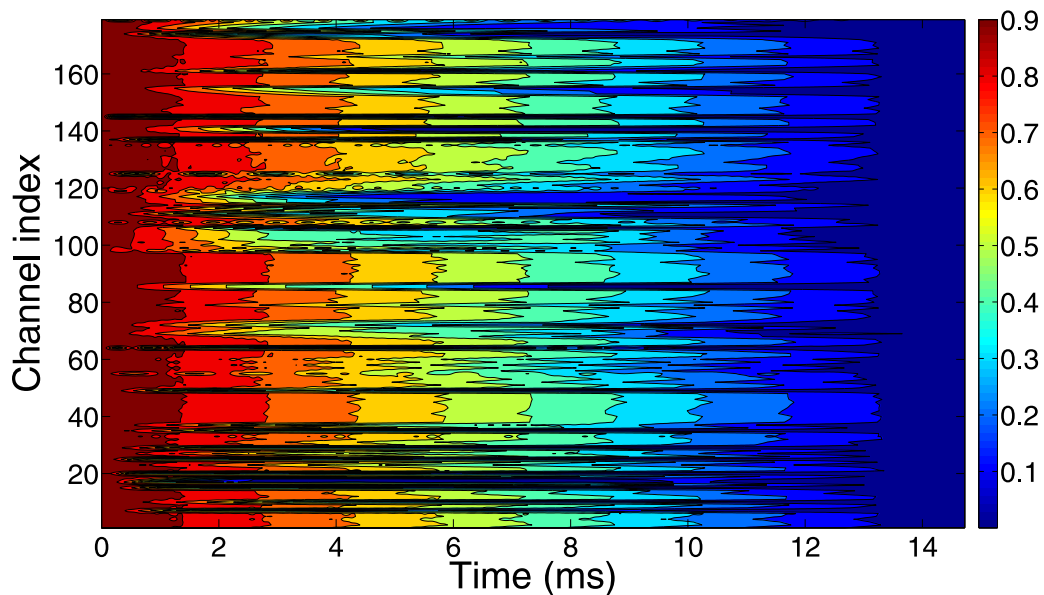


Figure 36: Coherence time of the measured in-home PLC channel.

The CDF of the CT for the three considered frequency bands are shown in Fig. 37, in which correlation levels of 0.85, 0.90, 0.95 and 0.99 are adopted. As we can note, the probability of a CT can be lower than a given value is almost the same for all analyzed frequency bands. These results suggest that the variability of the in-home PLC channel is more pronounced in the frequencies below 30 MHz. The CT surpasses 500  $\mu s$  for  $\beta = \{0.85, 0.90\}$  in 90% of the measured Brazilian in-home PLC channels. Also, the CT is independent of the frequency bandwidth.

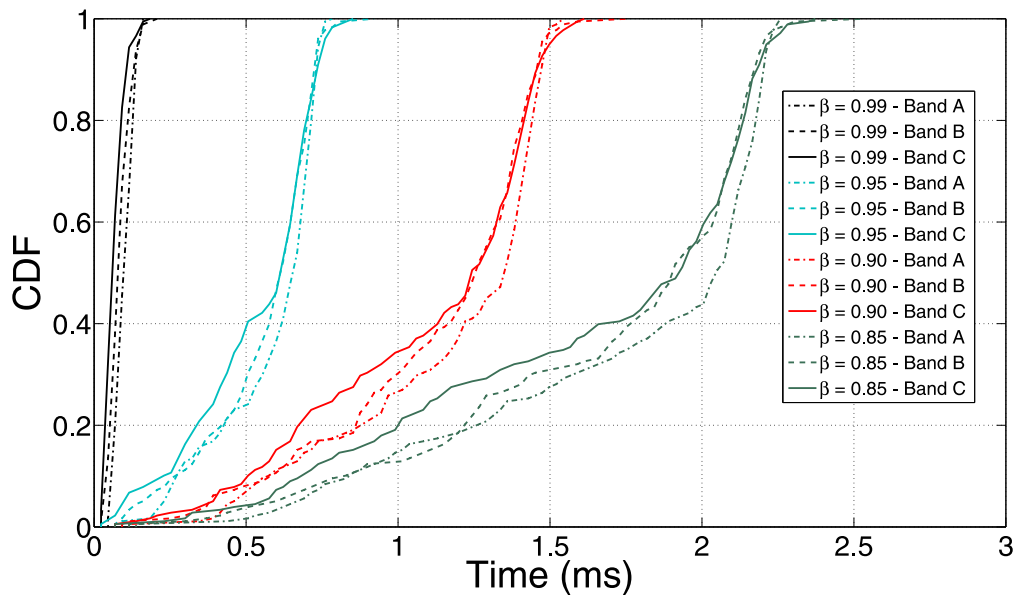


Figure 37: CDF of the coherence time for the three considered frequency bands.

#### 3.4.7.1 Statistical modeling

The dataset that represents the CT is constituted by less samples in comparison with the datasets for the ACA, RMS-DS and CB, due to the methodology applied to estimate this feature. In fact, the CT is derived from a set of consecutive CFR and only those combinations that rendered more than 640 consecutive CFR estimates were used. This means that the dataset for CT is composed of 178 estimates.

The histograms depicted in Figs. 38, 39 and 40 show some negative asymmetry of the dataset that represents the CT of the measured in-home PLC channels. This observation is reinforced by the fact that the Skew-normal is the best fitted statistical distribution, with a negative skewness (see the value of the parameter  $\gamma$  in Tabs. 24, 25 and 26, in Appendix C, for Band A, B and C, respectively). Also, the fit to the t-Student, the Weibull and the Normal distributions, for Band A, B and C, respectively, are presented for comparison purposes because they correspond to the second best statistical distribution model according to the value of the log-likelihood and the evaluated information criteria. The second statistical distribution that best fits the dataset presented a performance distant to those achieved by the first ones and because of that, they can not be chosen to model these in-home PLC channel feature at all.

#### 3.4.8 PSD of the additive noise

The measured additive noise is analyzed by means of PSD, and the results are shown in Fig. 41. As usually occurs in in-home PLC channels, the noise behaves as a sum of several kinds of disturbances. The higher peaks in the graphic are classified as narrowband noise components and summarize the broadcast signals, such as FM and

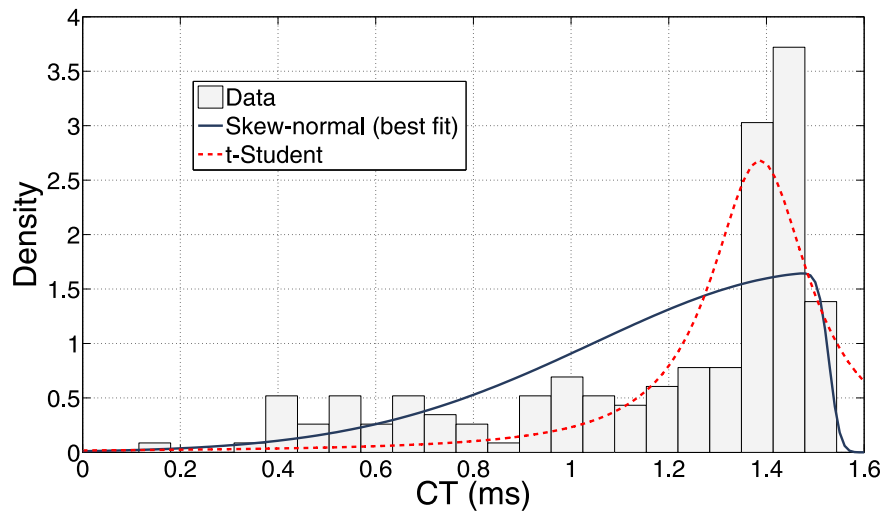


Figure 38: The histogram and distribution fitting of CT feature for Band A.

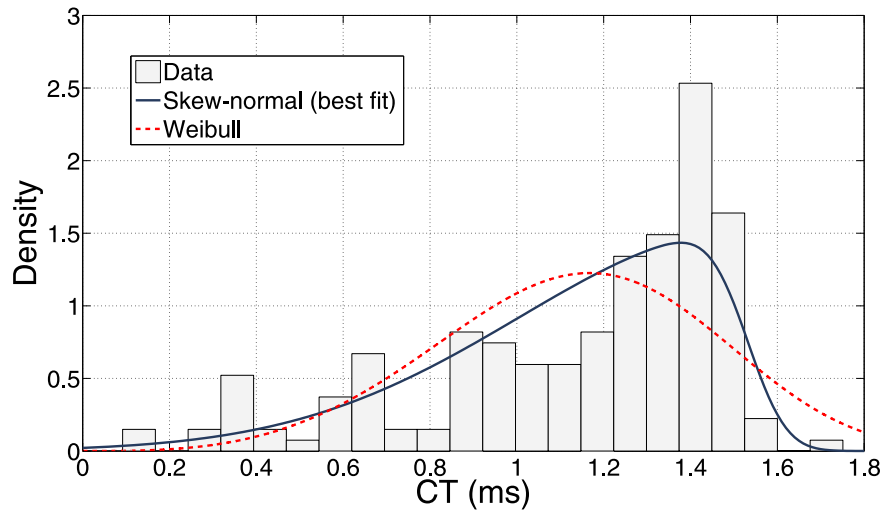


Figure 39: The histogram and distribution fitting of CT feature for Band B.

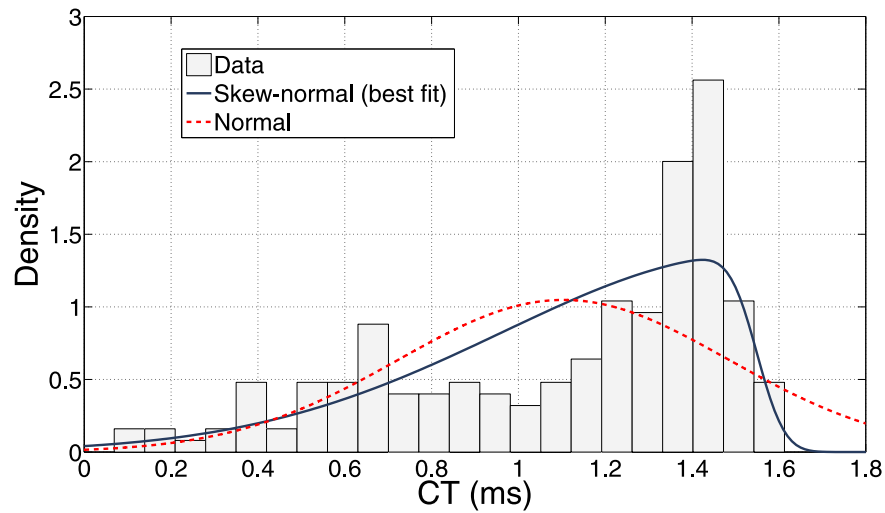


Figure 40: The histogram and distribution fitting of CT feature for Band C.

amateur radio, that are inducted in the in-home electric circuits. The decreasing PSD value with frequency is similar to what has been observed in previous works [97]. The analysis of several samples of measured additive noise shows that the PSD values range from  $-112$  dBm/Hz, approximately, up to almost  $-42$  dBm/Hz. The high PSD value is associated with the low-frequency components. The maximum-, mean- and minimum-value PSD curves reveal the presence of several primary users (each one associated to a narrowband signal).

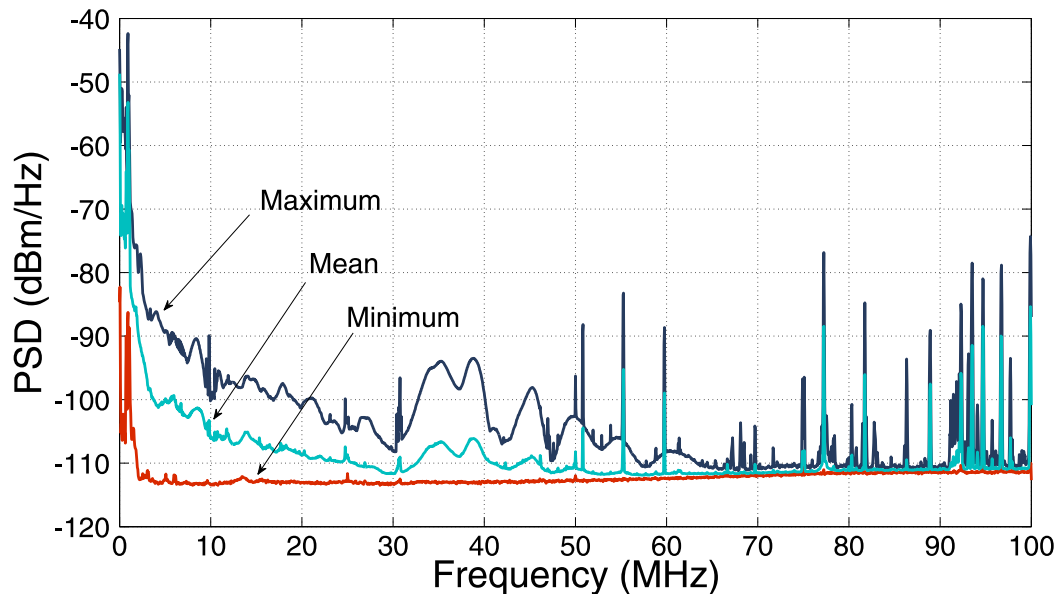


Figure 41: Estimated noise PSD in the measured in-home PLC channel.

### 3.4.9 Channel capacity

The maximum, mean and minimum channel capacities of the measured Brazilian in-home PLC channels are shown in Fig. 42. These curves were obtained by considering Band A, Band B and Band C, where the PSD for the transmitted signal ranges from  $-90$  up to  $-50$  dBm/Hz and estimated PSD of the noise. Based on these curves, the following observations can be drawn: (i) the mean channel capacities are closer to the maximum ones than to the minimum; (ii) considerable improvements in terms of channel capacity can be observed when comparing the results for the three analyzed frequency bands (e.g., the growth ratio between Band A and Band B is 1.5 and 1.8 for  $-80$  dBm/Hz and  $-50$  dBm/Hz, respectively and the similar results are achieved when Band B is compared with Band C).

The complementary CDF (CCDF) of the channel capacity when the measured additive noise and the modeled (as presented in [98]) one are shown in Fig. 43. To comply with the electric field emission regulation applied to PLC systems [99], the curves were obtained when the PSD of the transmitted signal is  $-55$  dBm/Hz in the frequency band that corresponds to Band A and  $-80$  dBm/Hz in the remaining frequencies up to 100 MHz.

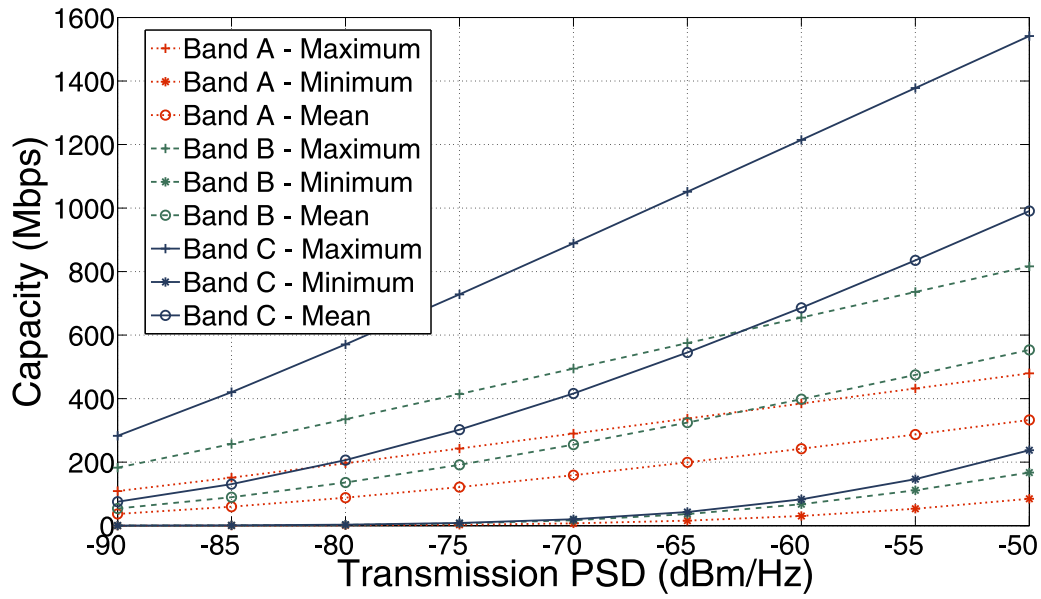


Figure 42: Channel capacity of the measured in-home PLC channels.

Comparing with the noise measurements, the model for the additive noise PSD seems to be very appropriate for the Band A and very optimistic for the Band B and Band C and should be avoided to represent the PSD of additive noise in Brazilian premises. Overall, the theoretical channel capacity of Brazilian in-home PLC channels achieved a maximum value higher than in Italy (see Fig. 11 and Tab. IX in [32]), for the same PSD model.

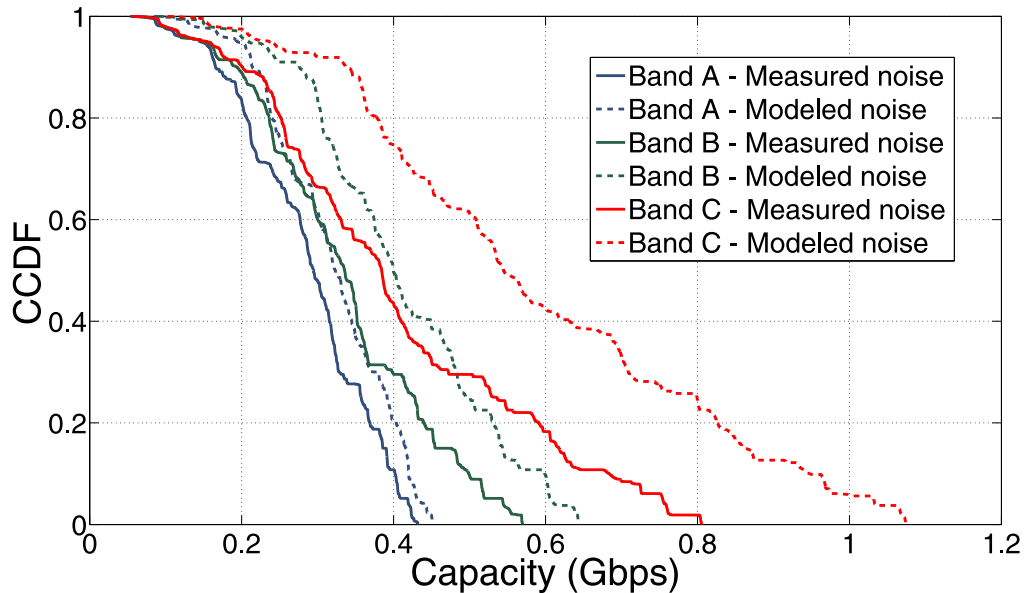


Figure 43: Complementary CDF of the channel capacity using the measured and colored noise.

### 3.5 SUMMARY

This chapter presented important results about the characterization of in-home PLC channels in developing countries. The next chapter will introduce a new communication media called hybrid PLC-wireless channel. Also, this communication channel will be characterized through measurements performed in in-home Brazilian scenarios.

#### 4 THE CHARACTERIZATION OF THE IN-HOME BRAZILIAN HYBRID PLC-WIRELESS CHANNELS

In a PLC system a physical connection is required between the PLC modem and the power cables by using, for instance, the power outlet. Therefore, mobility, which is the main attraction in wireless communications, is impractical in standard PLC systems and constitutes a major disadvantage of them. On the other hand, unshielded cabling infrastructure of electric power grids can radiate and be irradiated by wireless signals. This observation leads to a new paradigm that can potentially renew the R&D efforts in PLC technology for broadband application that exploits the interaction between the standard PLC and wireless technologies to provide mobility resulting in the so-called hybrid PLC-wireless technology. In this new scenario, some communication devices are physically connected to the power cables (PLC or wireline devices) while others (wireless devices) are not, with all of them operating in the same frequency bandwidth. Then, data communication between PLC and wireless devices is based on electromagnetic signals radiating from and induced into unshielded power cables. Based on this paradigm, a communication medium can be defined as hybrid PLC-wireless channel, consisting of unshield power cables belonging to the electric power grids and the air.

Regarding PLC and wireless systems, we point out that the exploitation of their combination has been recently addressed. These investigations assume that the signal transmission occur through the PLC and wireless channels in order to increase the system coverage or reliability by adopting some cooperative scheme. For instance, [24] presents results from the evaluation of some diversity combining schemes when a simultaneous communication over wireless and PLC is performed, with both data communication systems operating at their regulated frequency bandwidths. Other similar investigations can be found in [25, 26, 27] and references therein.

Different from the aforementioned works, this chapter addresses a communication media established between a device that makes use of the wireline to receive/transmit signals with a wireless device. A comprehensive characterization of the hybrid PLC-wireless channel for bi-directional data communication is timely and of utmost importance to quantify precisely the possibilities of such novel and challenging data-communication medium. Therefore, this chapter presents a statistical characterization of the hybrid PLC-wireless channel, based on a measurement campaign, carried out on several medium-size apartments and residences, in the frequency band from 1.7 MHz up to 100 MHz. Statistical analyzes of average channel gain (ACG), coherence bandwidth (CB), coherence time (CT), root mean squared delay spread (RMS-DS), and channel capacity highlight the limitations, restriction, and potential of this data communication medium. Furthermore, the symmetry of the hybrid PLC-wireless channel magnitude response is verified when the transmitter and the receiver have the same access impedance (i.e., 50  $\Omega$ ). Moreover, we reveal how the

wireless device distance to the unshielded power cable is related to the resulting channel capacity. In addition, differences between the noise power spectral densities from wireline (PLC) and from the wireless devices are reported. To the author's best knowledge, this is the first attempt to provide a complete and comprehensive characterization of hybrid PLC-wireless channels, for useful bidirectional communication.

The remainder of this chapter is organized as follows: the hybrid PLC-wireless channel and problem formulation are addressed in Sec. 4.1. Section 4.2 briefly describes the measurement setup and campaign that supported the characterization of the hybrid PLC-wireless channel. Results and analyses are summarized in Sec. 4.3.

#### 4.1 THE HYBRID PLC-WIRELESS CHANNEL: PROBLEM FORMULATION

The main idea behind the hybrid PLC-wireless channel lies in the fact that the infrastructure of electric power grids consists mainly by unshielded cables. As a result, the power cables radiate signals and, conversely, wireless signals are inductively injected into them. These signal interactions have been treated in the realms of unwanted interference from and into electric power grids, see [3, 4, 5, 6] and references therein. However, these usually unwanted interferences can be seen as useful signals that may potentially carry information that can be exchanged among wireline and wireless devices, leading to the hybrid PLC-wireless scenario illustrated in Fig. 44. In this framework, a PLC signal that is coupled into and propagated along the power cables is also radiated, and can be sensed by a nearby wireless device, which is connected to an antenna. On the other direction, a signal radiated in the air by the wireless-device antenna can, in part, be induced in unshield power cables and reach a PLC device. Thus, a useful full-duplex communication channel can be established between the PLC and wireless devices through the hybrid PLC-wireless channel, as depicted Fig. 44, where both wireline and wireless devices are operating in the same frequency band.

In fact, the hybrid PLC-wireless channel introduces mobility to the PLC systems that is the main disadvantage of them if compared with wireless-based ones. The following application motivates the investigation of this novel communication channel:

- safety monitoring/control/maintenance of smart grids, mainly those that involve high voltage levels. In fact, the connection in a purely PLC system can be dangerous and expensive. By using the hybrid principle, the electric utility can easily access information and interact with the electric power grids;
- in home networks (HN) the hybrid PLC-wireless system seems to be more convenient from the consumer point of view than purely PLC systems, since in the last one a physical connection to the power line is required;

- in vehicles, such as cars, ships and aircrafts, that make use of PLC systems, the hybrid PLS-wireless system can facilitate the interaction/maintenance of the devices, since the access to the power cables can be difficult and/or expensive;
- the reduction of digital divide problem in developing and underdeveloped countries owning a pervasive electric power system infrastructure;
- hybrid PLC-wireless systems, operating at frequencies of up to 100 MHz, may be healthier for living beings than the traditional wireless systems [100, 101, 102, 103] which operate at frequencies in the order of some GHz.

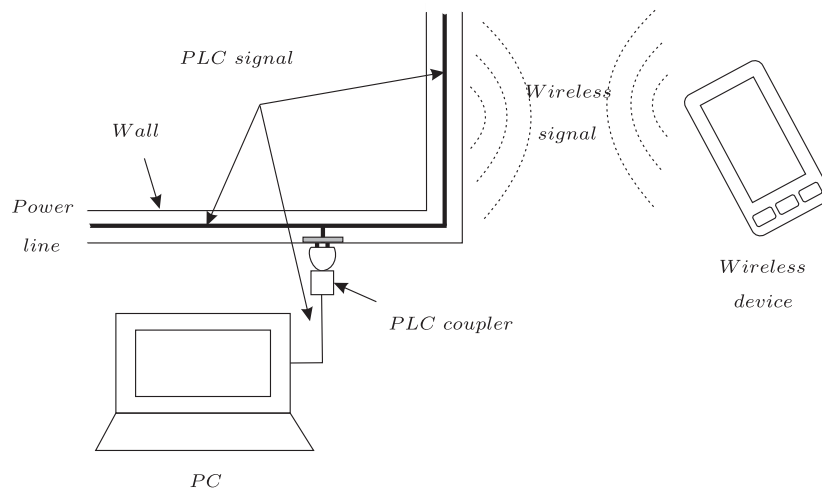


Figure 44: A hybrid PLC-wireless scenario.

A hybrid PLC-wireless communication system is composed of the following components (see Fig. 45):

- the hybrid-PLC transceiver, which is connected to the outlet and responsible for injecting/receiving signals into/from the electric power grid;
- the PLC coupler, which is a high-pass analog filter that promotes the interface between the PLC transceiver and the electric power grid, blocking the main frequency to prevent damage to the hybrid-PLC transceiver;
- the hybrid PLC-wireless channel, which constitutes the communication medium established between the hybrid-PLC and hybrid-wireless transceivers;
- the hybrid-wireless transceiver, namely the device that makes use of the wireless channel to provide data communication;
- antenna, which is the transducer of the hybrid-wireless transceiver that is designed to inject/receive signals into/from the wireless channel.

Now, assuming that the hybrid PLC-wireless channel is linear and time varying, then the channel output can be written as

$$y_{pw}(t) = \int_0^t x(\tau)h_{pw}(t, \tau)d\tau + w(t), \quad (4.1)$$

for the signal propagation from the PLC-to-wireless device and,

$$y_{wp}(t) = \int_0^t x(\tau)h_{wp}(t, \tau)d\tau + v(t), \quad (4.2)$$

for the reverse path from the wireless-to-PLC device. Note that  $h_{pw}(t, \tau)$  and  $h_{wp}(t, \tau)$  denote the two channel responses at time  $t$  when an impulse at instant  $\tau$  is applied to the PLC-to-wireless and wireless-to-PLC directions, respectively;  $x(\tau)$  is an input signal;  $w(t)$  and  $v(t)$  are, respectively, the additive noise components in the PLC-to-wireless and wireless-to-PLC channels.

By considering the hybrid PLC-wireless channel for data communication purposes, the following questions arise:

- Is the magnitude response of the hybrid PLC-wireless channel symmetric, i.e.  $|H_{pw}(f, \tau)| = |H_{wp}(f, \tau)|$ ?
- What kind of attenuation levels can be expected in such channels?
- How strong is the influence of the wireless-device localization in the hybrid-channel magnitude responses?
- What level of selectivity can be expected in the hybrid PLC-wireless channel frequency responses?
- How dispersive is the hybrid PLC-wireless channel?
- What kind of channel capacity can be expected in the hybrid communication channel?
- Are there differences in terms of channel capacities according to the signal propagation direction?
- How long can the hybrid PLC-wireless channels be considered time invariant, i.e.  $h_{wp}(t, \tau) = h_{wp}(t - \tau)$ ?
- Are there any significant differences between  $w(t)$  and  $v(t)$ ?

Based on measures of hybrid PLC-wireless channels, answers to all aforementioned questions are provided in the following sections.

## 4.2 MEASUREMENT SETUP AND CAMPAIGN

The block diagram of the measurement scheme is depicted in Fig. 45. The hybrid-PLC and hybrid-wireless transceivers are rugged computers equipped with a high-speed data acquisition board and a high-speed arbitrary signal generation board that operate as receiver and transmitter, respectively. The designed PLC coupler has a magnitude response almost flat in the passband range, with a maximum attenuation less than 3 dB (see Fig. 19) and the adopted omnidirectional and monopole antenna operate in the frequency band ranging from 1 MHz up to 1 GHz.

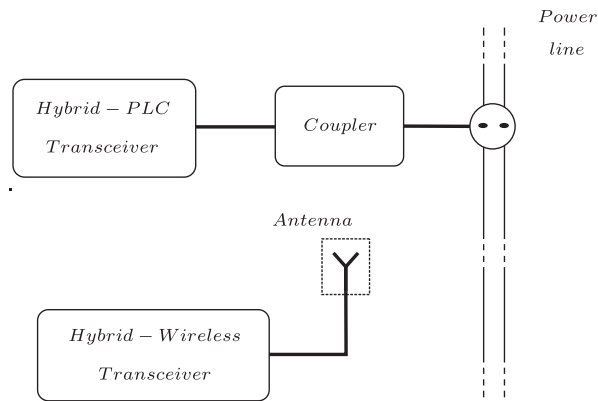


Figure 45: Block diagram of the measurement setup.

The measurement setup makes use of a sounding technique described in Chap. 2. The setup parameters for the measurement campaign of the hybrid PLC-wireless channels are summarized in Tab. 1. From Tab. 1, the frequency responses of all channel estimates are determined every  $23 \mu\text{s}$ , approximately, which is shorter than the sweep time of vector network analyzers (e.g., 300 ms for the same frequency resolution adopted) and the minimum coherence time of the indoor PLC channels ( $600 \mu\text{s}$ ) [35]. Thus, the adopted methodology constitutes an important tool for use in the characterization task for PLC and hybrid PLC-wireless channels and is superior to the use of vector network analyzers.

The locations in which the measurement campaigns were carried out are those listed in Tab. 4. These facilities comprise typical residences and apartments in an urban area of Juiz de Fora, Brazil. Potential scattering objects and the transceivers were stationary during the measurement campaign in order to avoid Doppler effects in the wireless portion of the hybrid PLC-wireless channel.

Into carrying out the measurements, the following cases were considered:

- *short-path channel*: The wireless-PLC transceiver was randomly positioned within a 2-m radius circle centered at the outlet in which the PLC-wireless transceiver is connected;

- *long-path channel*: The wireless-PLC transceiver was randomly placed into an area defined as a swept circle, having an outer and inner radius of 6 m and 2 m, respectively, centered in the outlet in which the PLC-wireless transceiver is connected.

By taking into account all facilities, 293 different combinations of locations for both PLC-wireless and wireless-PLC transceivers were evaluated. The wireless-PLC transceiver was positioned near to (*short-path channel*) and far from (*long-path channel*) the outlet in 200 and 93 combinations, respectively. Furthermore, approximately 600 estimates of the channel frequency response were measured for each combination. As a result, a total of 175,428 estimates of the hybrid PLC-wireless channel frequency responses were obtained during the campaign. Additionally, additive noise in the localization of both PLC-wireless and wireless-PLC transceivers were measured. In what follows we present all details about the estimated parameters and the results obtained.

### 4.3 RESULTS AND ANALYSIS

The presented results and analysis are based on the estimates of the channel features listed in Sec. 3.2, obtained from the hybrid PLC-wireless channels in the frequency range from 1.7 MHz up to 100 MHz. In addition, the frequency bands listed in Tab. 11 are considered to analyze the behavior of hybrid PLC-wireless channels in a regulated frequency band as well as in a frequency band that can be considered for future standardization efforts of PLC and hybrid PLC-wireless technology.

Table 11: Chosen Subbands for Analysis.

Notation	Frequency band (MHz)
FB <sub>01</sub>	1.7–30
FB <sub>02</sub>	30–70
FB <sub>03</sub>	70–100
FB <sub>T</sub>	1.7–100

#### 4.3.1 Channel frequency response analyses

##### 4.3.1.1 Comparison between PLC-PLC, PLC-wireless, Wireless-PLC and Wireless-wireless transmission

The scenario in Fig. 46, which is a typical room in Brazilian residences (house or apartment), was investigated in order to exemplify the differences that can be verified by adopting different transmission strategies (PLC-PLC, wireless-wireless, and wireless-PLC to PLC-wireless). Channel frequency responses were estimated (see Fig. 47), adopting the transmission direction from the wall on the top to that at the bottom of Fig. 46. As we can see, for the frequency band ranging from 1.7 up to 100 MHz, the PLC-PLC

communication suffers less attenuation in almost the entire frequency band, while the wireless-wireless communication is a little better in the frequencies around 70 MHz. In its turn, the hybrid PLC-wireless channel offers the highest channel attenuation regardless the transmission direction. On the other hand, as discussed before, the hybrid channel can be exploited as an artifice to introduce mobility into a pure PLC system.

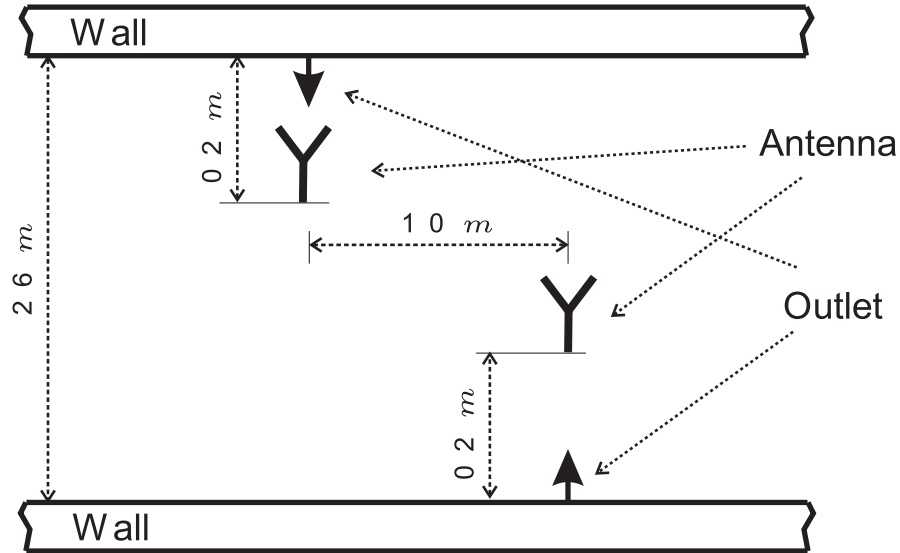


Figure 46: Measured scenario.

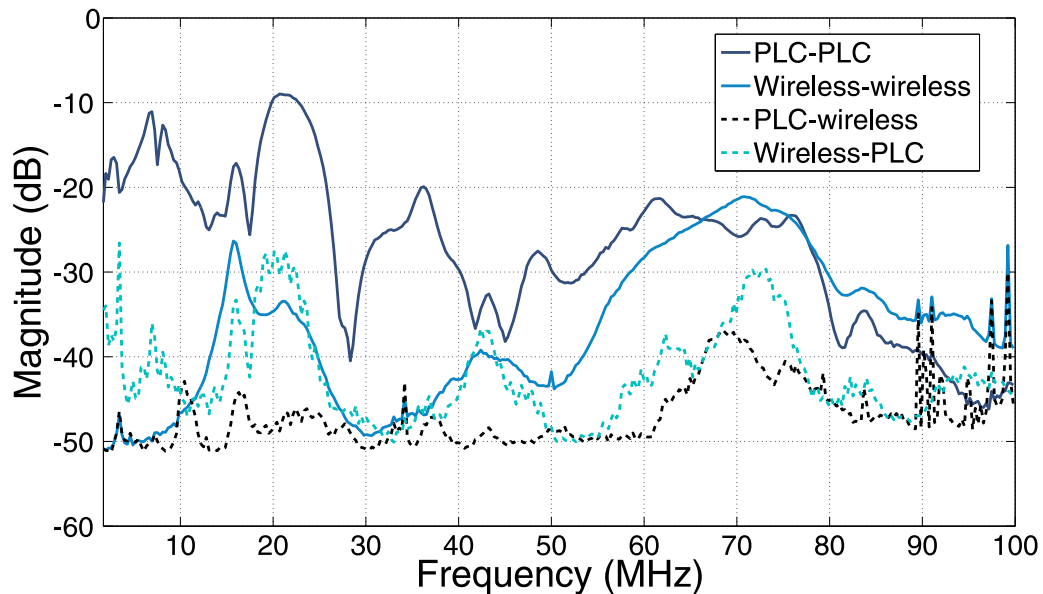


Figure 47: Magnitude responses of some measured channels.

#### 4.3.1.2 Magnitude Response Symmetry

Measurements of channels were carried out in both PLC-wireless and wireless-PLC directions in order to verify the symmetry of hybrid PLC-wireless channels. Figures 48

and 49 show magnitude responses of four distinct but typical hybrid channel estimates – each one obtained from different combinations of two different positions of PLC-wireless and wireless-PLC transceivers. Figure 48 shows results for wireless-PLC direction and Fig. 49 for the reverse path. From these figures, the hybrid PLC-wireless channel can be seen to be symmetrical in terms of the magnitude function, i.e., the magnitude response is independent of the transmission direction. This behavior is confirmed in all measured channels. Minor differences, as those seen in Fig. 50, which considers the two directions of a single scenario, may be associated to background noise and slow channel variation, since measurements in both directions are not simultaneous.

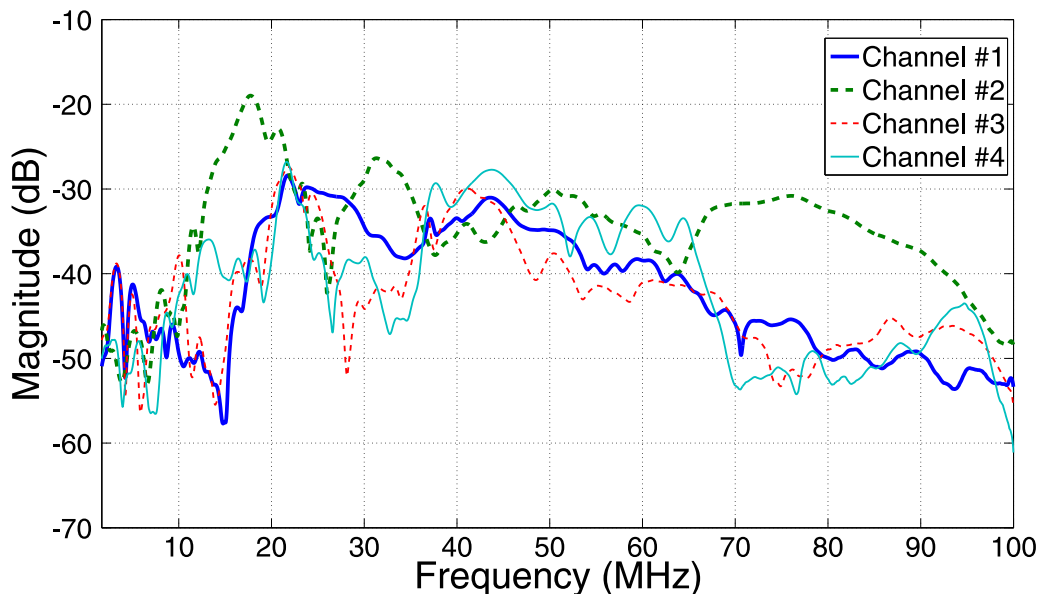


Figure 48: Magnitude responses of measured hybrid PLC-wireless channels for the transmission from wireless-PLC to PLC-wireless transceiver.

#### 4.3.1.3 Influence of small distance variations on the magnitude response

Figure 51 shows four different scenarios where only the wireless-PLC transceiver was displaced in four different locations 0.4 meters, on average, apart. From this plot, small position variations of wireless-PLC transceiver can significantly affect the hybrid channel magnitude response for frequencies above 30 MHz.

#### 4.3.1.4 Statistics

The maximum, minimum, mean, 50<sup>th</sup> and 90<sup>th</sup> percentiles statistical parameters of the magnitude response of the measured hybrid PLC-wireless channels were extracted. In Fig. 52, which refers to *short-path channels*, the magnitude responses range from  $-5$  to  $-120$  dB, approximately, and 90% of observations stay within the magnitude range of  $-20$  and  $-40$  dB for the frequency band ranging from 10 to 100 MHz. For *long-path channels*, as depicted in Fig. 53, 90% of the cases exhibit values below  $-30$  dB, approximately,

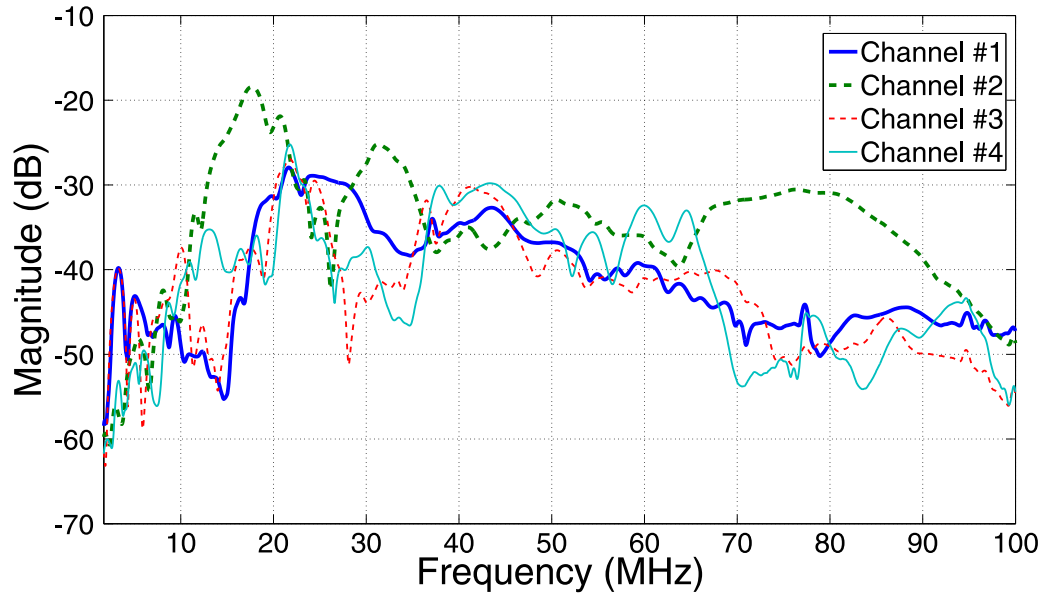


Figure 49: Magnitude responses of measured hybrid PLC-wireless channels for the transmission from PLC-wireless to wireless-PLC transceiver.

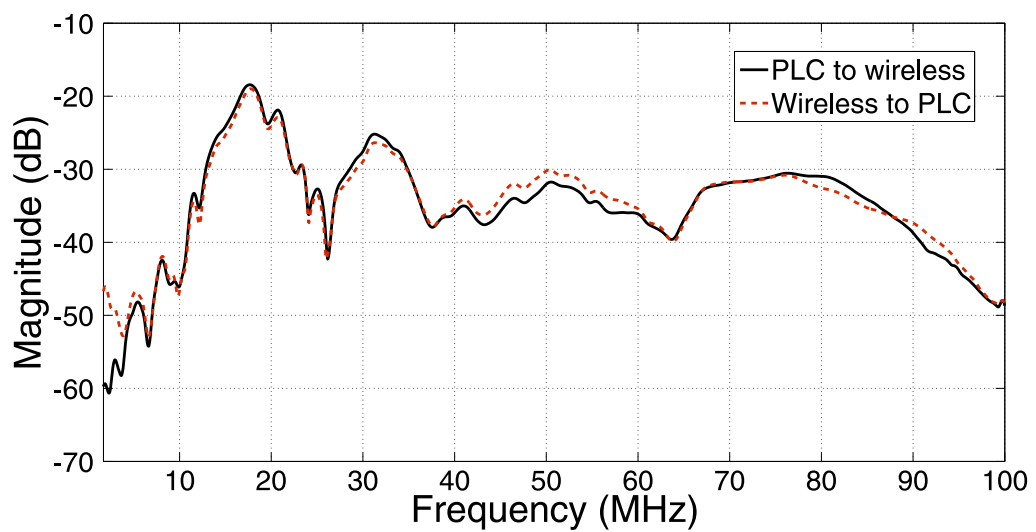


Figure 50: Magnitude responses of a single channel in both directions.

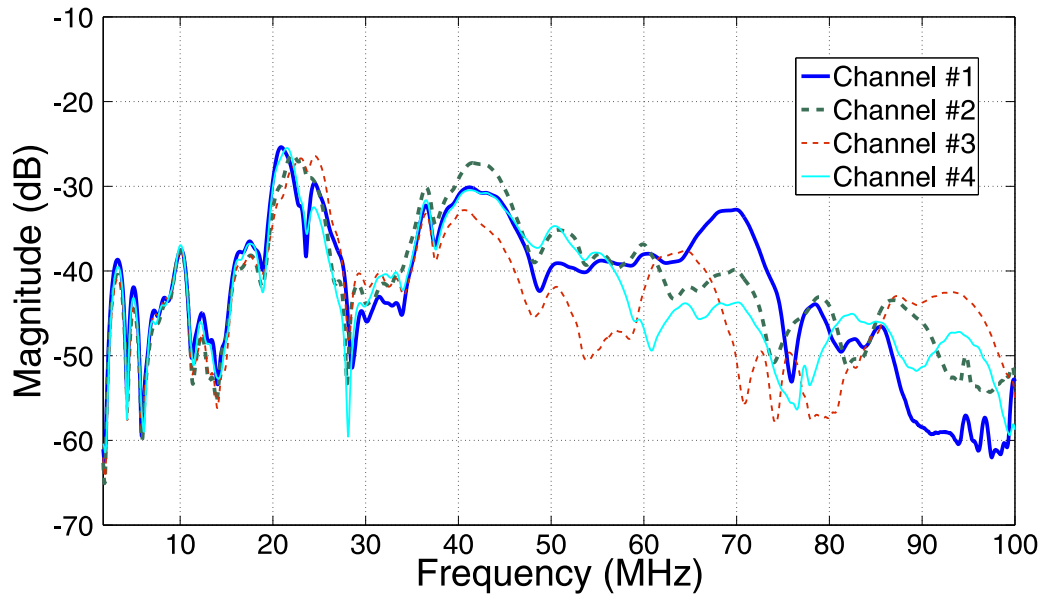


Figure 51: Magnitude responses of some measured hybrid PLC-wireless for different locations of the wireless-PLC transceiver.

and in the frequency band from 1.7 MHz up to 10 MHz, their values are below  $-50$  dB. Comparing these two scenarios, one observes significantly higher attenuation levels along *long-path channels*, as expected.

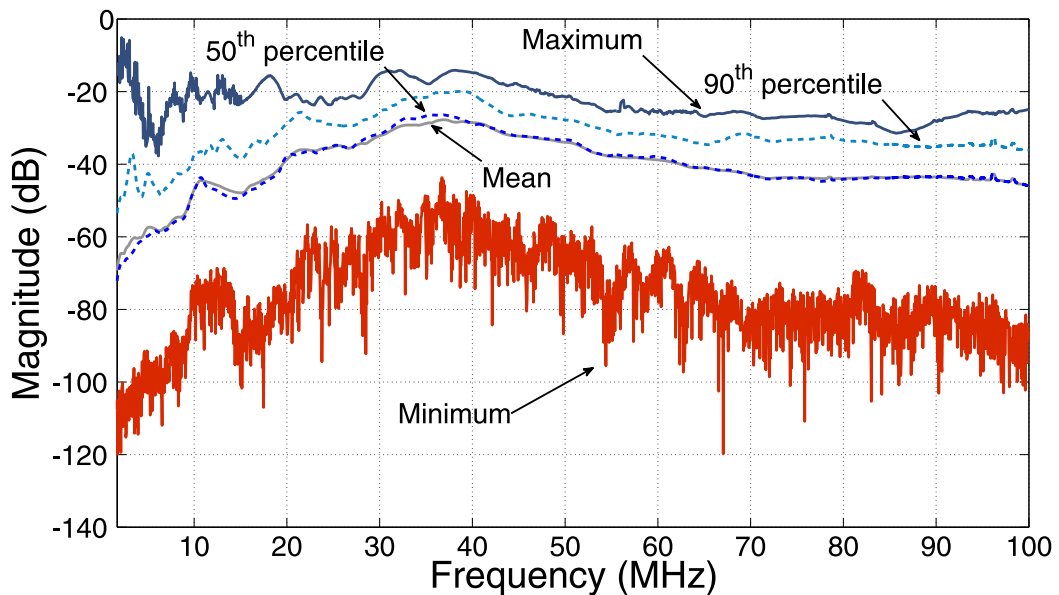


Figure 52: Statistical parameters extracted from estimated magnitude responses of the *short-path* hybrid PLC-wireless channels.

#### 4.3.2 Average channel attenuation (ACA)

ACA statistics are presented in Tab. 12, for frequency bands listed in Tab. 11, where *std* denotes the standard deviation. Subband  $FB_{02}$  shows the lowest ACA achieving

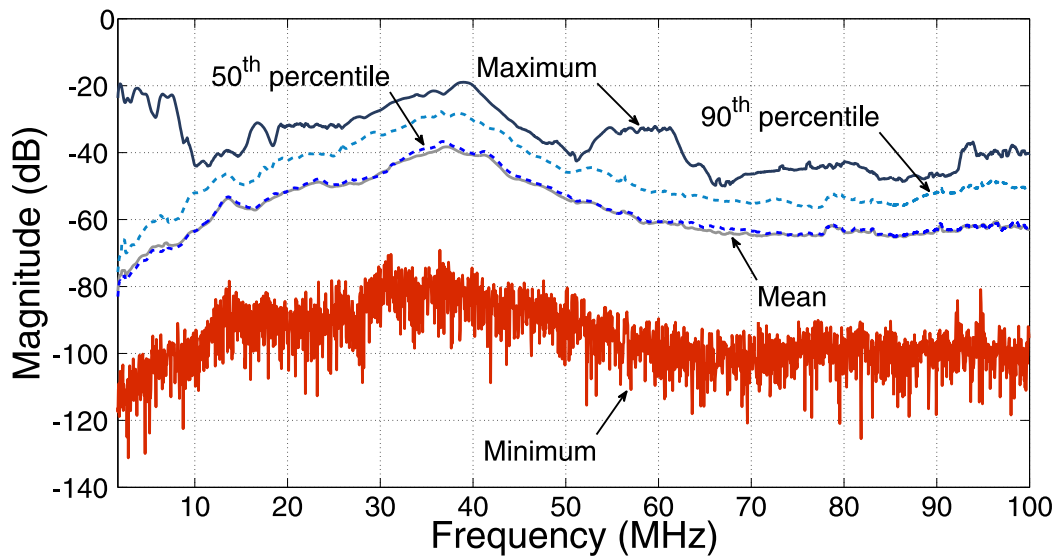


Figure 53: Statistical parameters extracted from estimated magnitude responses of the *long-path* hybrid PLC-wireless channels.

mean attenuation levels of 30 and 42 dB for the *short-* and *long-path channels*, respectively. On the other hand, subband  $FB_{03}$  presented the highest ACA values, reaching a maximum of 55.55 dB for *short-path* and 71.53 dB for *long-path channels*. Regarding the entire frequency band  $FB_T$  and considering *short-path channel*, ACA values are below 36.79 dB in 90% of the observations, while for *long-path channel* they are below 52.35 dB. In general, these results emphasize that magnitude responses of hybrid PLC-wireless channels show significantly high attenuation levels.

Table 12: ACA for the Measured Hybrid PLC-Wireless Channels.

		ACA (dB)					
		Maximum	Minimum	Mean	Std	50% below	90% below
<i>Short-path channel</i>	$FB_{01}$	50.57	24.39	36.38	4.68	36.72	41.94
	$FB_{02}$	42.12	20.94	30.77	3.79	30.98	36.02
	$FB_{03}$	55.55	26.65	41.69	5.41	42.32	48.28
	$FB_T$	41.69	24.61	33.03	3.17	33.04	36.79
<i>Long-path channel</i>	$FB_{01}$	63.54	21.83	48.99	7.79	49.92	57.94
	$FB_{02}$	64.73	28.64	42.66	5.92	42.14	49.62
	$FB_{03}$	71.53	28.49	56.14	5.61	55.79	63.33
	$FB_T$	63.06	27.11	44.89	6.33	45.29	52.35

Considering some reported results for the PLC scenario, we can verify that the mean ACA for *short-path channels* is less than that reported for in-home PLC channels in US [77] (41.5 dB), for  $FB_{01}$  but 13 dB higher than the value estimated for in-home Brazilian places. Considering  $FB_T$  the mean ACA is almost the same achieved in Italy [32] (35.4 dB) and only 3 dB higher than the Brazilian results. The mean attenuation observed in *long-path channels* are higher than those reported for in-home PLC channels in Brazil,

Italy and US. With respect to the results achieved for in-home Brazilian PLC channels, the differences are of 26 dB and 15 dB, approximately, for  $FB_{01}$  and  $FB_T$ , respectively.

#### 4.3.2.1 Statistical modeling

The statistical modeling of the channel features were performed considering only  $FB_T$ . The attained results revealed that the ACA is better fitted by the Skew-normal distribution in both *short-* (Fig. 54) and *long-path channels* (Fig. 55), according to all information criteria.

The asymmetry of the dataset for the ACA in both scenarios, *short-* and *long-path channels*, is not clear by the histograms in Figs. 54 and 55. On the other hand, the asymmetry of the ACA can be inferred looking at Tabs. 27 and 28, in Appendix D, for *short-path* and *long-path channels*, respectively. Also, for comparison purposes, the normal fit to the dataset is also depicted. As can be noted, the estimated values for  $(\mu, \sigma)$  to the Skew-normal and Normal distribution are close, but the Skew-normal distribution achieved the best fit by introducing a negative skewness (asymmetry) through its third parameter ( $\gamma$ ).

The modeling parameters of all considered statistical distributions fitted to the ACA for both, *short-* and *long-path channels*, are summarized in Tabs. 27 and 28, for *short-path* and *long-path channels*, respectively.

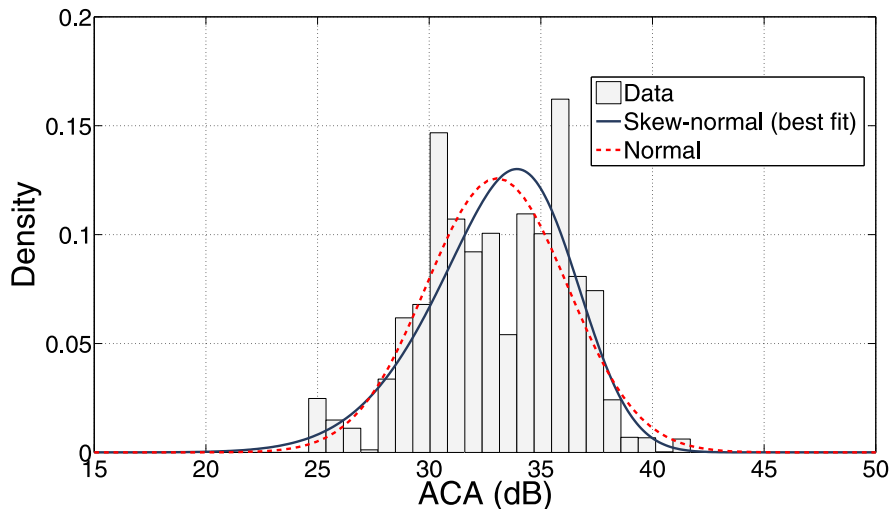


Figure 54: The histogram and distribution fitting of ACA for *short-path channels*.

### 4.3.3 Coherence bandwidth (CB)

Table 13 summarizes the estimated coherence bandwidth for measured PLC-wireless channels, considering correlation levels of 0.5 ( $B_{05}$ ), 0.7 ( $B_{07}$ ) and 0.9 ( $B_{09}$ ). In this analysis, subband  $FB_{03}$  shows the highest mean CB values when compared to subbands  $FB_{01}$  and  $FB_{02}$  for *short-path channel*. For *long-path channels* the highest mean value is observed

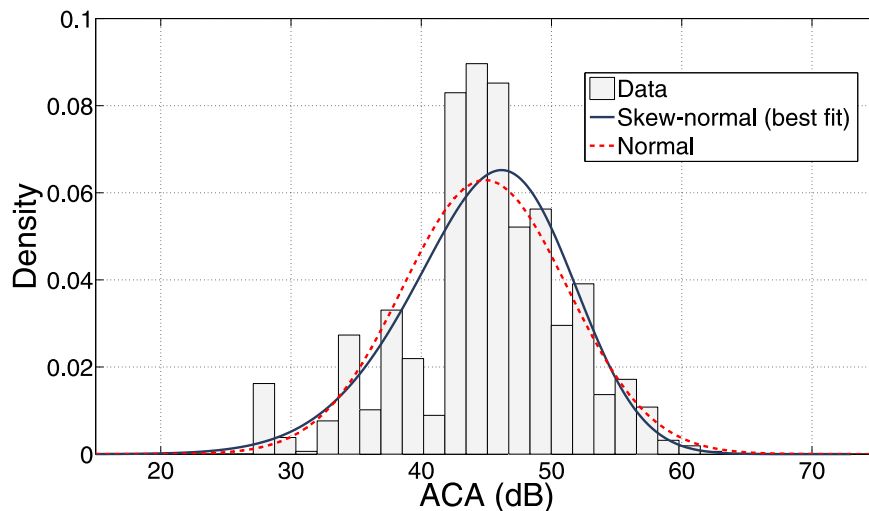


Figure 55: The histogram and distribution fitting of ACA for *long-path channels*.

in subband  $FB_{02}$ . For a correlation level of 0.9 in *short-path channels*, subband  $FB_{02}$  shows CB values greater than 1.51 MHz for 50% of observations, while the minimum CB value is 1.27 MHz and 0.68 MHz for subbands  $FB_{03}$  and  $FB_{01}$ , respectively, for the same percentage level. For *long-path channels*, CB values for subbands  $FB_{01}$  and  $FB_{03}$  are greater than 0.29 MHz and 0.27 MHz, respectively, while for subband  $FB_{02}$  the CB is greater than 0.98 MHz in 50% of observations.

When considering the correlation level of 0.9, subband  $FB_T$  offers a mean CB value of 1.62 MHz with a standard deviation of 0.66 MHz for the *short-path channel*. Also, a CB value greater than 1.42 MHz is observed in 50% of the observations and greater than 2.57 MHz in only 10% of the estimates. On the other hand, the *long-path channel* presents a mean CB value of 1.00 MHz with a standard deviation of 505.64 kHz and a CB value greater than 0.93 MHz and 1.61 MHz for 50% and 10%, respectively, of the observations. Thus, we conclude that *long-path channels* are more selective than its *short-path* counterpart, as expected. This behavior is verified in all considered correlation levels. Also, the minimal value was 48.83 kHz, for several evaluated scenarios. However, since this value is the frequency resolution (see Tab. 1), the CB value could, eventually, be lower than the frequency resolution. For the sake of conciseness, in the remainder of this contribution, only the CB value at a correlation level of 0.9 ( $B_{09}$ ) will be considered.

Comparing with the results achieved for in-home PLC channels and considering only  $B_{09}$ , we can verify that hybrid PLC-channel presented higher values of CB in some cases. For instance, the mean value of CB in hybrid PC-wireless channels is higher than those reported for the PLC case, with respect to  $FB_T$ . For  $FB_{01}$  only *short-path channel* presented mean values of CB higher than for the PLC case.

Table 13: CB for the Measured Hybrid PLC-Wireless Channels.

		CB (kHz)						
		Maximum	Minimum	Mean	Standard deviation	50% below	90% below	
<i>Short-path channel</i>	$B_{05}$ (FB <sub>01</sub> )	$16.45 \times 10^3$	97.66	$4.95 \times 10^3$	$3.62 \times 10^3$	$4.05 \times 10^3$	$10.47 \times 10^3$	
	$B_{05}$ (FB <sub>02</sub> )	$39.99 \times 10^3$	244.14	$10.09 \times 10^3$	$7.72 \times 10^3$	$7.23 \times 10^3$	$18.75 \times 10^3$	
	$B_{05}$ (FB <sub>03</sub> )	$29.93 \times 10^3$	97.66	$12.32 \times 10^3$	$9.43 \times 10^3$	$8.74 \times 10^3$	$29.32 \times 10^3$	
	$B_{05}$ (FB <sub>T</sub> )	$57.96 \times 10^3$	97.66	$8.67 \times 10^3$	$6.78 \times 10^3$	$6.73 \times 10^3$	$14.65 \times 10^3$	
	$B_{07}$ (FB <sub>01</sub> )	$10.84 \times 10^3$	97.66	$2.49 \times 10^3$	$1.82 \times 10^3$	$1.90 \times 10^3$	$5.08 \times 10^3$	
	$B_{07}$ (FB <sub>02</sub> )	$30.45 \times 10^3$	195.31	$4.58 \times 10^3$	$3.79 \times 10^3$	$3.71 \times 10^3$	$7.47 \times 10^3$	
	$B_{07}$ (FB <sub>03</sub> )	$29.93 \times 10^3$	48.83	$6.55 \times 10^3$	$6.82 \times 10^3$	$4.44 \times 10^3$	$13.57 \times 10^3$	
	$B_{07}$ (FB <sub>T</sub> )	$27.49 \times 10^3$	48.83	$4.40 \times 10^3$	$2.95 \times 10^3$	$3.76 \times 10^3$	$6.59 \times 10^3$	
	$B_{09}$ (FB <sub>01</sub> )	$3.76 \times 10^3$	97.66	$0.81 \times 10^3$	$0.54 \times 10^3$	$0.68 \times 10^3$	$1.32 \times 10^3$	
	$B_{09}$ (FB <sub>02</sub> )	$6.05 \times 10^3$	97.66	$1.57 \times 10^3$	$6.02 \times 10^3$	$1.51 \times 10^3$	$2.29 \times 10^3$	
	$B_{09}$ (FB <sub>03</sub> )	$13.91 \times 10^3$	48.83	$1.75 \times 10^3$	$1.90 \times 10^3$	$1.27 \times 10^3$	$4.35 \times 10^3$	
	$B_{09}$ (FB <sub>T</sub> )	$4.69 \times 10^3$	195.31	$1.62 \times 10^3$	$0.66 \times 10^3$	$1.42 \times 10^3$	$2.57 \times 10^3$	
	<i>Long-path channel</i>	$B_{05}$ (FB <sub>01</sub> )	$17.87 \times 10^3$	97.66	$3.26 \times 10^3$	$3.42 \times 10^3$	$2.09 \times 10^3$	$8.69 \times 10^3$
		$B_{05}$ (FB <sub>02</sub> )	$17.53 \times 10^3$	97.66	$4.08 \times 10^3$	$2.48 \times 10^3$	$3.47 \times 10^3$	$7.17 \times 10^3$
$B_{05}$ (FB <sub>03</sub> )		$29.93 \times 10^3$	48.83	$1.33 \times 10^3$	$2.93 \times 10^3$	$2.11 \times 10^3$	$8.00 \times 10^3$	
$B_{05}$ (FB <sub>T</sub> )		$12.01 \times 10^3$	146.48	$3.84 \times 10^3$	$2.14 \times 10^3$	$3.47 \times 10^3$	$6.59 \times 10^3$	
$B_{07}$ (FB <sub>01</sub> )		$11.77 \times 10^3$	97.66	$1.43 \times 10^3$	$1.43 \times 10^3$	$1.12 \times 10^3$	$2.98 \times 10^3$	
$B_{07}$ (FB <sub>02</sub> )		$6.93 \times 10^3$	48.89	$2.32 \times 10^3$	$1.09 \times 10^3$	$2.20 \times 10^3$	$3.56 \times 10^3$	
$B_{07}$ (FB <sub>03</sub> )		$7.52 \times 10^3$	48.83	$0.38 \times 10^3$	$0.90 \times 10^3$	$0.88 \times 10^3$	$4.34 \times 10^3$	
$B_{07}$ (FB <sub>T</sub> )		$6.10 \times 10^3$	48.83	$2.27 \times 10^3$	$1.19 \times 10^3$	$2.19 \times 10^3$	$3.86 \times 10^3$	
$B_{09}$ (FB <sub>01</sub> )		$3.27 \times 10^3$	48.83	$0.40 \times 10^3$	$0.39 \times 10^3$	$0.29 \times 10^3$	$0.93 \times 10^3$	
$B_{09}$ (FB <sub>02</sub> )		$2.78 \times 10^3$	48.83	$0.99 \times 10^3$	$0.48 \times 10^3$	$0.98 \times 10^3$	$1.51 \times 10^3$	
$B_{09}$ (FB <sub>03</sub> )		$2.29 \times 10^3$	48.83	$0.11 \times 10^3$	$0.14 \times 10^3$	273.44	$1.41 \times 10^3$	
$B_{09}$ (FB <sub>T</sub> )		$2.78 \times 10^3$	146.48	$1.00 \times 10^3$	505.64	$0.93 \times 10^3$	$1.61 \times 10^3$	

### 4.3.3.1 Statistical modeling

The CB presented distinct behavior, in terms of symmetry, if the *short-* and *long-path channels* are compared, when considering  $FB_T$ . The CB for *short-path channels* is better fitted by the Log-logistic distribution, as depicted in Fig. 56, whereas the best fit for the *long-path CB* was achieved by the t-Student distribution, as seen in Fig. 57. Also, the fit to the Log-normal and Normal distributions for the *short-* and *long-path channel*, respectively, are displayed to highlight the CB symmetry differences between the *short-* and *long-path channels*. These results suggest that the CB for *short-path channel* shows a positive asymmetry, while the same channel feature for *long-path channel* presents strong evidence of symmetry. Tables 29 and 30, in Appendix D, summarize the parameters estimates for all considered statistical distributions for the *short-* and *long-path channels*, respectively.

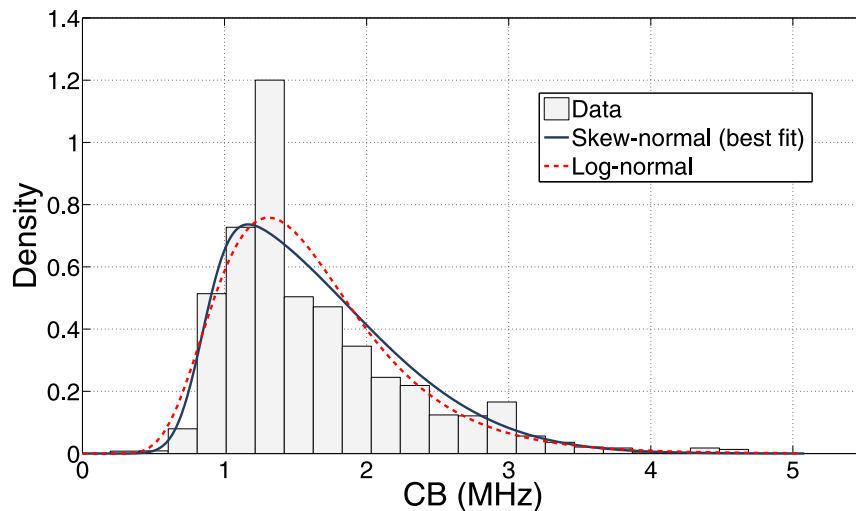


Figure 56: The histogram and distribution fitting of CB for *short-path channels*.

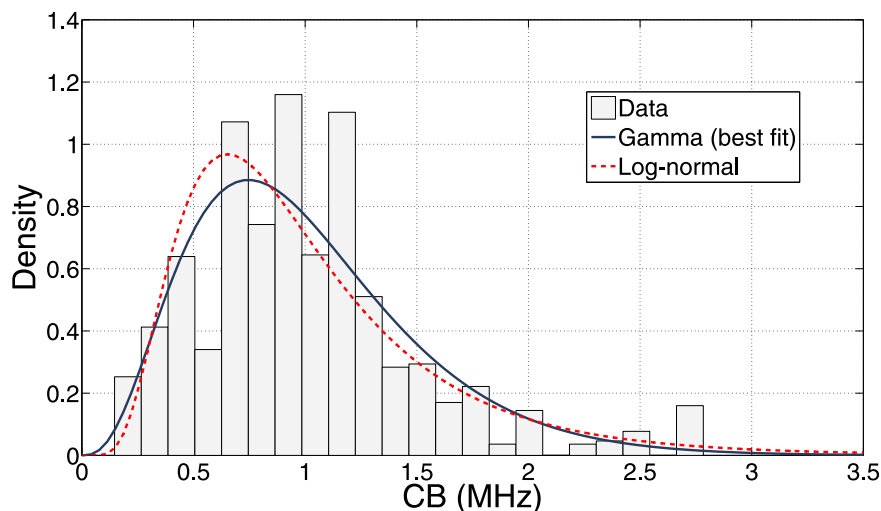


Figure 57: The histogram and distribution fitting of CB for *long-path channels*.

#### 4.3.4 Root mean squared delay spread (RMS-DS)

Statistical parameters of RMS-DS are presented in Tab. 14. subband  $FB_{02}$  exhibited the lowest values for the mean RMS-DS in all evaluated scenarios, whereas subband  $FB_{03}$  presented the highest ones. An RMS-DS below  $0.168 \mu s$ ,  $0.085 \mu s$ , and  $0.533 \mu s$  was observed in subbands  $FB_{01}$ ,  $FB_{02}$ , and  $FB_{03}$ , respectively, in 90% of observations of *short-path channel*. For *long-path channels* the corresponding threshold values were  $0.419 \mu s$ ,  $0.179 \mu s$ , and  $1.425 \mu s$ .

For the complete frequency band  $FB_T$ , *long-path channel* exhibited a maximum value of  $1.476 \mu s$  for the RMS-DS, whereas in *short-path channel* such value was  $1.196 \mu s$ . In 90% of the cases, the RMS-DS was above  $0.133 \mu s$  for *short-path channel*, compared with  $0.331 \mu s$  for *long-path channel*. Thus, the multipath effect is less pronounced in *short-path* than in *long-path channels*, as expected.

Table 14: RMS-DS of the Measured Hybrid PLC-Wireless Channels.

		RMS-DS ( $\mu s$ )					
		Maximum	Minimum	Mean	Std	50% below	90% below
<i>Short-path channel</i>	$FB_{01}$	1.685	0.024	0.129	0.064	0.122	0.168
	$FB_{02}$	0.936	0.031	0.066	0.035	0.059	0.085
	$FB_{03}$	1.857	0.013	0.180	0.288	0.056	0.533
	$FB_T$	1.196	0.018	0.085	0.069	0.071	0.133
<i>Long-path channel</i>	$FB_{01}$	1.742	0.029	0.214	0.219	0.139	0.419
	$FB_{02}$	1.540	0.025	0.108	0.094	0.079	0.178
	$FB_{03}$	1.928	0.011	0.440	0.556	0.095	1.425
	$FB_T$	1.476	0.019	0.162	0.147	0.107	0.331

The RMD-DS mean value observed for both the *short-path* and *long-path channels* are lower than that reported for in-home PLC channels in the urban area in US [77] ( $0.23 \mu s$ ) and in Italy (see Tab. I in [32]), considering  $FB_{01}$ . For  $FB_T$  the PLC channels in Italy presented lower RMS-DS values than the Brazilian hybrid channels evaluated in this thesis.

##### 4.3.4.1 Statistical modeling

The dataset that represents the RMD-DS for the hybrid PLC-wireless channel present a notorious positive asymmetry, as can be seen in the histograms depicted in Figs. 58 and 59, for *short-path* and *long-path channels*, respectively. The RMS-DS of *short-path channels* is better fitted by the Log-logistic statistical distribution, while the Inverse Gaussian is the one that best fits the RMS-DS of *long-path channels*. Also, the fit to the Log-normal distribution is depicted and it presents some similarities, if compared to the distribution that better fits to the dataset. Tables 31 and 32, in Appendix D, summarizes the estimates of the parameters of the fitted statistical distributions, for *short-path* and *long-path channels*, respectively.

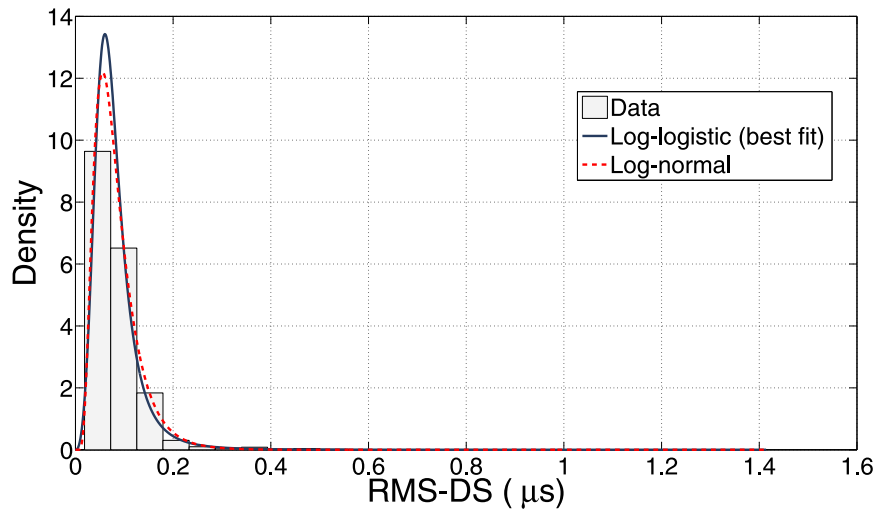


Figure 58: The histogram and distribution fitting of RMS-DS for *short-path channels*.

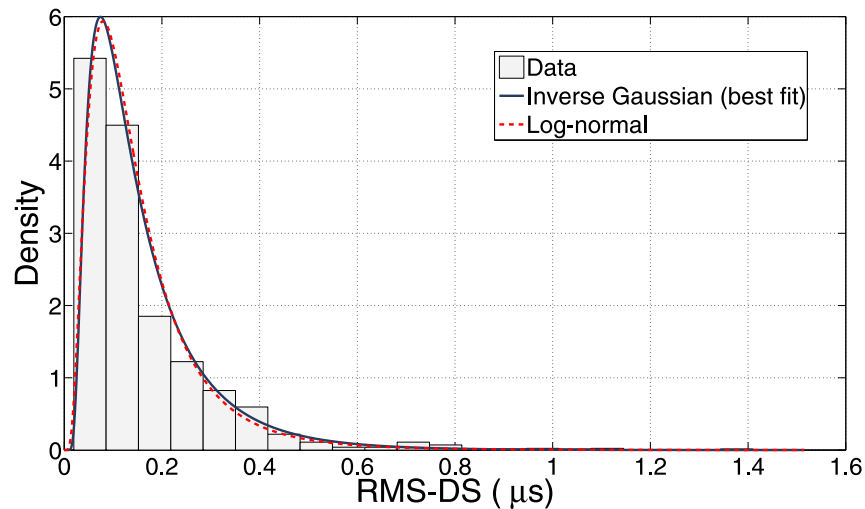


Figure 59: The histogram and distribution fitting of RMS-DS for *long-path channels*.

#### 4.3.5 CB versus RMS-DS

The relation between CB and RMS-DS parameters was given by (3.8) as  $\sigma_\tau \approx \gamma/B_{09}$ . The observed relation for the hybrid PLC-wireless channel is shown in Fig. 60, where the dotted line denotes the case  $\gamma = 111$ , which represents the best fit for the *short-path channel* according to the MMSE criterion. The analysis for *long-path channel* returned  $\gamma = 106$ , which is close to that achieved for the *short-path channel*. For comparison purposes, reference [72] reported  $\gamma = 55$  for a standard PLC channel, whereas [104] provided  $\gamma \approx 150$  and [105] reported  $\gamma < 100$  for some wireless channels.

#### 4.3.6 Coherence time (CT)

CT was estimated using the procedure described in [36] with its parameters having the values listed in Tab. 10. Also, only those measurements that provided more than

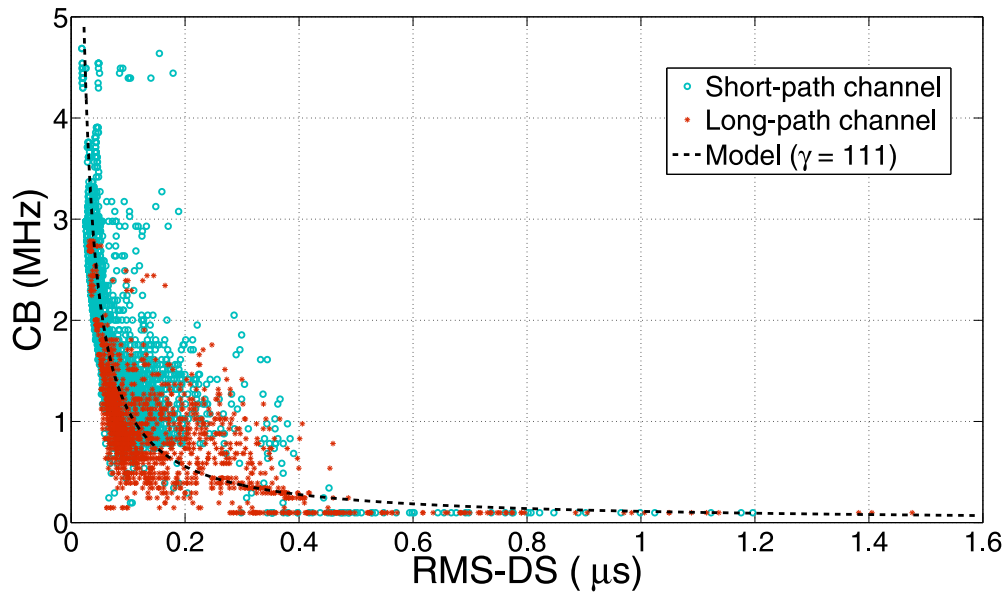


Figure 60: Scatter plot of CB versus RMS-DS.

640 consecutive estimates of frequency response of hybrid PLC-wireless channels were taken into account. Figure 61 shows the correlation evolution [36] for all measured hybrid PLC-wireless channels for *short-path channel*. Note that the  $y$ -axis refers to different channel configurations while the  $x$ -axis is the time evolution of the same channel through its several consecutive estimates and the correlation is evaluated with respect to the first channel impulse response as reference. It can be seen that most of the channels have a similar temporal variability of its channel impulse response. The CDF of the CT for *short-path channel* case is presented in Fig. 62, where different coherence levels are considered. This figure suggests that CT was below approximately  $156 \mu\text{s}$  for 90% of the observed cases, considering the coherence level ( $\beta$ ) of 0.99.

Figure 63 shows the correlation evolution of the hybrid PLC-wireless channel as defined in [36] for *long-path channel*. In this case, the analyzed hybrid PLC-wireless channels have distinct and severe variations of temporal correlation. That behavior indicates that these channels present shorter time intervals than *short-path channels* in which the channel impulse response can be considered time invariant, as confirmed by the coherence-time CDF plots depicted in Fig. 64. This plot also suggests that the CT for the *long-path channel* is shorter than  $39.5 \mu\text{s}$ , only one fourth of its *short-path* counterpart in 90% of the observed cases, for  $\beta = 0.99$ .

#### 4.3.6.1 Statistical modeling

The CT in *short-path channels* exhibits some kind of symmetry, which is confirmed by the best fit attained by the Logistic distribution, as seen in the histogram depicted in Fig. 65, where the Normal-distribution fit is also plotted for comparison purposes. For the

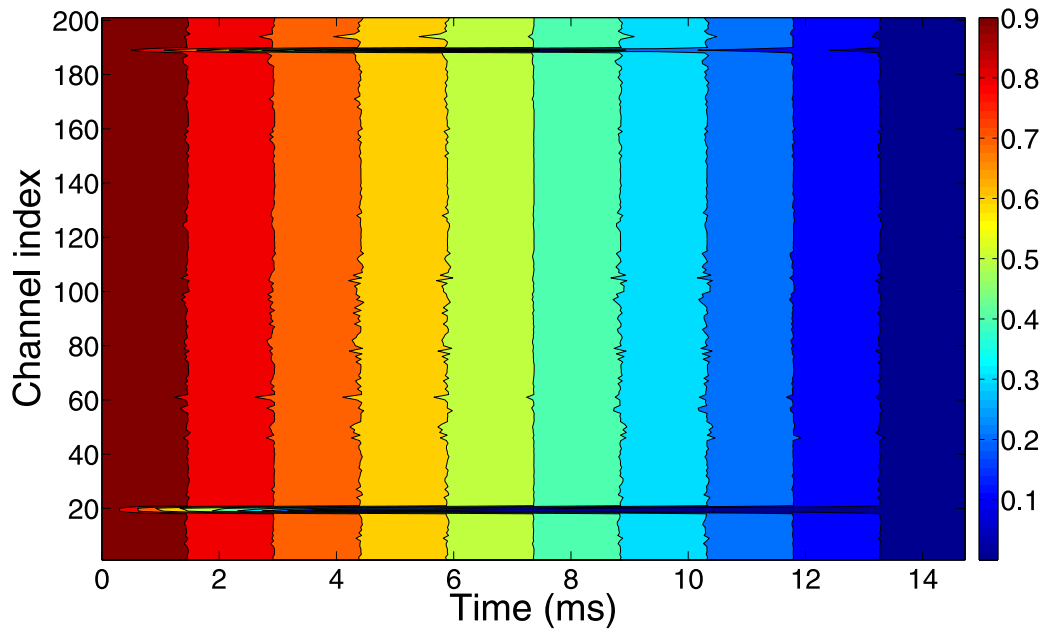


Figure 61: Correlation evolution for the *short-path channel*.

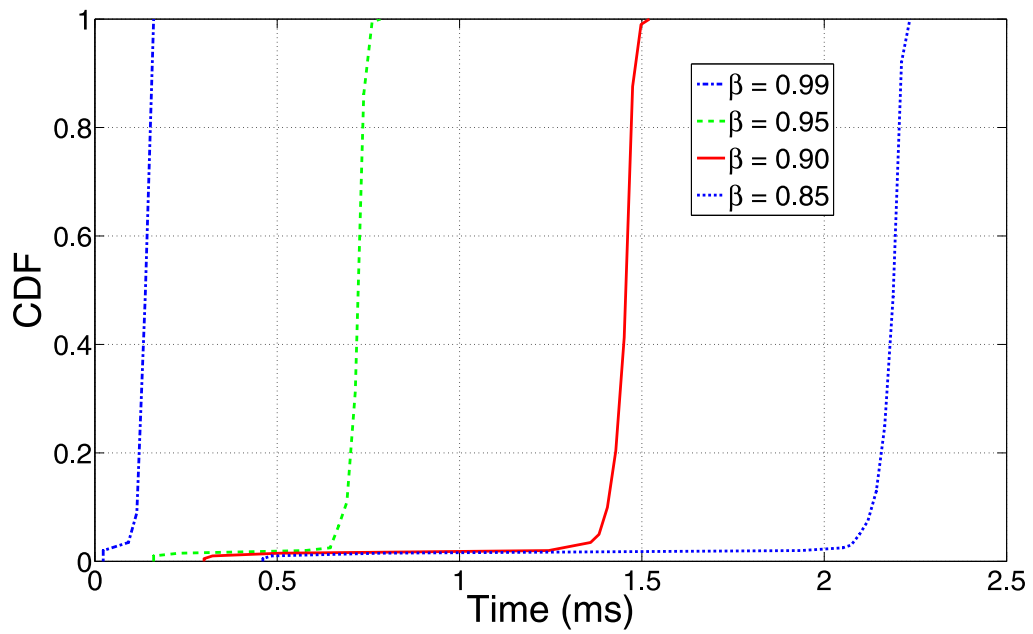


Figure 62: CT CDF of the *short-path channel* for distinct correlation levels.

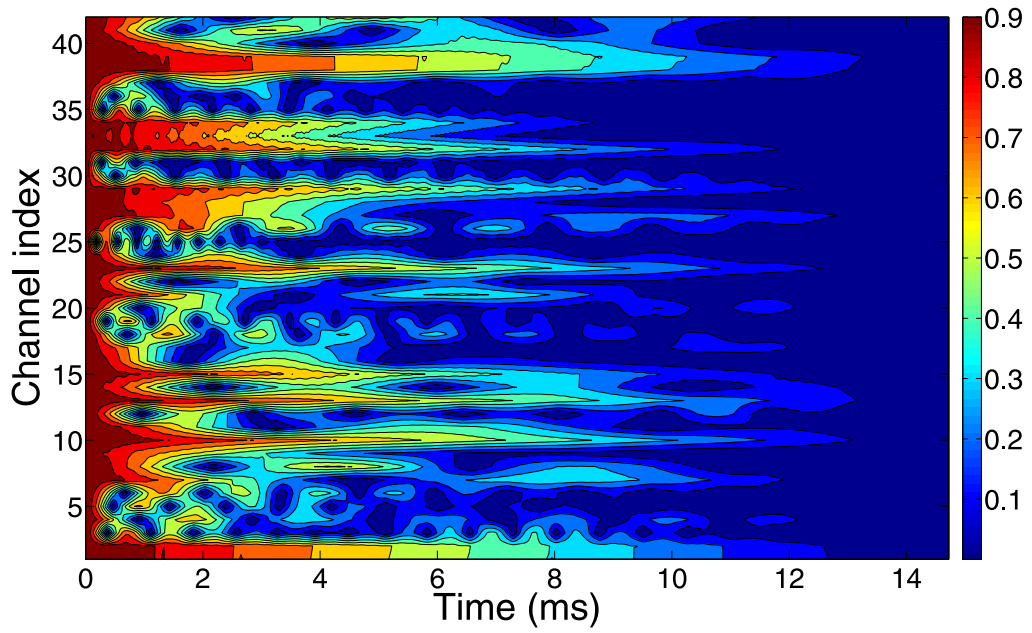


Figure 63: Correlation evolution for *long-path channel*.

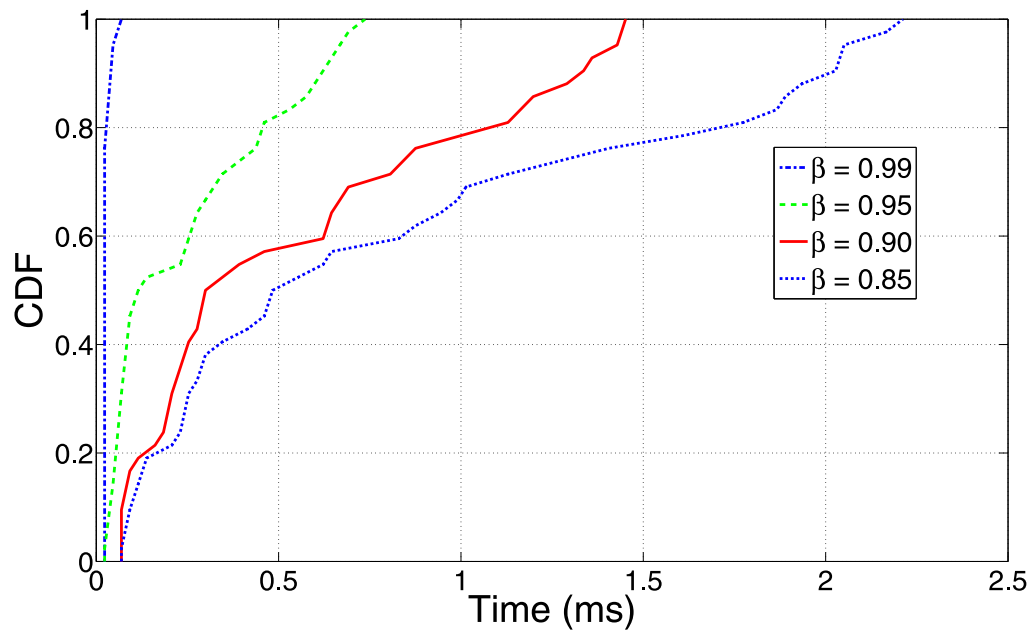


Figure 64: CDF of CT for *short-path channel* by considering distinct values of correlation levels.

*long-path channel* the best fit is achieved by the Skew-normal distribution, as shown in Fig.66. The parameter estimates for the fittings regarding the CT for *short-* and *long-path channels* are summarized in Tabs. 33 and 34, in Appendix D, respectively.

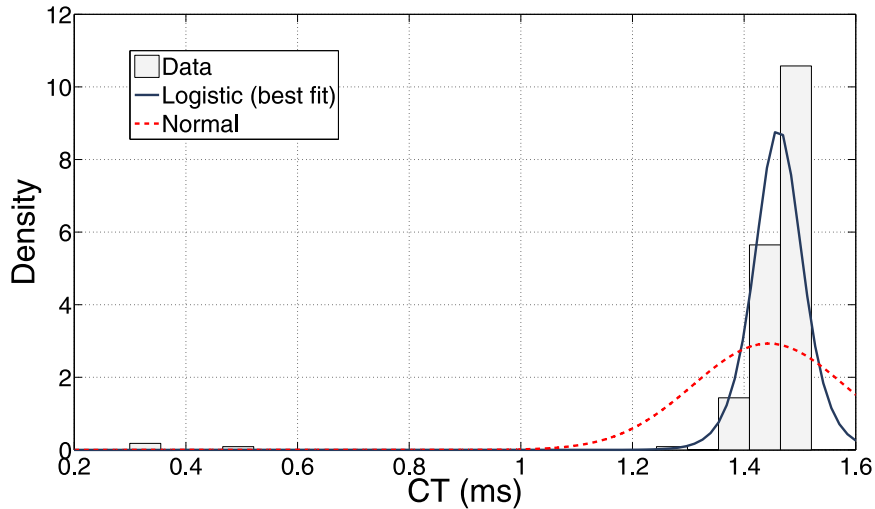


Figure 65: The histogram and distribution fitting of CT for *short-path channels*.

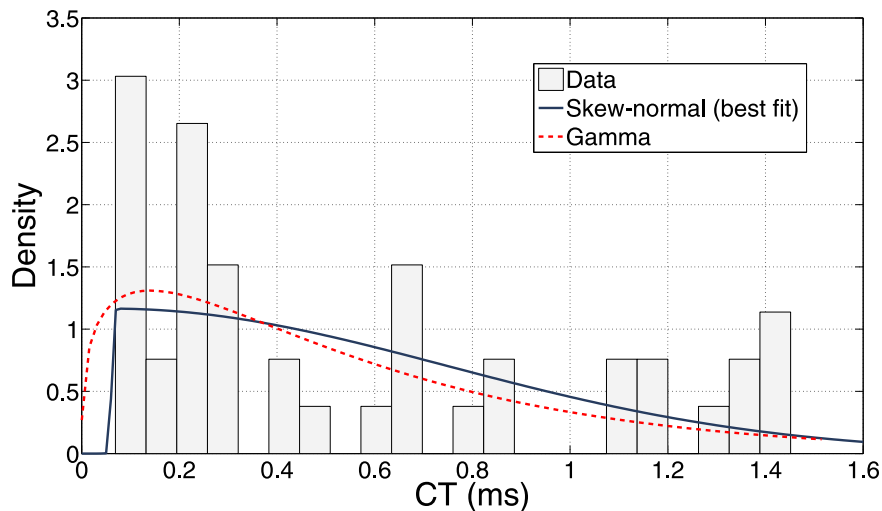


Figure 66: The histogram and distribution fitting of CT for *long-path channels*.

#### 4.3.7 Additive noise

Additive noise in both PLC and wireless interfaces was measured in order to estimate the channel capacity in the measured hybrid PLC-wireless channels. The statistical parameters of the measured noise in the wireless and PLC channels are shown in Figs. 67 and 68, respectively, in terms of power spectral density (PSD) in its maximum, minimum and mean values. In the wireless noise it is very clear the presence of narrowband noise, such as those from FM stations in frequencies around 100 MHz. Considering the entire ( $FB_T$ ) frequency band, background-noise PSD mean value was around  $-114$  dBm/Hz.

Figure 68 presents the noise measured in electric power grids, where the exponential behavior of background noise, which is typical in PLC channels, together with high energy in low frequencies is evident. Also, some high-frequency narrowband noise components can be identified, agreeing with those measured in the air. A comparison between PSDs obtained in both environments indicates that severe noise is observed in PLC channel, mainly for low frequencies but with less variations between minimum and maximum values for high frequencies.

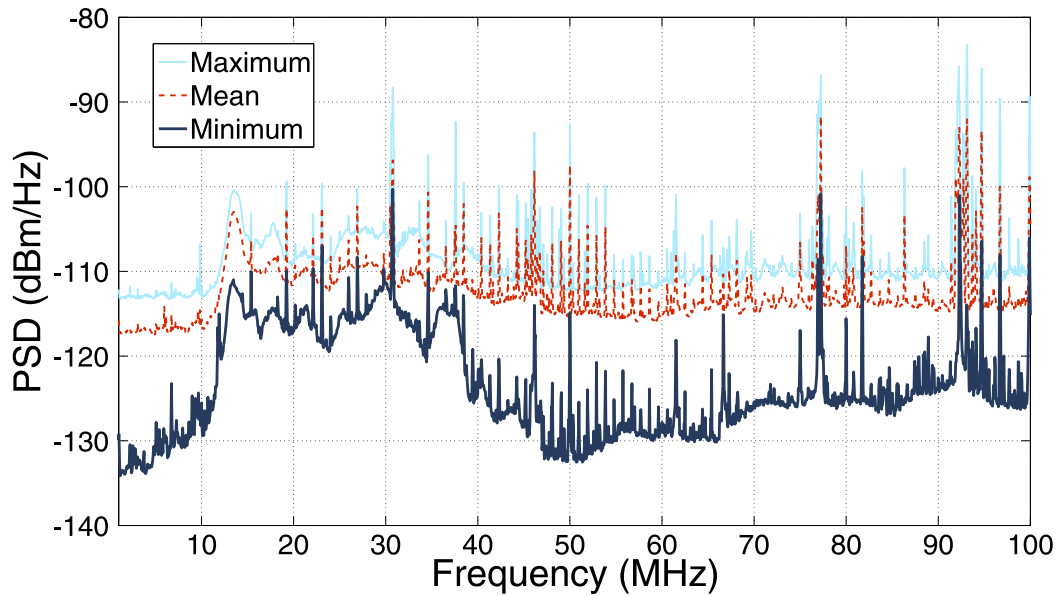


Figure 67: Statistical parameters of PSD of the additive noise at the input of the hybrid-wireless transceiver.

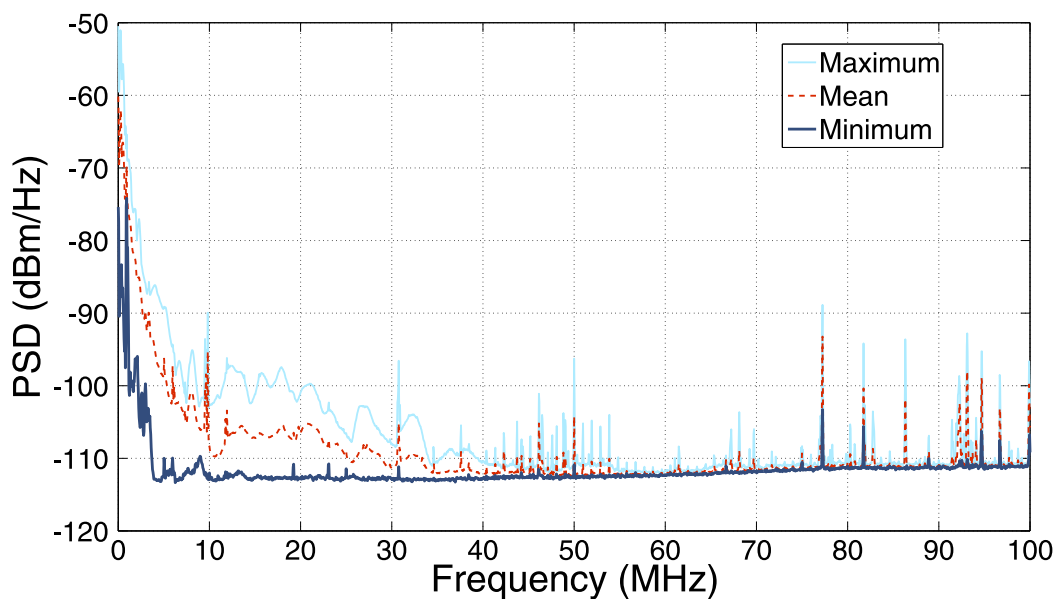


Figure 68: Statistical parameters of PSD of the additive noise at the input of the hybrid-PLC transceiver.

### 4.3.8 Channel capacity

The additive noise described in Subsection 4.3.7 was taken into account to estimate the channel capacity offered by the hybrid PLC-wireless channel, for the frequency band  $FB_T$ . Figure 69 shows the mean values of channel capacities for the *short-path* and *long-path channels*, respectively, considering both transmission directions (PLC-to-wireless and wireless-to-PLC). For this plot, the channel capacity was evaluated with PSD transmission power ranging from  $-90$  to  $-50$  dBm/Hz in steps of 5 dBm/Hz. As expected, *short-path channel* exhibits higher capacity than *long-path channel*. Also, higher capacities were observed in PLC-to-wireless transmission direction due to high power noise presence in the PLC channel. Thus, the hybrid PLC-wireless channels are asymmetrical from a channel capacity point of view, due to the additive noise.

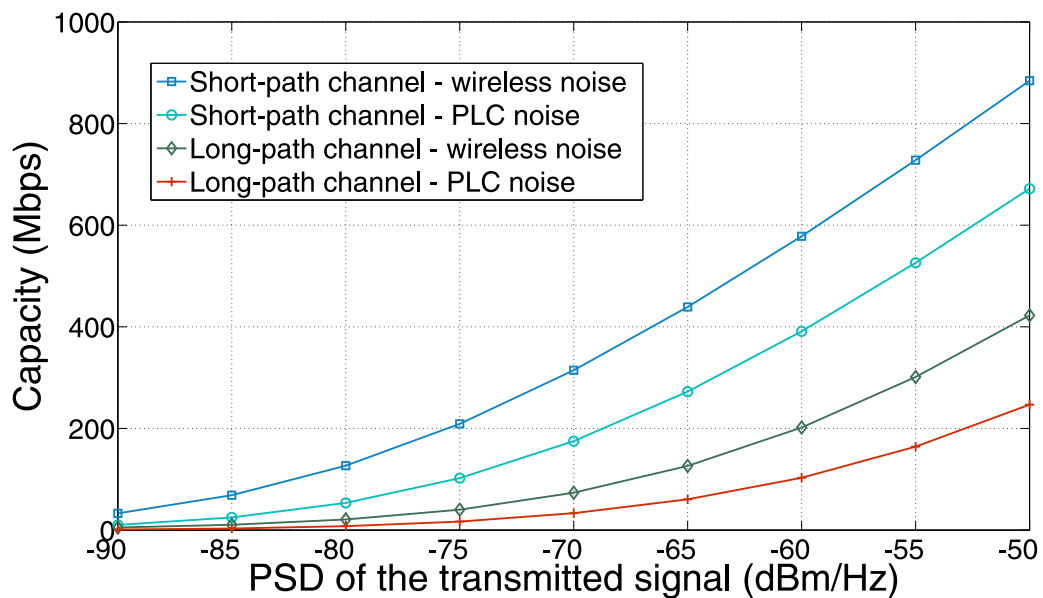


Figure 69: Mean values of channel capacity for the *short-path* and *long-path channels*.

Figure 70 shows the empirical complementary cumulative distribution function (CCDF) of the channel capacity for hybrid PLC-wireless in both transmission directions. In this case, the PSD of the transmitted signal was made  $-55$  dBm/Hz in the frequency band from 1.7 up to 30 MHz and  $-80$  dBm/Hz in the remainder frequencies. This PSD is the limit proposed for PLC systems [99]. For *short-path channel*, the minimal achieved capacity was 16 Mbps, whereas for *long-path channel* the minimal capacity was around 3 Mbps. Also, it is interesting to note that channel capacity is higher than 150 Mbps in 50% of the observed cases for the PLC-to-wireless direction of a *short-path channel* and can surpass 450 Mbps. If the transmission direction is considered, a difference of up to 139 Mbps and 46 Mbps in the capacity is observed for *short-path channel* and *long-path channel*, respectively.

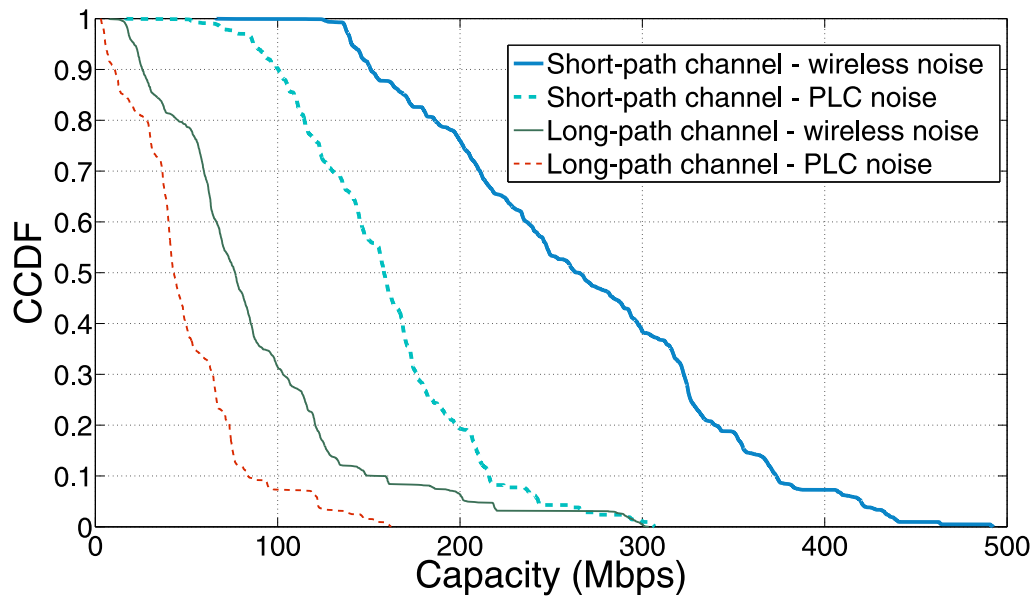


Figure 70: CCDF of channel capacity for *short-path channel* and *long-path channel*.

#### 4.4 SUMMARY

This chapter presented a new communication medium established between PLC and wireless devices, named hybrid PLC-wireless channel. Some statistical analyzes showed that hybrid PLC-wireless channels are strongly frequency selective, exhibit high attenuation levels and present symmetrical magnitude responses (irrespective to the transmission direction). The hybrid PLC-wireless channel is more flat and time varying than the measured PLC channels. Also, the hybrid PLC-wireless channel is asymmetric in terms of channel capacity, since the noise in PLC and wireless channels are completely different. Finally, capacities higher than 200 Mbps was observed when the PSD of the transmitted signal was assumed to be of -50 dBm/Hz. The follow chapter will summarize the main conclusions of this thesis.

## 5 CONCLUSIONS

Regarding the methodology for the estimation of the electric power grids, presented in Chap. 2, the following conclusions can be highlighted:

- A detailed description of a complete methodology to estimate CFR of electric power grids for power line communication was given. The presented methodology incorporates frequency sampling offset error estimation and correction, timing synchronization, channel estimation and channel estimation enhancement that improve the quality of the frequency response estimates.
- The reported results, based on both synthetic and measured data, showed that the methodology is effective. By using PLC channel models, it was verified that the proposed method contribute to offer reliable estimates of CFR. It was shown that the presented methodology is capable of estimating CFR of both linear time invariant and linear and periodically time varying PLC channels in low voltage and indoor electric power grids, while the VNA can only characterize linear time invariant PLC channels.
- The efficiency of the described methodology was corroborated by experimental results where estimates of CFR of a PLC coupler and monophasic transformers were compared to estimates provided by a VNA. Based on the attained results, the presented methodology can be very useful for both power line communication and power system applications.

With respect to the characterization of Brazilian in-home PLC channels, reported in Chap. 3, some important conclusions are:

- That chapter presented and discussed several features of Brazilian in-home PLC channels, which are quite relevant for modeling and designing PLC systems that will operate not only in electric power grids of developed countries, but also in developing ones. The analysis were performed considering three frequency bands: from 1.7 up to 30 MHz (Band A), from 1.7 up to 50 MHz (Band B) and from 1.7 up to 100 MHz (Band C).
- The analyzes for the frequency band regulated in Brazil for PLC operation (from 1.7 up to 50 MHz) constitute an important reference to the development of PLC systems to operate in Brazilian in-home electric power grids. The features considered here included the average channel gain or attenuation, the coherence bandwidth, the root mean squared delay spread, the coherence time, the channel capacity and the noise profile.

- Measurement framework (the setup and the HS-OFDM sounding-based approach) avoided the use of a vectorial network analyzer, which often requires a sweep time much longer than the typical coherence time of in-home PLC channel. Hence, the employed framework was able to characterize the time-varying behavior of the PLC channel in a reliable manner.
- The comparisons performed in this work reinforce the assumption that electric power grids in in-home facilities can have a strongly different behavior in different locations. For instance, Brazilian in-home PLC channels seem to be more suitable for communication purposes as they presented smaller attenuations than those analyzed in countries such as US, France and Spain, which are not well discussed in the literature. This may be associated with the fact that typical Brazilian residences are smaller and contain less electrical appliances than in US and Europe.
- Broadband applications can succeed if the PLC system operates in the frequency band of up to 100 MHz, because channel capacities higher than 1 Gbps can be achieved.
- The statistical modeling of the ACA, RMS-DS, CB and CT, was performed. The attained results indicates that the ACA feature is better fitted by the Skew-normal distribution in Band A, and by the Nakagami distribution in Band B and Band C. The RMS-DS is better fitted in all analyzed frequency bands by a Gamma distribution, having the Log-normal distribution quite similar fitting. Regarding CB, the best fit is associated with the Inverse Gaussian for Band A and Band C, while the Log-logistic distribution offers the best fit for Band B. Finally, the Skew-normal distribution is the statistical distribution that better fits the CT dataset all analyzed frequency bands.

Regarding the hybrid PLC-wireless channel, proposed and characterized in Chap. 4, the following conclusions are noteworthy:

- That chapter focused on the characterization of the hybrid PLC-wireless channels that emerge from the exploitation of the benefits of the intrinsic and traditionally unwanted radiation in unshield power cables to provide mobility in PLC systems. Several statistical parameters of hybrid PLC-wireless channels were presented and analyzed, considering an entire frequency band ranging from 1.7 MHz up to 100 MHz, as well as some subbands within it.
- Based on estimates of the hybrid PLC-wireless channels obtained in a measurement campaign carried out inside two residences and five apartments, two scenarios (*short-path* and *long-path channels*) were devised and thoroughly analyzed.

- The statistical analyzes showed that hybrid PLC-wireless channels are strongly frequency selective, exhibit high attenuation levels and present symmetrical magnitude responses (irrespective to the transmission direction).
- The statistical modeling of ACA, the RMS-DS, the CB and the CT was performed. The attained results revealed that the ACA feature is better fitted by the Skew-normal distribution for both *short-* and *long-path* channel types. The RMS-DS is better fitted by the Log-logistic distribution for the *short-path* case while the Inverse Gaussian is the statistical distribution that best fits the RMS-DS for the *long-path* case. Also, for the RMS-DS in both cases, the Log-normal distribution presented quite similar fitting. Regarding the CB, the best fit is associated to the Log-logistic distribution for the *short-path* channel and the t-Student distribution for the *long-path* channel. The Logistic distribution is the statistical distribution that better fits the CT dataset for the *short-path* channel and the Skew-normal provides the best fit for the *long-path* scenario.
- The presented statistical models can offer the means to design and evaluate hybrid PLC-wireless communication systems to facilitate the widespread of smart grid technologies into the power systems. Channel capacities surpassing 450 Mbps can be achieved for *short-path channel*, when transmitter-received distances are below 2 meters could be observed. When this distance is increased, within a range from 2 to 6 meters, channel capacities above 85 Mbps were still observed for more than 90% of measured hybrid PLC-wireless channels.
- This work will promote the development of PLC-based mobile and untethered communication applications such as in wireless sensor network, smart energy, intelligent buildings, and related areas. Finally, hybrid communication systems can be seen as an interesting and promising technology for dealing with digital divide in developing and underdeveloped countries.

## 5.1 FUTURE WORKS

Future efforts can be addressed in order to:

- Develop a prototype of a PLC analyzer based on the methodology described in Chap. 2, in which constitutes an important tool to be used for electric utilities in order to evaluate any electric power grid considered as a candidate to provide data communication.
- Propose a model for the channel impulse response and/or channel frequency response of Brazilian in-home PLC and hybrid PLC-wireless channels. Evaluate the impact

of other kind of antennas in the features related with hybrid PLC-wireless channels, and develop the own antenna.

- Perform a measurement campaign aiming at the characterization of outdoor Brazilian PLC and hybrid PLC-wireless channels. Additionally, complementary efforts can be made to characterize medium- and high voltage power lines. Develop a wireless device to be used in order to interact with a PLC system, operating at the same frequency band, by means of the hybrid PLC-wireless channel.

## REFERENCES

- [1] HRASNICA, H.; HAIDINE, A.; LEHNERT, R. *Broadband PowerLine Communications Network Design*. John Wiley & Sons, 2004.
- [2] GOTZ, M.; RAPP, M.; DOSTERT, K. Power line channel characteristics and their effect on communication system design. *IEEE Communications Magazine*, v. 42, n. 4, p. 78-86, Apr. 2004.
- [3] GEBHARDT, M.; WEINMANN, F.; DOSTERT, K. Physical and regulatory constraints for communication over the power supply grid. *IEEE Communications Magazine*, v. 41, n. 5, p. 84-90, May 2013.
- [4] IEC 610003-8, Electromagnect Compatibility (EMC) - Part 3: Limits - Section 8: Signaling on Low-Voltage Electrical Installations - Emission levels, Frequency bands and Electromagnect Disturbances levels. Geneva, Switzeland, 2002.
- [5] FCC, Code of Federal Regulations - Title 47: Telecommunication - Chapter I: FCC Part 15 - Radio Frequency Devices. Washington, DC, 2002.
- [6] CISPR 22, Information Technology Equipment - Radio Disturbance Characteristics - Limits and Methods of Measurement. Geneva, Switzeland, 2002.
- [7] DOSTERT, K. Telecommunications over the Power Distribution Grid - Possibilities and Limitations. *Proc. International Symposium on Powerline Communications and Its Applications*, 1997.
- [8] STIEVANO, I. S.; CANAVERO, F. G.; GARCIA VALVERDE, W. R.; GUERRIERI, L.; BISAGLIA, P. Multipath Modeling of Automotive Power Line Communication Channels. *IEEE Trans. on Industrial Informatics*, v. 10, n. 2, p. 1381-1391, May 2014.
- [9] LIENARD, M.; CARRION, M. O.; DEGARDIN, V.; DEGAUGUE, P. Modeling and Analysis of In-Vehicle Power Line Communication Channels. *IEEE Trans. on Vehicular Technology*, v. 57, n. 2, p. 670-679, Mar. 2008.
- [10] BARMADA, S.; RAUGI, M.; TUCCI, M.; ZHENG, T. Power Line Communication in a full electric vehicle: Measurements, modelling and analysis. *Proc. IEEE International Symposium on Power Line Communications and Its Applications*, p. 331-336, Mar. 2010.
- [11] VALLEJO-MORA, A. B.; SANCHEZ-MARTINEZ, J. J.; CANETE, F. J.; CORTES, J. A.; DIEZ, L. Analysis of In-vehicle Power Line Channel Response. *IEEE Latin America Transactions*, v. 9, n. 4, p. 445-450, Jul. 2011.
- [12] BASSI, E.; BENZI, F.; ALMEIDA, L.; NOLTE, T. Powerline communication in electric vehicles. *Proc. International Conference on Electric Machines and Drives*, p. 1749-1753, May. 2009.
- [13] MOHAMMADI, M.; LAMPE, L.; LOK, M.; MIRABBASI, S.; MIRVAKILI, M.; ROSALES, R.; VAN VEEN, P. Measurement study and transmission for in-vehicle power line communication. *Proc. IEEE International Symposium on Power Line Communications and Its Applications*, p. 73-78, Mar. 2009.

- [14] TAO ZHENG; RAUGI, M.; TUCCI, M. Time-Invariant Characteristics of Naval Power-Line Channels. *IEEE Trans. on Power Delivery*, v. 27, n. 2, p. 858-865, Apr. 2012.
- [15] BARMADA, S.; BELLANTI, L.; RAUGI, M.; TUCCI, M. Analysis of Power-Line Communication Channels in Ships. *IEEE Trans. on Vehicular Technology*, v. 59, n. 7, p. 3161-3170, 2010.
- [16] ANTONIALI, M.; TONELLO, A. M.; LENARDON, M.; QUALIZZA, A. Measurements and analysis of PLC channels in a cruise ship. *Proc. International Symposium on Power Line Communications and Its Applications*, p. 102-107, Apr. 2011.
- [17] BARMADA, S.; RAUGI, M.; TUCCI, M.; ZHENG TAO. Analysis of time-varying properties of Power Line Communication Channels in ships. *Proc. International Symposium on Power Line Communications and Its Applications*, p. 72-77, Apr. 2011.
- [18] DEGARDIN, V.; JUNQUA, I.; LIENARD, M.; DEGAUQUE, P.; BERTOUOL, S. Theoretical Approach to the Feasibility of Power-Line Communication in Aircrafts. *IEEE Trans. on Vehicular Technology*, v. 62, n. 3, p. 1362-1366, Mar. 2013.
- [19] DEGARDIN, V.; LALY, P.; LIENARD, M.; DEGAUQUE, P. Investigation on power line communication in aircrafts. *IET Communications*, v. 8, n. 10, p. 1868-1874, Jul. 2014.
- [20] DEGARDIN, V.; SIMON, E. P.; MORELLE, M.; LIENARD, M.; DEGAUQUE, P.; JUNQUA, I.; BERTUOL, S. On the possibility of using PLC in aircraft. *Proc. International Symposium on Power Line Communications and Its Applications*, p. 337-340, Mar. 2010.
- [21] BARMADA, S.; GAGGELLI, A.; MUSOLINO, A.; RIZZO, R.; RAUGI, M.; TUCCI, M. *Proc. International Symposium on Power Line Communications and Its Applications*, p. 13-17, Apr. 2008.
- [22] JINGCHENG LI; WHISNER, B.; WAYNERT, J. A. Measurements of Medium-Frequency Propagation Characteristics of a Transmission Line in an Underground Coal Mine. *IEEE Trans. on Industry Applications*, v. 49, n. 5, p. 1984-1991, Sep. 2013.
- [23] YAZDANI, J.; GLANVILLE, K.; CLARKE, P. Modelling, developing and implementing sub-sea power-line communications networks. *Proc. International Symposium on Power Line Communications and Its Applications*, p. 310-316, Apr. 2005.
- [24] LAI, S. W.; MESSIER, G. G. Using the Wireless and PLC Channels for Diversity. *IEEE Trans. on Communications*, v. 60, n. 12, p. 3865-3875, Dec. 2012.
- [25] LEE, JONG-HO; KINM, YOUNG-HWAS. Diversity Relaying for Parallel Use of Power-Line and Wireless Communication Networks. *IEEE Trans. on Power Delivery*, v. 29, n. 3, p. 1301-1310, Jun. 2014.
- [26] KUHN, M.; BERGER, S.; HAMMERSTROM, I.; WITTNEBEN, A. Power line enhanced cooperative wireless communications. *IEEE Journal on Selected Areas in Communications*, v. 24, n. 7, p. 1401-1410, 2006.

- [27] GONZALEZ, O. A.; URMINSKY, J.; CALVO, M.; DE-HARO, L. Performance analysis of hybrid broadband access technologies using PLC and Wi-Fi. *Proc. International Conference on Wireless Networks, Communications and Mobile Computing*, p. 564-569, Jun. 2005.
- [28] TLICH, M.; ZEDDAM, A.; MOULIN, F.; GAUTHIER, F. Indoor Power-Line Communications Channel Characterization Up to 100 MHz – Part I: One-Parameter Deterministic Model. *IEEE Trans. on Power Delivery*, v. 23, n. 3, p. 1392-1401, Jul. 2008.
- [29] PARSONS, J. D.; DEMERY, D. A.; TURKMANI, A. M. D. Sounding techniques for wideband mobile radio channels: a review. *IEEE Proceedings in Communications, Speech and Vision*, v. 138, n. 5, p. 437-446, Oct. 1991.
- [30] TANG, L. T.; SO, P. L.; GUNAWAN, E.; GUAN, Y. L.; CHEN, S.; LIE, T. T. Characterization and modeling of in-building power lines for high-speed data transmission. *IEEE Transactions on Power Delivery*, v. 18, n. 1, p. 69-77, Jan. 2003.
- [31] VERSOLATTO, F.; TONELLO, A. M. On the relation between geometrical distance and channel statistics in in-home PLC networks. *Proc. IEEE International Symposium on Power Line Communications and Its Applications*, p. 280-285, Mar. 2012.
- [32] TONELLO, A. M.; VERSOLATTO, F.; PITTOLO, A. In-Home Power Line Communication Channel: Statistical Characterization. *IEEE Transactions on Communications*, v. 62, n. 6, p. 2096-2106, Jun. 2014.
- [33] GASSARA, H.; ROUISSI, F.; GHAZEL, A. Statistical Characterization of the Indoor Low-Voltage Narrowband Power Line Communication Channel. *IEEE Transactions on Electromagnetic Compatibility*, v. 56, n. 1, p. 123-131, Feb. 2014.
- [34] TAHERINEJAD, N.; ROSALES, R.; LAMPE, L.; MIRABBASI, S. Channel characterization for power line communication in a hybrid electric vehicle. *Proc. IEEE International Symposium on Power Line Communications and Its Applications*, p. 328-333, Mar. 2012.
- [35] CANETE, F. J.; CORTES, J. A.; DIEZ, L.; ENTRANBASAGUAS, J. T. Analysis of the cyclic short-term variation of indoor power line channels. *IEEE Journal on Selected Areas in Communications*, v. 24, n. 7, p. 1327-1338, Jul. 2006.
- [36] PICORONE, A. A. M.; NETO, R. S.; RIBEIRO, M. V. Coherence time and sparsity of Brazilian outdoor PLC channels: A preliminary analysis. *Proc. IEEE International Symposium on Power Line Communications and its Applications*, p. 1-5, Mar. 2014.
- [37] WELCH, P. The use of fast Fourier transform for the estimation of power spectra: A method based on time averaging over short, modified periodograms. *IEEE Trans. on Audio and Electroacoustics*, v. 15, n. 2, p. 70-73, Jun. 1967.
- [38] ZHAI MINGYUE. Measurements and Channel Characteristics of LV Power Line Communications Networks in China. *Proc. IEEE International Symposium on Power Line Communications and Its Applications*, p. 212-216, Mar. 2006.
- [39] NAVARRO, M.; MORENO, J. A. Field channel measurements in a medium voltage overhead power line. *Proc. IEEE International Symposium on Power Line Communications and Its Applications*, p. 458-462, Apr. 2011.

- [40] HAITAO LIU; JIAN SONG; BINGZHEN ZHAO; XIAO LI. Channel Study for Medium-Voltage Power Network. *Proc. IEEE International Symposium on Power Line Communications and Its Applications*, p. 245-250, Mar. 2006.
- [41] ZIMMERMANN, M.; DOSTERT, K. A multipath model for the powerline channel. *IEEE Trans. on Communications*, v. 50, n. 4, p. 553-559, Apr. 2002.
- [42] GALLI, S. A simple two-tap statistical model for the power line channel. *Proc. IEEE International Symposium on Power Line Communications and its Applications*, p. 242-248, Mar. 2010.
- [43] Vector Network analyzer E5061B, Agilent. <http://cp.literature.agilent.com/litweb/pdf/5990-4392EN.pdf>.
- [44] HOLGER PHILIPPS. Performance Measurements of Power line Channels at High Frequencies. *Proc. International Symposium on Power Line Communications and Its Applications*, p. 229-237, Mar. 1998.
- [45] DA COSTA PINTO, F.; SCORALICK, F. S. O.; DE CAMPOS, F. P. V.; ZHI QUAN; RIBEIRO M. V. A low cost OFDM based modulation schemes for data communication in the passband frequency. *Proc. IEEE International Symposium on Power Line Communications and Its Applications*, p. 424-429, Apr. 2011.
- [46] , HANZO, L.; KELLER, T. *OFDM and MC-CDMA*. John Wiley & Sons, 2006.
- [47] MINN, H.; BHARGAVA, V. K.; LETAIEF, K. B. A robust timing and frequency synchronization for OFDM systems. *IEEE Transactions on Wireless Communications*, v. 2, n. 4, p. 822-839, Jul. 2003.
- [48] MENG-HAN HSIEH; CHE-HO WEI. A low-complexity frame synchronization and frequency offset compensation scheme for OFDM systems over fading channels. *IEEE Transactions on Vehicular Technology*, v. 48, n. 5, p. 1596-1609, Sep. 1999.
- [49] MULLER-WEINFUTER, S. H. On the optimality of metrics for coarse frame synchronization in OFDM: a comparison. *Proc. IEEE International Symposium on Personal, Indoor and Mobile Radio Communications*, p. 533-537, Sep. 1998.
- [50] TZI-DAR CHEUEH; PEI-YUN TSAI. *OFDM Baseband Receiver Design for Wireless Communications*. John Wiley & Sons, 2007.
- [51] KELLER, T.; HANZO, L. Orthogonal frequency division multiplex synchronisation techniques for wireless local area networks. *Proc. IEEE International Symposium on Personal Indoor and Mobile Radio Communications*, p. 963-967, Oct. 1996.
- [52] VAN DE BEEK, J. J.; BORJESSON, P. O.; BOUCHERET, M. L.; LANDSTROM, D.; ARENAS, J. M.; and ODLING, P.; OSTBERG, C.; WAHLQVIST, M.; WILSON, S. K. A time and frequency synchronization scheme for multiuser OFDM *IEEE Journal on Selected Areas in Communications*, v. 17, n. 11, p. 1900-1914, Nov. 1999.
- [53] VAN DE BEEK, J. J.; SANDELL, M.; BORJESSON, P. O. ML estimation of time and frequency offset in OFDM systems. *IEEE Trans. on Signal Processing*, v. 45, n. 7, p. 1800-1805, Jul. 1997.

- [54] CHEVILLAT, P.; MAIWALD, D.; UNGERBOECK, G. Rapid Training of a Voiceband Data-Modem Receiver Employing an Equalizer with Fractional-T Spaced Coefficients. *IEEE Trans. on Communications*, v. 35, n. 9, p. 869-876, Sep. 1987.
- [55] CARDOSO, D. F.; BACKX, F. D.; SAMPAIO-NETO, R. Improved Pilot-Aided Channel Estimation in Zero Padded MC-CDMA Systems. *Proc. International Symposium on Wireless Pervasive Computing*, p. 1-5, Feb. 2009.
- [56] GARDNER, F. M. Interpolation in digital modems. I - Fundamentals. *IEEE Transactions on Communications*, v. 41, n. 3, Mar. 1993.
- [57] ERUP, L.; GARDNER, FLOYD M.; HARRIS, R. A. Interpolation in digital modems. II - Implementation and performance. *IEEE Transactions on Communications*, v. 41, n. 6, Jun. 1993.
- [58] Brazilian resolution for PLC. ANATEL. <http://legislacao.anatel.gov.br/resolucoes/2009/101-resolucao-527>, 2009.
- [59] CHO, Y. S.; KIM, J.; YANG, W. Y.; KANG, C. G. *MIMO-OFDM Wireless Communications with MATLAB*. Wiley, 2011.
- [60] MARTINEZ, S. J. J.; CORTES, J. A.; DIEZ, L.; CANETE, F. J.; TORRES, L. M. Performance analysis of OFDM modulation on indoor PLC channels in the frequency band up to 210 MHz. *Proc. IEEE International Symposium on Power Line Communications and Its Applications*, p. 38-43, Mar. 2010.
- [61] PLATERO, C. A.; BLAZQUEZ, F.; FRIAS, P.; RAMIREZ, D. Influence of Rotor Position in FRA Response for Detection of Insulation Failures in Salient-Pole Synchronous Machines. *IEEE Transactions on Energy Conversion*, v. 26, n. 2, p. 671-676, Jun. 2011.
- [62] MAREK, F.; JAKUB, F. Detection of winding faults in electrical machines using the frequency response analysis method. *Measurement Science and Technology*, v. 15, n. 10, p. 2067-2074, 2004.
- [63] ZHONGDONG, W.; JIE LI; SOFIAN, D. M. Interpretation of Transformer FRA Responses - Part I: Influence of Winding Structure. *IEEE Transactions on Power Delivery*, v. 24, n. 2, p. 703-710, Apr. 2009.
- [64] NARAYANA, G. S.; BADGUJAR, K. P.; KULKARNI, S. V. Factorisation-based transfer function estimation technique for deformation diagnostics of windings in transformers. *Electric Power Applications*, v. 7, n. 1, p. 39-46, Jan. 2013.
- [65] SETAYESHMEHR, A.; BORSI, H.; GOCKENBACH, E.; FOFANA, I. On-line monitoring of transformer via transfer function. *Proc. IEEE Electrical Insulation Conference*, p. 278-282, May 2009.
- [66] LAMARRE, L.; PICHER, P. Impedance Characterization of Hydro Generator Stator Windings and Preliminary Results of FRA Analysis. *Proc. IEEE International Symposium on Electrical Insulation*, p. 227-230, Jun. 2008.
- [67] FANG YANG; WENBO DING; JIAN SONG. Non-intrusive power line quality monitoring based on power line communications. *Proc. IEEE International Symposium on Power Line Communications and Its Applications*, p. 191-196, Mar. 2013.

- [68] MING-YUE ZHAI. Transmission Characteristics of Low-Voltage Distribution Networks in China Under the Smart Grids Environment. *IEEE Trans. on Power Delivery*, v. 26, n. 1, p. 173-180, Jan. 2011.
- [69] LAZAROPOULOS, A. G.; COTTIS, P. G. Transmission Characteristics of Overhead Medium-Voltage Power-Line Communication Channels. *IEEE Trans. on Power Delivery*, v. 24, n. 3, p. 1164-1173, Jul. 2009.
- [70] ZAJC, M.; SULJANOVIC, N.; MUJICIC, A.; TASIC, J. F. High voltage power line constraints for high speed communications. *Proc. Mediterranean Electrotechnical Conference*, v. 1, p. 285-288, May 2004.
- [71] AQUILUE, R.; RIBO, M.; REGUE, J. R.; PIJOAN, J. L.; SANCHEZ, G. Scattering Parameters-Based Channel Characterization and Modeling for Underground Medium-Voltage Power-Line Communications. *IEEE Trans. on Power Delivery*, v. 24, n. 3, p. 1122-1131, Jul. 2009.
- [72] TLICH, M.; ZEDDAM, A.; MOULIN, F.; GAUTHIER, F. Indoor Power-Line Communications Channel Characterization up to 100MHz - Part II: Time-Frequency Analysis. *IEEE Trans. on Power Delivery*, v. 23, n. 3, p. 1402-1409, Jul. 2008.
- [73] JONES, C. H. Communications Over Aircraft Power Lines. *Proc. IEEE International Symposium on Power Line Communications and Its Applications*, p. 149-154, Mar. 2006.
- [74] GALLI, S.; SCAGLIONE, A.; ZHIFANG WANG. For the Grid and Through the Grid: The Role of Power Line Communications in the Smart Grid. *Proceedings of the IEEE*, v. 99, n. 6, p. 998-1027, Jun. 2011.
- [75] WENQUING LIU; SIGLE, M.; DOSTERT, K. Channel characterization and system verification for narrowband power line communication in smart grid applications. *IEEE Communications Magazine*, v. 49, n. 12, p. 28-35, Dec. 2011.
- [76] VERSOLATTO, F.; TONELLO, A. M. PLC channel characterization up to 300 MHz: Frequency response and line impedance. *Proc. IEEE Global Communications Conference*, p. 3525-3530, Dec. 2012.
- [77] GALLI, S. A Novel Approach to the Statistical Modeling of Wireline Channels. *IEEE Trans. on Communications*, v. 59, n. 5, p. 1332-1345, May 2011.
- [78] CANETE, F. J.; DIEZ, L.; CORTES, J. A.; ENTRAMBASAGUAS, J. T. Broadband modelling of indoor power-line channels. *IEEE Trans. on Consumer Electronics*, v. 48, n. 1, p. 175-183, Feb. 2002.
- [79] CANETE, F. J.; CORTES, J. A.; DIEZ, L.; ENTRAMBASAGUAS, J. T. A channel model proposal for indoor power line communications. *IEEE Communications Magazine*, v. 49, n. 12, p. 166-174, Dec. 2011.
- [80] CORTES, J. A.; CANETE, F. J.; DIEZ, L.; MORENO, J. L. G. On the statistical properties of indoor power line channels: Measurements and models. *Proc. IEEE International Symposium on Power Line Communications and Its Applications*, p. 271-276, Apr. 2011.

- [81] GALLI, S. A simplified model for the indoor power line channel. *Proc. IEEE International Symposium on Power Line Communications and Its Applications*, p. 13-19, Mar. 2009.
- [82] TONELLO, A. M.; VERSOLATTO, F.; BEJAR, B.; ZAZO, S. A Fitting Algorithm for Random Modeling the PLC Channel. *IEEE Trans. on Power Delivery*, v. 27, n. 3, p. 1477-1484, Jul. 2012.
- [83] PROAKIS, J. *Digital Communications*. New York, NY, USA: McGraw-Hill, 2007.
- [84] THOMAS M. COVER; JOY A. THOMAS. *Elements of Information Theory*. John Wiley & Sons, 2006.
- [85] SIMON, M. K.; ALOUINI, M. S. *Digital Communication over Fading Channels*. John Wiley & Sons, 2000.
- [86] PAVLOVIC, D. C.; SEKULOVIC, N. M.; MILOVANOVIC, G. V.; PANAJOTOVIC, A. S.; STEFANOVIC, M. C.; POPOVIC, Z. J. Statistics for Ratios of Rayleigh, Rician, Nakagami-m, and Weibull Distributed Random Variables. *Mathematical Problems in Engineering*, 2013.
- [87] SHANKAR, P. M. Performance Analysis of Diversity Combining Algorithms in Shadowed Fading Channels. *Wireless Personal Communications*, v. 37, n. 1, p. 61-72, 2006.
- [88] TRIGUI, I.; LAOURINE, A.; AFFES, S.; STEPHENNE, A. The Inverse Gaussian Distribution in Wireless Channels: Second-Order Statistics and Channel Capacity. *IEEE Transactions on Communications*, v. 60, n. 11, p. 3167-3173, Nov. 2012.
- [89] MOOD, A. M.; GRAYBILL, F. A.; BOES, D. C. *Introduction to the Theory of Statistics*. McGraw Hill, 1974.
- [90] CASELLA, G.; BERGER, R. *Statistical Inference*. Duxbury, 2002.
- [91] CABRAL, C. R. B.; LACHOS, V. H.; ZELLER, C. B. Multivariate measurement error models using finite mixtures of skew-Student t distributions. *Journal of Multivariate Analysis*, v. 124, n. C, p. 179-198, 2014.
- [92] O'MAHONY, B. Field Testing of High-Speed Power Line Communications in North American Homes. *Proc. IEEE International Symposium on Power Line Communications and Its Applications*, p. 155-159, Mar. 2006.
- [93] ZAR, J. H. *Biostatistical Analysis*. Pearson, 2010.
- [94] LIN, M.; LUCAS, H. C. and SHMUELI, G. Too Big to Fail: Large Samples and the p-Value Problem. *Information Systems Research*, v. 24, n. 4, p. 906-917, 2013.
- [95] ROYALL, R. M. The Effect of Sample Size on the Meaning of Significance Tests. *The American Statistician*, v. 40, n. 4, p. 313-315, Nov. 1986.
- [96] GALLI, S.; BANWELL, T. A novel approach to the modeling of the indoor power line channel-Part II: Transfer function and its properties. *IEEE Trans. on Power Delivery*, v. 20, n. 3, p. 1869-1878, Jul. 2005.

- [97] ZIMMERMANN, M.; DOSTERT, K. Analysis and modeling of impulsive noise in broad-band powerline communications. *IEEE Trans. on Electromagnetic Compatibility*, v. 44, n. 1, p. 249-258, Feb. 2002.
- [98] HASHMAT, R.; PAGANI, P.; ZEDDAM, A.; CHONAVEL, T. MIMO communications for inhome PLC networks: Measurements and results up to 100 MHz. *Proc. IEEE International Symposium on Power Line Communications and Its Applications*, p. 120-124, Mar. 2010.
- [99] PRAHO, B.; TLICH, M.; PAGANI, P.; ZEDDAM, A.; NOUVEL, F. Cognitive detection method of radio frequencies on power line networks. *Proc. IEEE International Symposium on Power Line Communications and Its Applications*, p. 225-230, Mar. 2010.
- [100] BOICE JR, J. D.; TARONE, R. E. Cell Phones, Cancer and Children. *Journal of the National Cancer Institute*, v. 103, n. 16, p. 1211-1213, Jul. 2011.
- [101] HIRATA, A.; MORITA, M.; SHIOZAWA, T. Temperature increase in the human head due to a dipole antenna at microwave frequencies. *IEEE Trans. on Electromagnetic Compatibility*, v. 45, n. 1, p. 109-116, Feb. 2003.
- [102] HIRATA, A., SHIOZAWA, T. Correlation of maximum temperature increase and peak SAR in the human head due to handset antennas. *IEEE Trans. on Microwave Theory and Techniques*, v. 51, n. 7, p. 1834-1841, Jul. 2003.
- [103] WAINWRIGHT, P. Thermal effects of radiation from cellular telephones. *Physics in Medicine and Biology*, v. 45, n. 8, p. 2363-2372, 2000.
- [104] PAHLAVAN, K.; HOWARD, S. J. Frequency domain measurements of indoor radio channels. *Electronics Letters*, v. 25, n. 24, p. 1645-1647, Nov. 1989.
- [105] JANSSEN, G. J. M.; STIGER, P. A.; PRASAD, R. Wideband indoor channel measurements and BER analysis of frequency selective multipath channels at 2.4, 4.75, and 11.5 GHz. *IEEE Trans. on Communications*, v. 44, n. 10, p. 1272-1288, Oct. 1996.

## APPENDIX A – List of Contributions

### A.1 Related with Chap. 2

- Journals:
  - Oliveira, Thiago R.; Marques, Cristiano A. G.; Finamore, Weiler A.; Netto, Sérgio L.; Ribeiro, Moisés V. A Methodology for Estimating Frequency Responses of Electric Power Grids. *Journal of Control, Automation and Electrical Systems*, v. 25, p. 720-731, 2014.
  - Picorone, Antônio. A. M.; Oliveira, Thiago. R.; Ribeiro, Moisés. V. PLC Channel Estimation Based on Pilot Signals for OFDM Modulation: A Review. *Revista IEEE América Latina*, v. 12, p. 580, 2014.
- Conference Papers:
  - Oliveira, Thiago R.; Finamore, Weiler A.; Ribeiro, Moisés V. A Sounding Method based on OFDM Modulation for PLC Channel Measurement. *Proc IEEE International Symposium on Power Line Communications and Its Applications (ISPLC)*, 2013, Johannesburg.
  - Ribeiro, Moisés V.; Marques, Cristiano A. G.; Colen, Guilherme; Oliveira, Thiago R.; Campos, Fabricio P. Measurement Setup for Characterizing Low-Voltage and Outdoor Electric Distribution Grids for PLC Systems. *Proc. Conference on Innovative Smart Grid Technologies (ISGT-LA)*, 2013, São Paulo.
  - Marques, Cristiano A. G.; Campos, Fabricio P.; Oliveira, Thiago R.; Menezes, Alan; Ribeiro, Moisés V. Analysis of a Hybrid OFDM Synchronization Algorithm for Power Line Communication. *Proc IEEE International Symposium on Power Line Communications and Its Applications (ISPLC)*, 2010, Rio de Janeiro.
- Patent Filing:
  - Oliveira, Thiago R.; Ribeiro, Moisés V. Metodologia e Equipamentos para a Estimaco da Resposta em Frequncia de Canais PLC (Power Line Communication) e a Deteco e Segmentaco de Rudos Impulsivos em Redes Eltricas. Patente depositada no INPI em 05/07/2011, nmero 0200110070470, Brasil.

### A.2 Related with Chap. 3

- Conference Papers:

- Oliveira, Thiago R.; Zeller, Camila B.; Netto, Sérgio L.; Ribeiro, Moisés V. Statistical Modeling of the Average Channel Gain and Delay Spread in In-Home PLC Channels. Proc IEEE International Symposium on Power Line Communications and Its Applications (ISPLC), 2015, Austin.
- Valencia, Juan; Oliveira, Thiago R.; Andrade, Fernando J. A.; Ribeiro, Moisés V. Statistical Analysis of Brazilian In-Home PLC Channels: First Results. Proc IEEE International Symposium on Power Line Communications and Its Applications (ISPLC), 2014, Glasgow.
- Valencia, J.; Oliveira, Thiago R.; Ribeiro, Moisés V. Cooperative Power Line Communication: Analysis of Brazilian In-Home Channels. Proc IEEE International Symposium on Power Line Communications and Its Applications (ISPLC), 2014, Glasgow.
- Andrade, Fernando J. A.; Marques, Cristiano A. G.; Oliveira, Thiago R.; Campos, Fabricio P.; Oliveira, Edimar J.; Ribeiro, Moisés V. Preliminary Analysis of Additive Noise on Outdoor and Low Voltage Electric Power Grid in Brazil. Proc IEEE International Symposium on Power Line Communications and Its Applications (ISPLC), 2013, Johannesburg.
- Oliveira, Thiago R.; Sa, Pedro C.; Barbosa, Sergio L. P.; Ribeiro, Moisés V. HOS-Based Impulsive Noise Detection Technique for Power Line Communication Systems. Proc IEEE International Symposium on Power Line Communications and Its Applications (ISPLC), 2010, Rio de Janeiro.

### A.3 Related with Chap. 4

- Conference Papers:

- Oliveira, Thiago R.; Marques, Cristiano A. G.; Pereira, Michelle S.; Netto, Sérgio L.; Ribeiro, Moisés V. The Characterization of Hybrid PLC-Wireless Channels: A preliminary Analysis. Proc IEEE International Symposium on Power Line Communications and Its Applications (ISPLC), 2013, Johannesburg.
- Oliveira, Thiago R.; Andrade, Fernando J. A.; Guilherme, Luis; Pereira, Michelle S.; Ribeiro, Moisés V. Measurement of Hybrid PLC-wireless Channels for Indoor and Broadband Data Communication. Proc XXXI Simpósio Brasileiro de Telecomunicações (SBrT), 2013, Fortaleza.

## APPENDIX B – Statistical Distributions

This appendix summarizes the pdf's of the statistical distributions applied in this work to model some channel features.

- Exponential:

$$f(x|\mu) = \frac{1}{\mu} e^{-\frac{x}{\mu}}, \quad \mu > 0. \quad (\text{B.1})$$

Parameter description:

- $\mu$  (mean).

- Gamma:

$$f(x|a, b) = \frac{1}{b^a \Gamma(a)} x^{a-1} e^{-\frac{x}{b}}, \quad x > 0. \quad (\text{B.2})$$

Parameters description:

- $a$  (shape parameter).
- $b$  (shape parameter).

- Inverse Gaussian:

$$f(x|\mu, \lambda) = \sqrt{\frac{\lambda}{2\pi^2 x^3}} \exp\left\{-\frac{\lambda}{2\mu^2 x}(x - \mu)^2\right\}, \quad x > 0. \quad (\text{B.3})$$

Parameters description:

- $\mu$  (shape parameter).
- $\lambda$  (shape parameter).

- Logistic:

$$f(x|\mu, \sigma) = \frac{\exp\left\{\frac{x-\mu}{\sigma}\right\}}{\sigma \left(1 + \exp\left\{\frac{x-\mu}{\sigma}\right\}\right)^2}, \quad -\infty < x < \infty. \quad (\text{B.4})$$

Parameters description:

- $\mu$  (mean).
- $\sigma$  (scale parameter).

- Log-logistic:

$$f(x|\mu, \sigma) = \frac{1}{\sigma} \frac{1}{x} \frac{e^z}{(1 + e^z)^2}, \quad x \geq 0, \quad (\text{B.5})$$

where  $z = \frac{\log(x) - \mu}{\sigma}$ .

Parameters description:

- $\mu$  (log mean).
- $\sigma$  (log scale parameter).

- Log-normal:

$$f(x|\mu, \sigma) = \frac{1}{x\sigma\sqrt{2\pi}} \exp\left\{-\frac{(\ln x - \mu)^2}{2\sigma^2}\right\}, \quad x > 0. \quad (\text{B.6})$$

Parameters description:

- $\mu$  (mean).
- $\sigma$  (log standard deviation).

- Nakagami:

$$f(x|\mu, \omega) = 2 \left(\frac{\mu^\mu}{\omega}\right) \frac{1}{\Gamma(\mu)} x^{2\mu-1} \exp\left\{-\frac{\mu}{\omega} x^2\right\}, \quad x > 0, \quad (\text{B.7})$$

where  $\Gamma(\cdot)$  is the Gamma function.

Parameters description:

- $\mu$  (shape parameter).
- $\omega$  (scale parameter).

- Normal:

$$f(x|\mu, \sigma) = \frac{1}{\sigma\sqrt{2\pi}} e^{-\frac{(x-\mu)^2}{2\sigma^2}}, \quad -\infty < x < \infty. \quad (\text{B.8})$$

Parameters description:

- $\mu$  (mean).
- $\sigma$  (standard deviation).

- Rayleigh:

$$f(x|b) = \frac{x}{b^2} \exp\left\{-\frac{x^2}{2b^2}\right\}, \quad x \geq 0. \quad (\text{B.9})$$

Parameter description:

- $b$  (defining parameter).

- Rician:

$$f(x|s, \sigma) = I_0\left(\frac{xs}{\sigma^2}\right) \left(\frac{x}{\sigma^2}\right) \exp\left\{-\frac{x^2 + s^2}{2\sigma^2}\right\}, \quad x \geq 0, \quad (\text{B.10})$$

where  $I_0$  is the zero-order modified Bessel function of the first kind.

Parameters description:

- $s$  (noncentrality parameter).
- $\sigma$  (scale parameter).

- Skew-normal:

$$f(x|\gamma, \mu, \sigma) = 2\phi(x)\Phi(\gamma x), \quad -\infty < x < \infty, \quad (\text{B.11})$$

where  $\phi(\cdot)$  and  $\Phi(\cdot)$  denotes the probability density function (PDF) and the CDF of the standard Normal statistical distribution in which the pdf is denoted by  $f(x|\mu, \sigma)$ .

Parameters description:

- $\gamma$  (shape parameter).
- $\mu$  (mean).
- $\sigma$  (standard deviation).

- t-Student:

$$f(x|\mu, \sigma, \nu) = \frac{\Gamma\left(\frac{\nu+1}{2}\right)}{\sigma\sqrt{\nu\pi}\Gamma\left(\frac{\nu}{2}\right)} \left[ \frac{\nu + \left(\frac{x-\mu}{\sigma}\right)^2}{\nu} \right]^{-\left(\frac{\nu+1}{2}\right)}, \quad -\infty < x < \infty. \quad (\text{B.12})$$

Parameters description:

- $\mu$  (location parameter).
- $\sigma$  (scale parameter).
- $\nu$  (shape parameter).

- Weibull:

$$f(x|A, B) = \frac{B}{A} \left(\frac{x}{A}\right)^{B-1} \exp\left\{-\left(\frac{x}{A}\right)^B\right\}, \quad x \geq 0. \quad (\text{B.13})$$

Parameters description:

- $A$  (scale parameter).
- $B$  (shape parameter).

## APPENDIX C – MLE Results for PLC Channel Features

This appendix summarizes the results of the log-likelihood, AIC, BIC and EDC for several statistical distributions when applied to model ACA, CB, RMS-DS and CT estimated from the measured Brazilian in-door PLC channels.

Table 15: MLE results of the statistical distribution fitting of the ACA (dB) for Band A (SE is the estimated standard error).

Distribution	Parameter	Estimate	SE	Log-likelihood	AIC	BIC	EDC
Exponential Gamma	$\mu$	23.2804	0.0820	$-2.7412 \times 10^4$	$5.4825 \times 10^4$	$5.4827 \times 10^4$	$5.4839 \times 10^4$
	$a$	6.9369	0.0139	$-2.3451 \times 10^4$	$4.6906 \times 10^4$	$4.6909 \times 10^4$	$4.6934 \times 10^4$
	$b$	3.3560	0.0035				
Inverse Gaussian	$\mu$	23.2804	0.0137	$-2.3525 \times 10^4$	$4.7054 \times 10^4$	$4.7057 \times 10^4$	$4.7082 \times 10^4$
	$\lambda$	139.8050	5.9148				
Logistic	$\mu$	23.0296	0.0124	$-2.3802 \times 10^4$	$4.7608 \times 10^4$	$4.7612 \times 10^4$	$4.7637 \times 10^4$
	$\sigma$	5.1032	0.0026				
Log-logistic	$\mu$	3.0939	0.2621	$-2.3766 \times 10^4$	$4.7536 \times 10^4$	$4.7539 \times 10^4$	$4.7564 \times 10^4$
	$\sigma$	0.2346	0.0556				
Log-normal	$\mu$	3.0738	$0.2357 \times 10^{-4}$	$-2.3547 \times 10^4$	$4.7099 \times 10^4$	$4.7102 \times 10^4$	$4.7127 \times 10^4$
	$\sigma$	0.3946	$0.1179 \times 10^{-4}$				
Nakagami	$\mu$	1.9633	0.0010	$-2.3434 \times 10^4$	$4.6873 \times 10^4$	$4.6876 \times 10^4$	$4.6901 \times 10^4$
	$\omega$	616.0890	29.2519				
Normal	$\mu$	23.2804	0.0112	$-2.3606 \times 10^4$	$4.7215 \times 10^4$	$4.7219 \times 10^4$	$4.7244 \times 10^4$
	$\sigma$	8.6094	0.0056				
Rayleigh	$B$	17.5512	0.0117	$-2.4165 \times 10^4$	$4.8333 \times 10^4$	$4.8335 \times 10^4$	$4.8347 \times 10^4$
Rician	$s$	21.1317	0.0174	$-2.3542 \times 10^4$	$4.7088 \times 10^4$	$4.7092 \times 10^4$	$4.7117 \times 10^4$
	$\sigma$	9.2071	0.0093				
	$\mu$	22.7062	$1.2380 \times 10^{-2}$	$-2.3359 \times 10^4$	$4.6726 \times 10^4$	$4.6731 \times 10^4$	$4.6768 \times 10^4$
Skew-normal	$\sigma$	9.4122	$0.8141 \times 10^{-2}$				
	$\gamma$	0.9625	$1.5147 \times 10^{-3}$				
	$\mu$	23.2802	0.0112	$-2.3606 \times 10^4$	$4.7217 \times 10^4$	$4.7223 \times 10^4$	$4.7260 \times 10^4$
t-Student	$\sigma$	8.6091	0.0056				
	$\nu$	$1.0684 \times 10^7$	$3.0323 \times 10^9$				
	$A$	26.1488	0.0132	$-2.3471 \times 10^4$	$4.6945 \times 10^4$	$4.6949 \times 10^4$	$4.6974 \times 10^4$
Weibull	$B$	2.9580	0.0008				

Table 16: MLE results of the statistical distribution fitting of the ACA (dB) for Band B (SE is the estimated standard error).

Distribution	Parameter	Estimate	SE	Log-likelihood	AIC	BIC	EDC
Exponential Gamma	$\mu$	25.244	0.0964	$-2.7947 \times 10^4$	$5.5895 \times 10^4$	$5.5897 \times 10^4$	$5.5910 \times 10^4$
	$a$	8.5236	0.0212	$-2.3368 \times 10^4$	$4.6741 \times 10^4$	$4.6744 \times 10^4$	$4.6769 \times 10^4$
	$b$	2.9617	0.0027				
Inverse Gaussian	$\mu$	25.2440	0.0132	$-2.3549 \times 10^4$	$4.7102 \times 10^4$	$4.7106 \times 10^4$	$4.7131 \times 10^4$
	$\lambda$	184.5420	10.3958				
Logistic	$\mu$	25.1994	0.0109	$-2.3478 \times 10^4$	$4.6960 \times 10^4$	$4.6964 \times 10^4$	$4.6988 \times 10^4$
	$\sigma$	4.8178	0.0024				
Log-logistic	$\mu$	3.19647	$0.1971 \times 10^{-4}$	$-2.3630 \times 10^4$	$4.7264 \times 10^4$	$4.7268 \times 10^4$	$4.7293 \times 10^4$
	$\sigma$	0.2058	$0.0441 \times 10^{-4}$				
Log-normal	$\mu$	3.1688	$0.1947 \times 10^{-4}$	$-2.3543 \times 10^4$	$4.7091 \times 10^4$	$4.7094 \times 10^4$	$4.7119 \times 10^4$
	$\sigma$	0.3587	$0.0974 \times 10^{-4}$				
Nakagami	$\mu$	2.4072	0.0015	$-2.3289 \times 10^4$	$4.6582 \times 10^4$	$4.6586 \times 10^4$	$4.6611 \times 10^4$
	$\omega$	705.8651	31.3180				
Normal	$\mu$	25.2445	0.0104	$-2.3350 \times 10^4$	$4.6705 \times 10^4$	$4.6708 \times 10^4$	$4.6733 \times 10^4$
	$\sigma$	8.2835	0.0052				
Rayleigh	$B$	18.7865	0.0134	$-2.4437 \times 10^4$	$4.8875 \times 10^4$	$4.8877 \times 10^4$	$4.8890 \times 10^4$
Rician	$s$	23.3614	0.0135	$-2.3326 \times 10^4$	$4.6656 \times 10^4$	$4.6660 \times 10^4$	$4.6684 \times 10^4$
	$\sigma$	8.6429	0.0070				
Skew-normal	$\mu$	25.2377	$1.0401 \times 10^{-2}$	$-2.3335 \times 10^4$	$4.6676 \times 10^4$	$4.6682 \times 10^4$	$4.6719 \times 10^4$
	$\sigma$	8.2875	0.0054				
	$\gamma$	0.1779	$1.1403 \times 10^{-3}$				
t-Student	$\mu$	25.2445	0.0104	$-2.3350 \times 10^4$	$4.6707 \times 10^4$	$4.6712 \times 10^4$	$4.6750 \times 10^4$
	$\sigma$	8.2829	0.0052				
	$\nu$	$1.2079 \times 10^6$	$1.7073 \times 10^9$				
Weibull	$A$	28.1449	0.0119	$-2.3296 \times 10^4$	$4.6595 \times 10^4$	$4.6599 \times 10^4$	$4.6624 \times 10^4$
	$B$	3.3479	0.0010				

Table 17: MLE results of the statistical distribution fitting of the ACA (dB) for Band C (SE is the estimated standard error).

Distribution	Parameter	Estimate	SE	Log-likelihood	AIC	BIC	EDC
Exponential	$\mu$	30.2112	0.1381	$-2.9134 \times 10^4$	$5.8270 \times 10^4$	$5.8272 \times 10^4$	$5.8284 \times 10^4$
	$a$	10.1338	0.0301	$-2.4027 \times 10^4$	$4.8058 \times 10^4$	$4.8062 \times 10^4$	$4.8087 \times 10^4$
	$b$	2.9812	0.0027				
Inverse Gaussian	$\mu$	30.2112	0.0154	$-2.4165 \times 10^4$	$4.8335 \times 10^4$	$4.8338 \times 10^4$	$4.8363 \times 10^4$
	$\lambda$	270.2152	22.0960				
Logistic	$\mu$	30.1738	0.0135	$-2.4163 \times 10^4$	$4.8330 \times 10^4$	$4.8333 \times 10^4$	$4.8358 \times 10^4$
	$\sigma$	5.3523	0.0029				
Log-logistic	$\mu$	3.3809	$0.1667 \times 10^{-4}$	$-2.4287 \times 10^4$	$4.8577 \times 10^4$	$4.8581 \times 10^4$	$4.8606 \times 10^4$
	$\sigma$	0.1889	$0.0369 \times 10^{-4}$				
Log-normal	$\mu$	3.3581	$0.1610 \times 10^{-4}$	$-2.4167 \times 10^4$	$4.8339 \times 10^4$	$4.8342 \times 10^4$	$4.8367 \times 10^4$
	$\sigma$	0.3262	$0.0805 \times 10^{-4}$				
Nakagami	$\mu$	2.8123	0.0021	$-2.3962 \times 10^4$	$4.7928 \times 10^4$	$4.7931 \times 10^4$	$4.7956 \times 10^4$
	$\omega$	996.5721	53.4341				
Normal	$\mu$	30.2112	0.0127	$-2.4014 \times 10^4$	$4.8032 \times 10^4$	$4.8035 \times 10^4$	$4.8060 \times 10^4$
	$\sigma$	9.1581	0.0063				
Rayleigh	$B$	22.3223	0.0188	$-2.5465 \times 10^4$	$5.0932 \times 10^4$	$5.0934 \times 10^4$	$5.0947 \times 10^4$
Rician	$s$	28.5925	0.0155	$-2.3998 \times 10^4$	$4.8001 \times 10^4$	$4.8005 \times 10^4$	$4.8029 \times 10^4$
	$\sigma$	9.4616	0.0079				
Skew-normal	$\mu$	30.2037	$1.2715 \times 10^{-2}$	$-2.4004 \times 10^4$	$4.8015 \times 10^4$	$4.8020 \times 10^4$	$4.8058 \times 10^4$
	$\sigma$	9.1627	$0.6591 \times 10^{-2}$				
	$\gamma$	0.1488	$1.2825 \times 10^{-3}$				
t-Student	$\mu$	30.2115	0.0127	$-2.4014 \times 10^4$	$4.8034 \times 10^4$	$4.8039 \times 10^4$	$4.8076 \times 10^4$
	$\sigma$	9.1574	0.0063				
	$\nu$	$6.3036 \times 10^6$	$2.9163 \times 10^9$				
Weibull	$A$	33.5333	0.0143	$-2.3977 \times 10^4$	$4.7957 \times 10^4$	$4.7961 \times 10^4$	$4.7986 \times 10^4$
	$B$	3.6440	0.0012				

Table 18: MLE results of the statistical distribution fitting of the RMS-DS ( $\mu s$ ) for Band A (SE is the estimated standard error).

Distribution	Parameter	Estimate	SE	Log-likelihood	AIC	BIC	EDC
Exponential	$\mu$	0.1481	$3.3180 \times 10^{-6}$	$6.0141 \times 10^3$	$-1.2026 \times 10^4$	$-1.2024 \times 10^4$	$-1.2012 \times 10^4$
	$a$	5.3806	0.0083	$9.2350 \times 10^3$	$-1.8466 \times 10^4$	$-1.8462 \times 10^4$	$-1.8437 \times 10^4$
	$b$	0.0275	0.0002				
Inverse Gaussian	$\mu$	0.1481	$0.0007 \times 10^{-3}$	$9.1701 \times 10^3$	$-1.8336 \times 10^4$	$-1.8333 \times 10^4$	$-1.8308 \times 10^4$
	$\lambda$	0.6674	$0.1348 \times 10^{-3}$				
Logistic	$\mu$	0.14373	$0.5951 \times 10^{-6}$	$8.8357 \times 10^3$	$-1.7667 \times 10^4$	$-1.7664 \times 10^4$	$-1.7639 \times 10^4$
	$\sigma$	0.0358	$0.1321 \times 10^{-6}$				
Log-logistic	$\mu$	-1.9881	$0.3114 \times 10^{-4}$	$9.0858 \times 10^3$	$-1.8168 \times 10^4$	$-1.8164 \times 10^4$	$-1.8139 \times 10^4$
	$\sigma$	0.2584	$0.0687 \times 10^{-4}$				
Log-normal	$\mu$	-2.0058	$0.3044 \times 10^{-4}$	$9.1779 \times 10^3$	$-1.8352 \times 10^4$	$-1.8348 \times 10^4$	$-1.8323 \times 10^4$
	$\sigma$	0.4485	$0.1522 \times 10^{-4}$				
Nakagami	$\mu$	1.5153	$0.5768 \times 10^{-3}$	$9.1241 \times 10^3$	$-1.8244 \times 10^4$	$-1.8241 \times 10^4$	$-1.8216 \times 10^4$
	$\omega$	0.02608	$0.0001 \times 10^{-3}$				
Normal	$\mu$	0.1481	$0.6280 \times 10^{-6}$	$8.7462 \times 10^3$	$-1.7488 \times 10^4$	$-1.7485 \times 10^4$	$-1.7460 \times 10^4$
	$\sigma$	0.0644	$0.0644 \times 10^{-6}$				
Rayleigh	$B$	0.1142	$4.9324 \times 10^{-7}$	$8.8165 \times 10^3$	$-1.7631 \times 10^4$	$-1.7629 \times 10^4$	$-1.7617 \times 10^4$
Rician	$s$	0.1222	$0.2104 \times 10^{-5}$	$8.9461 \times 10^3$	$-1.7888 \times 10^4$	$-1.7885 \times 10^4$	$-1.7860 \times 10^4$
	$\sigma$	0.0746	$0.1056 \times 10^{-5}$				
Skew-normal	$\mu$	0.1477	$6.2367 \times 10^{-7}$	$9.2045 \times 10^3$	$-1.8403 \times 10^4$	$-1.8398 \times 10^4$	$-1.8360 \times 10^4$
	$\sigma$	0.0649	$4.1255 \times 10^{-7}$				
	$\gamma$	0.8453	$1.7173 \times 10^{-4}$				
t-Student	$\mu$	0.1442	$6.2515 \times 10^{-7}$	$8.8602 \times 10^3$	$-1.7714 \times 10^4$	$-1.7709 \times 10^4$	$-1.7672 \times 10^4$
	$\sigma$	0.0566	$5.1078 \times 10^{-7}$				
	$\nu$	9.2055	0.6177				
Weibull	$A$	0.1672	$0.0008 \times 10^{-3}$	$9.0239 \times 10^3$	$-1.8044 \times 10^4$	$-1.8040 \times 10^4$	$-1.8015 \times 10^4$
	$B$	2.4300	$0.4811 \times 10^{-3}$				

Table 19: MLE results of the statistical distribution fitting of the RMS-DS ( $\mu s$ ) for Band B (SE is the estimated standard error).

Distribution	Parameter	Estimate	SE	Log-likelihood	AIC	BIC	EDC
Exponential	$\mu$	0.1384	$2.8962 \times 10^{-6}$	$6.4634 \times 10^3$	$-1.2925 \times 10^4$	$-1.2923 \times 10^4$	$-1.2911 \times 10^4$
	$a$	4.6809	0.0062	$9.2915 \times 10^3$	$-1.8579 \times 10^4$	$-1.8575 \times 10^4$	$-1.8550 \times 10^4$
	$b$	0.0295	0.0004				
Inverse Gaussian	$\mu$	0.1384	$0.0078 \times 10^{-4}$	$9.1057 \times 10^3$	$-1.8207 \times 10^4$	$-1.8204 \times 10^4$	$-1.8179 \times 10^4$
	$\lambda$	0.5105	$0.7888 \times 10^{-4}$				
Logistic	$\mu$	0.1342	$0.5661 \times 10^{-6}$	$8.9580 \times 10^3$	$-1.7912 \times 10^4$	$-1.7908 \times 10^4$	$-1.7883 \times 10^4$
	$\sigma$	0.0351	$0.1274 \times 10^{-6}$				
Log-logistic	$\mu$	-2.0601	$0.3524 \times 10^{-4}$	$9.1259 \times 10^3$	$-1.8248 \times 10^4$	$-1.8244 \times 10^4$	$-1.8219 \times 10^4$
	$\sigma$	0.2767	$0.0801 \times 10^{-4}$				
Log-normal	$\mu$	-2.0886	$0.3625 \times 10^{-4}$	$9.1479 \times 10^3$	$-1.8292 \times 10^4$	$-1.8288 \times 10^4$	$-1.8263 \times 10^4$
	$\sigma$	0.4895	$0.1813 \times 10^{-4}$				
Nakagami	$\mu$	1.3543	$0.4528 \times 10^{-3}$	$9.2203 \times 10^3$	$-1.8347 \times 10^4$	$-1.8433 \times 10^4$	$-1.8408 \times 10^4$
	$\omega$	0.0232	$0.0001 \times 10^{-3}$				
Normal	$\mu$	0.1384	$0.6109 \times 10^{-6}$	$8.8374 \times 10^3$	$-1.7671 \times 10^4$	$-1.7667 \times 10^4$	$-1.7642 \times 10^4$
	$\sigma$	0.0635	$0.3055 \times 10^{-6}$				
Rayleigh	$B$	0.1076	$4.3838 \times 10^{-7}$	$9.0486 \times 10^3$	$-1.8095 \times 10^4$	$-1.8093 \times 10^4$	$-1.8081 \times 10^4$
Rician	$s$	0.1062	$0.3890 \times 10^{-5}$	$9.0973 \times 10^3$	$-1.8191 \times 10^4$	$-1.8187 \times 10^4$	$-1.8162 \times 10^4$
	$\sigma$	0.0771	$0.1642 \times 10^{-5}$				
Skew-normal	$\mu$	0.1383	$6.0740 \times 10^{-7}$	$9.2278 \times 10^3$	$-1.8450 \times 10^4$	$-1.8444 \times 10^4$	$-1.8407 \times 10^4$
	$\sigma$	0.0636	$3.9489 \times 10^{-7}$				
	$\gamma$	0.7747	$3.1647 \times 10^{-4}$				
t-Student	$\mu$	0.1344	$5.8888 \times 10^{-7}$	$8.9774 \times 10^3$	$-1.7949 \times 10^4$	$-1.7943 \times 10^4$	$-1.7906 \times 10^4$
	$\sigma$	0.0548	$5.0551 \times 10^{-7}$				
	$\nu$	8.1067	0.4104				
Weibull	$A$	0.1564	$0.0008 \times 10^{-3}$	$9.1580 \times 10^3$	$-1.8312 \times 10^4$	$-1.8308 \times 10^4$	$-1.8283 \times 10^4$
	$B$	2.3007	$0.4367 \times 10^{-3}$				

Table 20: MLE results of the statistical distribution fitting of the RMS-DS ( $\mu s$ ) for Band C (SE is the estimated standard error).

Distribution	Parameter	Estimate	SE	Log-likelihood	AIC	BIC	EDC
Exponential	$\mu$	0.1327	$2.6647 \times 10^{-6}$	$6.7386 \times 10^3$	$-1.3475 \times 10^4$	$-1.3473 \times 10^4$	$-1.3461 \times 10^4$
	$a$	4.1178	0.0048	$9.2151 \times 10^3$	$-1.8426 \times 10^4$	$-1.8423 \times 10^4$	$-1.8398 \times 10^4$
Gamma	$b$	0.0322	0.0001				
	$\mu$	0.1327	$0.0085 \times 10^{-4}$	$9.0035 \times 10^3$	$-1.8003 \times 10^4$	$-1.7999 \times 10^4$	$-1.7974 \times 10^4$
Inverse Gaussian	$\lambda$	0.4167	$0.5256 \times 10^{-4}$				
	$\mu$	0.1285	$0.5914 \times 10^{-6}$	$8.8334 \times 10^3$	$-1.7663 \times 10^4$	$-1.7659 \times 10^4$	$-1.7634 \times 10^4$
Logistic	$\sigma$	0.0358	$0.1324 \times 10^{-6}$				
	$\mu$	-2.1128	$0.4106 \times 10^{-4}$	$9.0088 \times 10^3$	$-1.8014 \times 10^4$	$-1.8010 \times 10^4$	$-1.7985 \times 10^4$
Log-logistic	$\sigma$	0.2984	$0.0932 \times 10^{-4}$				
	$\mu$	-2.1459	$0.4191 \times 10^{-4}$	$9.0471 \times 10^3$	$-1.8090 \times 10^4$	$-1.8087 \times 10^4$	$-1.8062 \times 10^4$
Log-normal	$\sigma$	0.5263	$0.2096 \times 10^{-4}$				
	$\mu$	1.2160	$0.3587 \times 10^{-3}$	$9.1591 \times 10^3$	$-1.8314 \times 10^4$	$-1.8311 \times 10^4$	$-1.8286 \times 10^4$
Nakagami	$\omega$	0.0218	$0.0001 \times 10^{-3}$				
	$\mu$	0.1327	$0.6290 \times 10^{-6}$	$8.7409 \times 10^3$	$-1.7478 \times 10^4$	$-1.7474 \times 10^4$	$-1.7449 \times 10^4$
Normal	$\sigma$	0.0645	$0.3146 \times 10^{-6}$				
	$B$	0.1043	$4.1171 \times 10^{-7}$	$9.0844 \times 10^3$	$-1.8167 \times 10^4$	$-1.8165 \times 10^4$	$-1.8152 \times 10^4$
Rayleigh	$s$	$0.194 \times 10^{-3}$	$0.3422 \times 10^{-5}$	$9.0844 \times 10^3$	$-1.8165 \times 10^4$	$-1.8161 \times 10^4$	$-1.8136 \times 10^4$
	$\sigma$	0.1043	$0.0177 \times 10^{-5}$				
Rician	$\mu$	0.1323	$6.3203 \times 10^{-7}$	$9.1509 \times 10^3$	$-1.8296 \times 10^4$	$-1.8290 \times 10^4$	$-1.8253 \times 10^4$
	$\sigma$	0.0649	$4.2056 \times 10^{-7}$				
	$\gamma$	0.8127	$2.6454 \times 10^{-4}$				
Skew-normal	$\mu$	0.1288	$6.2274 \times 10^{-7}$	$8.8528 \times 10^3$	$-1.7700 \times 10^4$	$-1.7694 \times 10^4$	$-1.7657 \times 10^4$
	$\sigma$	0.0564	$5.3258 \times 10^{-7}$				
	$\nu$	8.8234	0.5668				
t-Student	$A$	0.1484	$0.0008 \times 10^{-3}$	$9.1259 \times 10^3$	$-1.8248 \times 10^4$	$-1.8244 \times 10^4$	$-1.8219 \times 10^4$
	$B$	2.1794	$0.4020 \times 10^{-3}$				

Table 21: MLE results of the statistical distribution fitting of the CB (MHz) for Band A (SE is the estimated standard error).

Distribution	Parameter	Estimate	SE	Log-likelihood	AIC	BIC	EDC
Exponential	$\mu$	0.6442	$6.2910 \times 10^{-5}$	$-3.7036 \times 10^3$	$7.4093 \times 10^3$	$7.4111 \times 10^3$	$7.4235 \times 10^3$
	$a$	3.6451	0.1767	$-1.5514 \times 10^3$	$3.1069 \times 10^3$	$3.1105 \times 10^3$	$3.1354 \times 10^3$
Gamma	$b$						
	$\mu$	0.6443	$1.9430 \times 10^{-5}$	$-1.1737 \times 10^3$	$2.3514 \times 10^3$	$2.3550 \times 10^3$	$2.3799 \times 10^3$
Inverse Gaussian	$\lambda$	2.0827	0.0013				
	$\mu$	0.5882	$0.1669 \times 10^{-4}$	$-2.5406 \times 10^3$	$5.0852 \times 10^3$	$5.0888 \times 10^3$	$5.1137 \times 10^3$
Logistic	$\sigma$	0.1936	$0.0406 \times 10^{-4}$				
	$\mu$	-0.6053	$0.4271 \times 10^{-4}$	$-1.3125 \times 10^3$	$2.6291 \times 10^3$	$2.6327 \times 10^3$	$2.6576 \times 10^3$
Log-logistic	$\sigma$	0.3015	$0.0926 \times 10^{-4}$				
	$\mu$	-0.5830	$0.4094 \times 10^{-4}$	$-1.2044 \times 10^3$	$2.4128 \times 10^3$	$2.4165 \times 10^3$	$2.4414 \times 10^3$
Log-normal	$\sigma$	0.5202	$0.2047 \times 10^{-4}$				
	$\mu$	0.9741	$0.2216 \times 10^{-3}$	$-2.1019 \times 10^3$	$4.2078 \times 10^3$	$4.2115 \times 10^3$	$4.2364 \times 10^3$
Nakagami	$\omega$	0.5646	$0.0495 \times 10^{-3}$				
	$\mu$	0.6443	$0.2263 \times 10^{-4}$	$-3.0980 \times 10^3$	$6.2001 \times 10^3$	$6.2037 \times 10^3$	$6.2286 \times 10^3$
Normal	$\sigma$	0.3867	$0.1132 \times 10^{-4}$				
	$B$	0.5313	$1.0679 \times 10^{-5}$	$-2.1034 \times 10^3$	$4.2088 \times 10^3$	$4.2106 \times 10^3$	$4.2231 \times 10^3$
Rayleigh	$s$	0.0042	0.6769	$-2.1034 \times 10^3$	$4.2108 \times 10^3$	$4.2145 \times 10^3$	$4.22383 \times 10^3$
	$\sigma$	0.5313	$2.1048 \times 10^{-5}$				
Skew-normal	$\mu$	0.6814	$1.6475 \times 10^{-5}$	$-1.3848 \times 10^3$	$2.7756 \times 10^3$	$2.7811 \times 10^3$	$2.8184 \times 10^3$
	$\sigma$	0.3428	$0.9767 \times 10^{-5}$				
	$\gamma$	0.9699	$0.4232 \times 10^{-5}$				
t-Student	$\mu$	0.5496	$1.7593 \times 10^{-5}$	$-2.31492 \times 10^3$	$4.6359 \times 10^3$	$4.6413 \times 10^3$	$4.6786 \times 10^3$
	$\sigma$	0.2394	$1.5248 \times 10^{-5}$				
	$\nu$	2.9499	0.0148				
Weibull	$A$	0.7303	$0.0276 \times 10^{-3}$	$-2.0371 \times 10^3$	$4.0782 \times 10^3$	$4.0818 \times 10^3$	$4.1067 \times 10^3$
	$B$	1.8162	$0.2462 \times 10^{-3}$				

Table 22: MLE results of the statistical distribution fitting of the CB (MHz) for Band B (SE is the estimated standard error).

Distribution	Parameter	Estimate	SE	Log-likelihood	AIC	BIC	EDC
Exponential	$\mu$	0.7205	$0.7855 \times 10^{-4}$	$-4.4430 \times 10^3$	$8.8879 \times 10^3$	$8.8897 \times 10^3$	$8.9002 \times 10^3$
	$a$	3.1311	0.0027	$-2.6785 \times 10^3$	$5.3610 \times 10^3$	$5.3647 \times 10^3$	$5.3896 \times 10^3$
Gamma	$b$	0.2301	$1.7070 \times 10^{-5}$				
	$\mu$	0.7205	$0.2823 \times 10^{-4}$	$-2.1633 \times 10^3$	$4.3306 \times 10^3$	$4.3342 \times 10^3$	$4.3591 \times 10^3$
Inverse Gaussian	$\lambda$	2.0051	0.0012				
	$\mu$	0.6429	$0.2380 \times 10^{-4}$	$-3.8558 \times 10^3$	$7.7156 \times 10^3$	$7.7193 \times 10^3$	$7.7442 \times 10^3$
Logistic	$\sigma$	0.2330	$0.0601 \times 10^{-4}$				
	$\mu$	-0.5283	$0.4779 \times 10^{-4}$	$-2.2875 \times 10^3$	$4.5790 \times 10^3$	$4.5826 \times 10^3$	$4.6075 \times 10^3$
Log-logistic	$\sigma$	0.3194	$0.1045 \times 10^{-4}$				
	$\mu$	-0.4958	$0.4652 \times 10^{-4}$	$-2.2029 \times 10^3$	$4.4099 \times 10^3$	$4.4135 \times 10^3$	$4.4384 \times 10^3$
Log-normal	$\sigma$	0.5545	$0.2327 \times 10^{-4}$				
	$\mu$	0.8270	$0.1550 \times 10^{-3}$	$-3.3894 \times 10^3$	$6.7827 \times 10^3$	$6.7864 \times 10^3$	$6.8113 \times 10^3$
Nakagami	$\omega$	0.7579	$0.1051 \times 10^{-3}$				
	$\mu$	0.7205	$0.3613 \times 10^{-4}$	$-4.6445 \times 10^3$	$9.2929 \times 10^3$	$9.2966 \times 10^3$	$9.3215 \times 10^3$
Normal	$\sigma$	0.4886	$0.1807 \times 10^{-4}$				
	$B$	0.6156	$1.4335 \times 10^{-5}$	$-3.4733 \times 10^3$	$6.9486 \times 10^3$	$6.9504 \times 10^3$	$6.9628 \times 10^3$
Rayleigh	$s$	0.0185	0.0356	$-3.4733 \times 10^3$	$6.9506 \times 10^3$	$6.9542 \times 10^3$	$6.9791 \times 10^3$
	$\sigma$	0.6155	$2.2377 \times 10^{-5}$				
Skew-normal	$\mu$	0.7852	$0.2417 \times 10^{-4}$	$-2.5880 \times 10^3$	$5.1821 \times 10^3$	$5.1876 \times 10^3$	$5.2249 \times 10^3$
	$\sigma$	0.4151	$0.1412 \times 10^{-4}$				
	$\gamma$	0.9777	$0.0026 \times 10^{-4}$				
t-Student	$\mu$	0.5729	$2.1287 \times 10^{-5}$	$-3.4213 \times 10^3$	$6.8486 \times 10^3$	$6.8541 \times 10^3$	$6.8914 \times 10^3$
	$\sigma$	0.2513	$1.9870 \times 10^{-5}$				
	$\nu$	2.2450	0.0063				
Weibull	$A$	0.8137	$0.0416 \times 10^{-3}$	$-3.1820 \times 10^3$	$6.3681 \times 10^3$	$6.3717 \times 10^3$	$6.3966 \times 10^3$
	$B$	1.6499	$0.1974 \times 10^{-3}$				

Table 23: MLE results of the statistical distribution fitting of the CB (MHz) for Band C (SE is the estimated standard error).

Distribution	Parameter	Estimate	SE	Log-likelihood	AIC	BIC	EDC
Exponential	$\mu$	0.7803	$9.2121 \times 10^{-5}$	$-4.9692 \times 10^3$	$9.9405 \times 10^3$	$9.9423 \times 10^3$	$9.9548 \times 10^3$
	$a$	3.1126	0.0027	$-3.2195 \times 10^3$	$6.4430 \times 10^3$	$6.4467 \times 10^3$	$6.4715 \times 10^3$
Gamma	$b$	0.2507	$0.2026 \times 10^{-4}$				
	$\mu$	0.7803	$0.3328 \times 10^{-4}$	$-2.6962 \times 10^3$	$5.3964 \times 10^3$	$5.4000 \times 10^3$	$5.4249 \times 10^3$
Inverse Gaussian	$\lambda$	2.1601	0.0014				
	$\mu$	0.6839	$0.2684 \times 10^{-4}$	$-4.4687 \times 10^3$	$8.9414 \times 10^3$	$8.9450 \times 10^3$	$8.9699 \times 10^3$
Logistic	$\sigma$	0.2508	$0.0731 \times 10^{-4}$				
	$\mu$	-0.4577	$0.4419 \times 10^{-4}$	$-2.7116 \times 10^3$	$5.4272 \times 10^3$	$5.4309 \times 10^3$	$5.4558 \times 10^3$
Log-logistic	$\sigma$	0.3107	$0.1021 \times 10^{-4}$				
	$\mu$	-0.4173	$0.4645 \times 10^{-4}$	$-2.7171 \times 10^3$	$5.4382 \times 10^3$	$5.4418 \times 10^3$	$5.4667 \times 10^3$
Log-normal	$\sigma$	0.5541	$0.2323 \times 10^{-4}$				
	$\mu$	0.8267	$0.1549 \times 10^{-3}$	$-3.9103 \times 10^3$	$7.8246 \times 10^3$	$7.8282 \times 10^3$	$7.8531 \times 10^3$
Nakagami	$\omega$	0.8872	$0.1441 \times 10^{-3}$				
	$\mu$	0.7803	$0.4212 \times 10^{-4}$	$-5.1517 \times 10^3$	$1.0307 \times 10^4$	$1.0311 \times 10^4$	$1.0336 \times 10^4$
Normal	$\sigma$	0.5276	$0.2107 \times 10^{-4}$				
	$B$	0.6660	$1.6780 \times 10^{-5}$	$-3.9945 \times 10^3$	$7.9911 \times 10^3$	$7.9929 \times 10^3$	$8.0053 \times 10^3$
Rayleigh	$s$	0.0192	0.0619	$-3.9945 \times 10^3$	$7.9931 \times 10^3$	$7.9967 \times 10^3$	$8.0216 \times 10^3$
	$\sigma$	0.6659	$0.2957 \times 10^{-4}$				
Skew-normal	$\mu$	0.8495	$0.2847 \times 10^{-4}$	$-3.1539 \times 10^3$	$6.3138 \times 10^3$	$6.3193 \times 10^3$	$6.3566 \times 10^3$
	$\sigma$	0.4489	$0.1664 \times 10^{-4}$				
	$\gamma$	0.9701	$0.0429 \times 10^{-4}$				
t-Student	$\mu$	0.5908	$0.1580 \times 10^{-4}$	$-3.6950 \times 10^3$	$7.3960 \times 10^3$	$7.4014 \times 10^3$	$7.4388 \times 10^3$
	$\sigma$	0.2203	$0.1535 \times 10^{-4}$				
	$\nu$	1.6706	0.0022				
Weibull	$A$	0.8818	$0.0488 \times 10^{-3}$	$-3.7171 \times 10^3$	$7.4383 \times 10^3$	$7.4419 \times 10^3$	$7.4668 \times 10^3$
	$B$	1.6517	$0.2030 \times 10^{-3}$				

Table 24: MLE results of the statistical distribution fitting of the CT (ms) for Band A (SE is the estimated standard error).

Distribution	Parameter	Estimate	SE	Log-likelihood	AIC	BIC	EDC
Exponential	$\mu$	1.1863	0.0079	-208.4095	418.8191	419.0695	419.4874
	$a$	8.2153	0.7288				
Gamma	$b$	0.1444	0.0002	-88.1016	180.2032	180.7040	181.5399
	$\mu$	1.1863	0.0015	-117.1688	238.3375	238.8384	238.6742
Inverse Gaussian	$\lambda$	6.3446	0.4523				
	$\mu$	1.24127	$0.6095 \times 10^{-3}$	-59.7283	123.4566	123.9575	124.7933
Logistic	$\sigma$	0.1883	$0.1440 \times 10^{-3}$				
	$\mu$	0.1858	$0.6190 \times 10^{-3}$	-92.6302	189.2604	189.7613	190.5971
Log-logistic	$\sigma$	0.1949	$0.1642 \times 10^{-3}$				
	$\mu$	0.1087	$0.8980 \times 10^{-3}$	-108.2377	220.4754	220.9762	221.8121
Log-normal	$\sigma$	0.3998	$0.4528 \times 10^{-3}$				
	$\mu$	2.6184	0.0685	-74.1036	152.2072	152.7080	153.5438
Nakagami	$\omega$	1.5226	0.0050				
	$\mu$	1.1863	$0.6515 \times 10^{-3}$	-60.3188	124.6375	125.1384	125.9742
Normal	$\sigma$	0.3405	$0.3285 \times 10^{-3}$				
	$B$	0.8725	0,0011	-110.0999	222.1998	222.4502	222.8681
Rayleigh	$s$	1.1305	$0.7709 \times 10^{-3}$	-61.3467	126.6934	127.1942	128.0301
	$\sigma$	0.3496	$0.3919 \times 10^{-3}$				
Skew-normal	$\mu$	1.1440	0.0004	-3.5299	13.0597	13.8110	15.0647
	$\sigma$	0.2909	0.0002				
	$\gamma$	-0.9898	$1.4123 \times 10^{-5}$				
t-Student	$\mu$	1.3867	$5.6459 \times 10^{-4}$	-57.7546	121.5093	122.2605	123.5143
	$\sigma$	0.1204	0.0011				
	$\nu$	1.0848	0.0878				
Weibull	$A$	1.3027	0.0005	-53.8489	111.6979	112.1987	113.0345
	$B$	4.5431	0.0939				

Table 25: MLE results of the statistical distribution fitting of the CT (ms) for Band B (SE is the estimated standard error).

Distribution	Parameter	Estimate	SE	Log-likelihood	AIC	BIC	EDC
Exponential	$\mu$	1.1374	0.0073	-200.9125	403.8249	404.0753	404.4932
	$a$	6.7627	0.4898	-96.2638	196.5276	197.0285	197.8643
Gamma	$b$	0.1682	0.0003	-136.0928	276.1856	276.6864	277.52222
	$\lambda$	4.3390	0.2115	-63.5261	131.0521	131.5530	132.3888
Logistic	$\mu$	1.1850	$0.6431 \times 10^{-3}$	-99.3000	202.6000	203.1009	203.9367
	$\sigma$	0.1924	$0.1485 \times 10^{-3}$	-121.5316	247.0631	247.5640	248.3998
Log-logistic	$\mu$	0.1366	$0.7225 \times 10^{-3}$	-80.2633	164.5266	165.0274	165.8632
	$\sigma$	0.2122	$0.1921 \times 10^{-3}$	-64.0309	132.0619	132.5627	133.3985
Log-normal	$\mu$	0.0530	0.0012	-106.8342	215.6684	215.9188	216.3367
	$\sigma$	0.4555	0.0006	-65.3746	134.7492	135.2500	136.0858
Nakagami	$\mu$	2.2325	0.0490	-31.5650	69.1300	69.8813	71.1350
	$\omega$	1.4138	0.0050	-63.6052	133.2104	133.9616	135.2154
Normal	$\mu$	1.1374	$0.6792 \times 10^{-3}$	-62.8862	129.7724	130.2733	131.1091
	$\sigma$	0.3477	$0.3425 \times 10^{-3}$				
Rayleigh	$B$	0.8408	0.0009				
	$s$	1.0751	$0.8329 \times 10^{-3}$				
Rician	$\sigma$	0.3591	$0.4242 \times 10^{-3}$				
	$\mu$	1.5311	0.0005				
Skew-normal	$\sigma$	0.3212	0.0003				
	$\gamma$	-0.9241	0.0005				
t-Student	$\mu$	1.1698	0.0018				
	$\sigma$	0.3124	0.0017				
	$\nu$	10.0589	137.5842				
Weibull	$A$	1.2527	0.0006				
	$B$	4.0363	0.0707				

Table 26: MLE results of the statistical distribution fitting of the CT (ms) for Band C (SE is the estimated standard error).

Distribution	Parameter	Estimate	SE	Log-likelihood	AIC	BIC	EDC
Exponential Gamma	$\mu$	1.1039	0.0068	-195.6078	393.2157	393.4661	393.8840
	$a$	5.4787	0.3180	-107.4669	218.9338	219.4346	220.2704
	$b$	0.2015	0.0005				
Inverse Gaussian	$\mu$	1.1039	0.0022	-45.4933	294.9865	295.4874	296.3232
	$\lambda$	3.3797	0.1283				
Logistic	$\mu$	1.1506	$0.8628 \times 10^{-3}$	-83.9979	171.9958	172.4967	173.3325
	$\sigma$	0.2209	$0.1876 \times 10^{-3}$				
Log-logistic	$\mu$	0.0916	0.0010	-116.0575	236.1149	236.6158	237.4516
	$\sigma$	0.2507	0.0003				
Log-normal	$\mu$	0.0049	0.0014	-131.0328	266.0655	266.5663	267.4022
	$\sigma$	0.5041	0.0007				
Nakagami	$\mu$	1.8166	0.0316	-92.9655	189.9390	190.4318	191.2676
	$\omega$	1.3629	0.0057				
Normal	$\mu$	1.1039	$0.8141 \times 10^{-3}$	-80.1585	164.3171	164.8179	165.6538
	$\sigma$	0.3807	$0.4105 \times 10^{-3}$				
Rayleigh	$B$	0.8255	0.0009	-108.8567	219.7134	219.9638	220.3817
Rician	$s$	1.0218	0.0011	-81.2115	166.4229	166.9238	167.7596
	$\sigma$	0.3992	0.0006				
Skew-normal	$\mu$	1.5492	0.0006	-44.4363	94.8727	95.6239	96.8777
	$\sigma$	0.3550	0.0003				
	$\gamma$	-0.9655	0.0002				
t-Student	$\mu$	1.1039	0.0008	-80.1571	166.3143	167.0655	168.3193
	$\sigma$	0.3796	0.0004				
	$\nu$	$6.2559 \times 10^6$	$7.4749 \times 10^{10}$				
Weibull	$A$	1.2267	0.0008	-81.1403	166.2806	166.7814	167.6173
	$B$	3.4355	0.0515				

## APPENDIX D – MLE Results for Hybrid PLC-wireless Channel Features

This appendix summarizes the results of the log-likelihood, AIC, BIC and EDC for several statistical distributions when applied to model ACA, CB, RMS-DS and CT estimated from the measured Brazilian in-door hybrid PLC-wireless channels.

Table 27: MLE results of the statistical distribution fitting of the ACA (dB) for *short path* channel (SE is the estimated standard error).

Distribution	Parameter	Estimate	SE	Log-likelihood	AIC	BIC	EDC
Exponential	$\mu$	33.0315	0.1679	$-2.9233 \times 10^4$	$5.8469 \times 10^4$	$5.8471 \times 10^4$	$5.8483 \times 10^4$
	$a$	105.4952	3.4136	$-1.6795 \times 10^4$	$3.3595 \times 10^4$	$3.3598 \times 10^4$	$3.3623 \times 10^4$
	$b$	0.3131	0.0005				
Inverse Gaussian	$\mu$	33.0315	0.0027	$-1.6846 \times 10^4$	$3.3696 \times 10^4$	$3.3699 \times 10^4$	$3.3724 \times 10^4$
	$\lambda$	$3403.9214$	$3.5651 \times 10^3$				
Logistic	$\mu$	33.1182	0.0017	$-1.6874 \times 10^4$	$3.3751 \times 10^4$	$3.3755 \times 10^4$	$3.3779 \times 10^4$
	$\sigma$	1.8625	0.0004				
Log-logistic	$\mu$	3.4975	$0.1562 \times 10^{-5}$	$-1.6942 \times 10^4$	$3.3888 \times 10^4$	$3.3891 \times 10^4$	$3.3916 \times 10^4$
	$\sigma$	0.0569	$0.0332 \times 10^{-5}$				
Log-normal	$\mu$	3.4927	$0.1486 \times 10^{-5}$	$-1.6846 \times 10^4$	$3.3695 \times 10^4$	$3.3699 \times 10^4$	$3.3723 \times 10^4$
	$\sigma$	0.0983	$0.0743 \times 10^{-5}$				
Nakagami	$\mu$	26.9567	0.2209	$-1.6754 \times 10^4$	$3.3512 \times 10^4$	$3.3516 \times 10^4$	$3.3541 \times 10^4$
	$\omega$	1101.1325	6.9198				
Normal	$\mu$	33.0315	0.0015	$-1.6723 \times 10^4$	$3.3449 \times 10^4$	$3.3453 \times 10^4$	$3.3478 \times 10^4$
	$\sigma$	3.1704	0.0008				
Rayleigh	$B$	23.4641	0.0212	$-2.4818 \times 10^4$	$4.9639 \times 10^4$	$4.9641 \times 10^4$	$4.9653 \times 10^4$
Rician	$s$	32.8775	0.0016	$-1.6723 \times 10^4$	$3.3450 \times 10^4$	$3.3453 \times 10^4$	$3.3478 \times 10^4$
	$\sigma$	3.1777	0.0008				
Skew-normal	$\mu$	33.0600	0.0016	$-1.6670 \times 10^4$	$3.3347 \times 10^4$	$3.3352 \times 10^4$	$3.3389 \times 10^4$
	$\sigma$	3.1998	0.0010				
	$\gamma$	-0.4696	0.0003				
t-Student	$\mu$	33.0314	0.0015	$-1.6723 \times 10^4$	$3.3451 \times 10^4$	$3.3457 \times 10^4$	$3.3494 \times 10^4$
	$\sigma$	3.1700	$7.6758 \times 10^{-4}$				
	$\nu$	$3.2365 \times 10^6$	$1.7785 \times 10^9$				
Weibull	$A$	34.4459	0.0014	$-1.6720 \times 10^4$	$3.3444 \times 10^4$	$3.3448 \times 10^4$	$3.3472 \times 10^4$
	$B$	11.8823	0.0126				

Table 28: MLE results of the statistical distribution fitting of the ACA (dB) for *long-path channel* (SE is the estimated standard error).

Distribution	Parameter	Estimate	SE	Log-likelihood	AIC	BIC	EDC
Exponential Gamma	$\mu$	44.8971	1.0471	$-9.2484 \times 10^3$	$1.8499 \times 10^4$	$1.8500 \times 10^4$	$1.8506 \times 10^4$
	$a$	46.4716	2.2278	$-6.3461 \times 10^3$	$1.2696 \times 10^4$	$1.2699 \times 10^4$	$1.2710 \times 10^4$
	$b$	0.9661	0.0010				
Inverse Gaussian	$\mu$	44.8971	0.0062	$-6.3925 \times 10^3$	$1.2789 \times 10^4$	$1.2792 \times 10^4$	$1.2803 \times 10^4$
	$\lambda$	$1952.7561$	$3.9618 \times 10^3$				
Logistic	$\mu$	45.1724	0.0186	$-6.2611 \times 10^3$	$1.2526 \times 10^4$	$1.2529 \times 10^4$	$1.2540 \times 10^4$
	$\sigma$	3.4788	0.0045				
Log-logistic	$\mu$	3.8067	$0.9718 \times 10^{-5}$	$-6.3221 \times 10^3$	$1.2648 \times 10^4$	$1.2651 \times 10^4$	$1.2662 \times 10^4$
	$\sigma$	0.0799	$0.2405 \times 10^{-5}$				
Log-normal	$\mu$	3.7936	$0.1178 \times 10^{-4}$	$-6.3893 \times 10^3$	$1.2783 \times 10^4$	$1.2785 \times 10^4$	$1.2796 \times 10^4$
	$\sigma$	0.1506	$0.0590 \times 10^{-4}$				
Nakagami	$\mu$	12.2722	0.1523	$-6.3126 \times 10^3$	$1.2629 \times 10^4$	$1.2632 \times 10^4$	$1.2643 \times 10^4$
	$\omega$	2055.8501	178.9079				
Normal	$\mu$	44.8971	0.0208	$-6.2845 \times 10^3$	$1.2573 \times 10^4$	$1.2576 \times 10^4$	$1.2587 \times 10^4$
	$\sigma$	6.3347	0.0104				
Rayleigh	$B$	32.0613	0.1335	$-7.9728 \times 10^3$	$1.5948 \times 10^4$	$1.5949 \times 10^4$	$1.5954 \times 10^4$
Rician	$s$	44.4386	0.0215	$-6.2850 \times 10^3$	$1.2574 \times 10^4$	$1.2577 \times 10^4$	$1.2588 \times 10^4$
	$\sigma$	6.3662	0.0108				
Skew-normal	$\mu$	44.8678	0.0206	$-6.2535 \times 10^3$	$1.2513 \times 10^4$	$1.2517 \times 10^4$	$1.2533 \times 10^4$
	$\sigma$	6.3050	0.1137				
	$\gamma$	-0.3703	0.0019				
t-Student	$\mu$	45.1986	0.0198	$-6.2658 \times 10^3$	$1.2538 \times 10^4$	$1.2541 \times 10^4$	$1.2558 \times 10^4$
	$\sigma$	5.3147	0.0327				
	$\nu$	6.2551	1.2922				
Weibull	$A$	47.5639	0.0198	$-6.2658 \times 10^3$	$1.2536 \times 10^4$	$1.2538 \times 10^4$	$1.2549 \times 10^4$
	$B$	8.1289	0.0196				

Table 29: MLE results of the statistical distribution fitting of the CB (MHz) for *short-path channel* (SE is the estimated standard error).

Distribution	Parameter	Estimate	SE	Log-likelihood	AIC	BIC	EDC
Exponential	$\mu$	1.6179	$4.1174 \times 10^{-4}$	$-9.4173 \times 10^3$	$1.8837 \times 10^4$	$1.8838 \times 10^4$	$1.8851 \times 10^4$
	$a$	7.0454	0.0149	$-5.5627 \times 10^3$	$1.1129 \times 10^4$	$1.1133 \times 10^4$	$1.1157 \times 10^4$
	$b$	0.2296	$0.1702 \times 10^{-4}$				
Inverse Gaussian	$\mu$	1.6179	0.0001	$-5.3886 \times 10^3$	$1.0781 \times 10^4$	$1.0785 \times 10^4$	$1.0809 \times 10^4$
	$\lambda$	10.6805	0.0359				
Logistic	$\mu$	1.5326	$0.5787 \times 10^{-4}$	$-6.1342 \times 10^3$	$1.2272 \times 10^4$	$1.2276 \times 10^4$	$1.2300 \times 10^4$
	$\sigma$	0.3509	$0.1383 \times 10^{-4}$				
Log-logistic	$\mu$	0.3913	$0.2211 \times 10^{-4}$	$-5.4356 \times 10^3$	$1.0875 \times 10^4$	$1.0879 \times 10^4$	$1.0903 \times 10^4$
	$\sigma$	0.2142	$0.0495 \times 10^{-4}$				
Log-normal	$\mu$	0.4085	$0.2212 \times 10^{-4}$	$-5.3822 \times 10^3$	$1.0768 \times 10^4$	$1.0772 \times 10^4$	$1.0796 \times 10^4$
	$\sigma$	0.3749	$0.1106 \times 10^{-4}$				
Nakagami	$\mu$	1.8267	$0.8947 \times 10^{-3}$	$-5.8662 \times 10^3$	$1.1736 \times 10^4$	$1.1740 \times 10^4$	$1.1764 \times 10^4$
	$\omega$	3.0498	$0.8008 \times 10^{-3}$				
Normal	$\mu$	1.6179	$0.6795 \times 10^{-4}$	$-6.3532 \times 10^3$	$1.2710 \times 10^4$	$1.2714 \times 10^4$	$1.2738 \times 10^4$
	$\sigma$	0.6573	$0.3398 \times 10^{-4}$				
Rayleigh	$B$	1.2349	$0.5996 \times 10^{-4}$	$-6.4432 \times 10^3$	$1.2888 \times 10^4$	$1.2890 \times 10^4$	$1.2902 \times 10^4$
Rician	$s$	1.4119	$1.4443 \times 10^{-4}$	$-6.2048 \times 10^3$	$1.2414 \times 10^4$	$1.2417 \times 10^4$	$1.2441 \times 10^4$
	$\sigma$	0.7267	$0.7872 \times 10^{-4}$				
Skew-normal	$\mu$	1.6469	$0.5815 \times 10^{-4}$	$-5.3577 \times 10^3$	$1.0721 \times 10^4$	$1.0727 \times 10^4$	$1.0763 \times 10^4$
	$\sigma$	0.6218	$0.3177 \times 10^{-4}$				
	$\gamma$	0.9080	$0.4504 \times 10^{-4}$				
t-Student	$\mu$	1.4877	0.0001	$-6.0825 \times 10^3$	$1.2171 \times 10^4$	$1.2176 \times 10^4$	$1.2213 \times 10^4$
	$\sigma$	0.4751	0.0001				
	$\nu$	3.7397	0.0488				
Weibull	$A$	1.8240	$0.9007 \times 10^{-4}$	$-6.1090 \times 10^3$	$1.2222 \times 10^4$	$1.2226 \times 10^4$	$1.2250 \times 10^4$
	$B$	2.5628	$5.1926 \times 10^{-4}$				

Table 30: MLE results of the statistical distribution fitting of the CB (MHz) for *long-path channel* (SE is the estimated standard error).

Distribution	Parameter	Estimate	SE	Log-likelihood	AIC	BIC	EDC
Exponential	$\mu$	1.0029	$6.2124 \times 10^{-4}$	$-1.6237 \times 10^3$	$3.2493 \times 10^3$	$3.2506 \times 10^3$	$3.2554 \times 10^3$
	$a$	3.9001	0.0173	$-1.0527 \times 10^3$	$2.1095 \times 10^3$	$2.1119 \times 10^3$	$2.1216 \times 10^3$
	$b$	0.2571	0.0001				
Inverse Gaussian	$\mu$	1.0029	0.0002	$-1.1323 \times 10^3$	$2.2685 \times 10^3$	$2.2710 \times 10^3$	$2.2806 \times 10^3$
	$\lambda$	2.8487	0.0100				
Logistic	$\mu$	0.9604	$0.1338 \times 10^{-3}$	$-1.1370 \times 10^3$	$2.2780 \times 10^3$	$2.2804 \times 10^3$	$2.2901 \times 10^3$
	$\sigma$	0.2702	$0.0319 \times 10^{-3}$				
Log-logistic	$\mu$	-0.0948	$0.1652 \times 10^{-3}$	$-1.0815 \times 10^3$	$2.1670 \times 10^3$	$2.1694 \times 10^3$	$2.1791 \times 10^3$
	$\sigma$	0.2994	$0.0394 \times 10^{-3}$				
Log-normal	$\mu$	-0.1308	$0.1835 \times 10^{-3}$	$-1.1027 \times 10^3$	$2.2094 \times 10^3$	$2.2118 \times 10^3$	$2.2215 \times 10^3$
	$\sigma$	0.5451	$0.0919 \times 10^{-3}$				
Nakagami	$\mu$	1.1509	0.0013	$-1.0747 \times 10^3$	$2.1533 \times 10^3$	$2.1558 \times 10^3$	$2.1654 \times 10^3$
	$\omega$	1.2613	0.0009				
Normal	$\mu$	1.0029	$0.1579 \times 10^{-3}$	$-1.1927 \times 10^3$	$2.3895 \times 10^3$	$2.3919 \times 10^3$	$2.4016 \times 10^3$
	$\sigma$	0.5056	$0.0790 \times 10^{-3}$				
Rayleigh	$B$	0.7941	$0.9738 \times 10^{-4}$	$-1.0844 \times 10^3$	$2.1707 \times 10^3$	$2.1719 \times 10^3$	$2.1767 \times 10^3$
Rician	$s$	0.0564	0.5033	$-1.0844 \times 10^3$	$2.1727 \times 10^3$	$2.1751 \times 10^3$	$2.1848 \times 10^3$
	$\sigma$	0.7932	0.0007				
Skew-normal	$\mu$	1.0092	$1.5325 \times 10^{-4}$	$-1.0721 \times 10^3$	$2.1503 \times 10^3$	$2.1539 \times 10^3$	$2.1685 \times 10^3$
	$\sigma$	0.4979	$0.9738 \times 10^{-4}$				
	$\gamma$	0.7598	$1.3841 \times 10^{-4}$				
t-Student	$\mu$	0.9473	0.0001	$-1.1288 \times 10^3$	$2.2636 \times 10^3$	$2.2672 \times 10^3$	$2.2818 \times 10^3$
	$\sigma$	0.3852	0.0001				
	$\nu$	4.5051	0.2593				
Weibull	$A$	1.1344	0.0002	$-1.0813 \times 10^3$	$2.1666 \times 10^3$	$2.1690 \times 10^3$	$2.1787 \times 10^3$
	$B$	2.0945	0.0015				

Table 31: MLE results of the statistical distribution fitting of the RMS-DS ( $\mu s$ ) for *short-path channel* (SE is the estimated standard error).

Distribution	Parameter	Estimate	SE	Log-likelihood	AIC	BIC	EDC
Exponential Gamma	$\mu$	0.0850	$1.1125 \times 10^{-6}$	$9.5202 \times 10^3$	$-1.9038 \times 10^4$	$-1.9037 \times 10^4$	$-1.9024 \times 10^4$
	$a$	3.3511	0.0031	$1.1424 \times 10^4$	$-2.2843 \times 10^4$	$-2.2840 \times 10^4$	$-2.2815 \times 10^4$
	$b$	0.0275	0.0001				
Inverse Gaussian	$\mu$	0.0850	$0.0035 \times 10^{-4}$	$1.2050 \times 10^4$	$-2.4095 \times 10^4$	$-2.4092 \times 10^4$	$-2.4067 \times 10^4$
	$\lambda$	0.2676	$0.2204 \times 10^{-4}$				
Logistic	$\mu$	0.0759	$0.2688 \times 10^{-6}$	$1.0557 \times 10^4$	$-2.1110 \times 10^4$	$-2.1106 \times 10^4$	$-2.1082 \times 10^4$
	$\sigma$	0.0250	$0.0700 \times 10^{-6}$				
Log-logistic	$\mu$	-2.6418	$0.3744 \times 10^{-4}$	$1.2258 \times 10^4$	$-2.4513 \times 10^4$	$-2.4509 \times 10^4$	$-2.4484 \times 10^4$
	$\sigma$	0.2835	$0.0854 \times 10^{-4}$				
Log-normal	$\mu$	-2.6212	$0.4059 \times 10^{-4}$	$1.2145 \times 10^4$	$-2.4287 \times 10^4$	$-2.4283 \times 10^4$	$-2.4259 \times 10^4$
	$\sigma$	0.5137	$0.2030 \times 10^{-4}$				
Nakagami	$\mu$	0.7314	$0.1205 \times 10^{-3}$	$9.9424 \times 10^3$	$-1.9881 \times 10^4$	$-1.9877 \times 10^4$	$-1.9852 \times 10^4$
	$\omega$	0.0120	$0.0001 \times 10^{-9}$				
Normal	$\mu$	0.0850	$0.7368 \times 10^{-6}$	$8.1368 \times 10^3$	$-1.6270 \times 10^4$	$-1.6266 \times 10^4$	$-1.6241 \times 10^4$
	$\sigma$	0.0692	$0.3685 \times 10^{-6}$				
Rayleigh	$B$	0.0775	$2.3116 \times 10^{-7}$	$9.7052 \times 10^3$	$-1.9408 \times 10^4$	$-1.9407 \times 10^4$	$-1.9394 \times 10^4$
	$s$	0.0018	$0.1331 \times 10^{-3}$	$9.7052 \times 10^3$	$-1.9406 \times 10^4$	$-1.9403 \times 10^4$	$-1.9378 \times 10^4$
Rician	$\sigma$	0.0775	$0.0002 \times 10^{-3}$				
	$\mu$	0.0989	$4.2516 \times 10^{-7}$	$1.0737 \times 10^4$	$-2.1470 \times 10^4$	$-2.1464 \times 10^4$	$-2.1427 \times 10^4$
Skew-normal	$\sigma$	0.0546	$2.4272 \times 10^{-7}$				
	$\gamma$	0.9878	$1.0782 \times 10^{-6}$				
t-Student	$\mu$	0.0702	$2.0588 \times 10^{-7}$	$1.1482 \times 10^4$	$-2.2958 \times 10^4$	$-2.2953 \times 10^4$	$-2.2916 \times 10^4$
	$\sigma$	0.0261	$1.9585 \times 10^{-7}$				
	$\nu$	2.3463	0.0068				
Weibull	$A$	0.0954	$0.0007 \times 10^{-3}$	$1.0578 \times 10^4$	$-2.1151 \times 10^4$	$-2.1147 \times 10^4$	$-2.1123 \times 10^4$
	$B$	1.5199	$0.1329 \times 10^{-3}$				

Table 32: MLE results of the statistical distribution fitting of the RMS-DS ( $\mu s$ ) for *long-path channel* (SE is the estimated standard error).

Distribution	Parameter	Estimate	SE	Log-likelihood	AIC	BIC	EDC
Exponential Gamma	$\mu$	0.1620	$1.3642 \times 10^{-5}$	$1.5782 \cdot 10^3$	$-3.1544 \cdot 10^3$	$-3.1531 \cdot 10^3$	$-3.1476 \cdot 10^3$
	$a$	2.0845	0.0039	$1.8248 \cdot 10^3$	$-3.6457 \cdot 10^3$	$-3.6431 \cdot 10^3$	$-3.6321 \cdot 10^3$
	$b$	0.0778	0.0001				
Inverse Gaussian	$\mu$	0.1620	$0.0786 \times 10^{-4}$	$2.0492 \cdot 10^3$	$-4.0943 \cdot 10^3$	$-4.0918 \cdot 10^3$	$-4.0808 \cdot 10^3$
	$\lambda$	0.2812	$0.8217 \times 10^{-4}$				
Logistic	$\mu$	0.1363	$0.6127 \times 10^{-5}$	$1.3124 \cdot 10^3$	$-2.6209 \cdot 10^3$	$-2.6183 \cdot 10^3$	$-2.6073 \cdot 10^3$
	$\sigma$	0.0645	$0.1629 \times 10^{-5}$				
Log-logistic	$\mu$	-2.1320	$0.2380 \times 10^{-3}$	$2.0113 \cdot 10^3$	$-4.0186 \cdot 10^3$	$-4.0160 \cdot 10^3$	$-4.0050 \cdot 10^3$
	$\sigma$	0.3854	$0.0528 \times 10^{-3}$				
Log-normal	$\mu$	-2.0785	$0.2362 \times 10^{-3}$	$2.0286 \cdot 10^3$	$-4.0532 \cdot 10^3$	$-4.0506 \cdot 10^3$	$-4.0396 \cdot 10^3$
	$\sigma$	0.6743	$0.1182 \times 10^{-3}$				
Nakagami	$\mu$	0.5597	$0.2265 \times 10^{-3}$	$1.5389 \cdot 10^3$	$-3.0738 \cdot 10^3$	$-3.0712 \cdot 10^3$	$-3.0602 \cdot 10^3$
	$\omega$	0.0478	$0.0021 \times 10^{-3}$				
Normal	$\mu$	0.1620	$0.1117 \times 10^{-4}$	964.2933	$-1.9246 \cdot 10^3$	$-1.9220 \cdot 10^3$	$-1.9110 \cdot 10^3$
	$\sigma$	0.1467	$0.0559 \times 10^{-4}$				
Rayleigh	$B$	0.1545	$3.1013 \times 10^{-6}$	$1.2632 \cdot 10^3$	$-2.5245 \cdot 10^3$	$-2.5232 \cdot 10^3$	$-2.5177 \cdot 10^3$
	$s$	0.0006	0.1363	$1.2632 \cdot 10^3$	$-2.5225 \cdot 10^3$	$-2.5199 \cdot 10^3$	$-2.5089 \cdot 10^3$
Rician	$\sigma$	0.1545	0.0002				
	$\mu$	0.1897	$6.9297 \times 10^{-6}$	$1.7199 \cdot 10^3$	$-3.4340 \cdot 10^3$	$-3.4301 \cdot 10^3$	$-3.4137 \cdot 10^3$
Skew-normal	$\sigma$	0.1171	$3.9944 \times 10^{-6}$				
	$\gamma$	0.9902	$7.8936 \times 10^{-6}$				
t-Student	$\mu$	0.0992	$3.1904 \times 10^{-6}$	$1.6115 \cdot 10^3$	$-3.2169 \cdot 10^3$	$-3.2131 \cdot 10^3$	$-3.1966 \cdot 10^3$
	$\sigma$	0.0435	$4.1117 \times 10^{-6}$				
	$\nu$	1.2546	0.0048				
Weibull	$A$	0.1785	$0.0106 \times 10^{-3}$	$1.7157 \cdot 10^3$	$-3.4274 \cdot 10^3$	$-3.4249 \cdot 10^3$	$-3.4139 \cdot 10^3$
	$B$	1.3305	$0.4347 \times 10^{-3}$				

Table 33: MLE results of the statistical distribution fitting of the CT (ms) for *short-path channel* (SE is the estimated standard error).

Distribution	Parameter	Estimate	SE	Log-likelihood	AIC	BIC	EDC
Exponential	$\mu$	1.4439	0.0104	-274.8445	551.6890	551.9922	552.5245
	$a$	51.3508	26.0686	38.0973	-72.1946	-71.5882	-70.5236
Gamma	$b$	0.0281	0.0002	-19.4690	42.9381	43.5445	44.6091
	$\mu$	1.4439	0.0004	277.1460	-550.2919	-549.6856	-548.6210
Inverse Gaussian	$\lambda$	41.1411	16.8417	196.9781	-389.9562	-389.3498	-388.2852
	$\mu$	1.4616	$0.9653 \times 10^{-5}$	-2.8988	9.7977	10.4041	11.4687
Logistic	$\sigma$	0.0282	$0.3190 \times 10^{-5}$	69.7586	-135.5173	-134.9109	-133.8463
	$\mu$	0.3786	$0.8484 \times 10^{-5}$	116.1389	-228.2778	-227.6714	-226.6068
Log-logistic	$\sigma$	0.0274	$0.3223 \times 10^{-5}$	-139.2548	280.5096	280.8128	281.3451
	$\mu$	0.3576	0.0001	115.6148	-227.2296	-226.6232	-225.5586
Log-normal	$\sigma$	0.1721	0.0074	228.1800	-450.3600	-449.4504	-447.8535
	$\mu$	17.8081	3.0975	257.5174	-511.0349	-510.4285	-509.3639
Nakagami	$\omega$	2.1034	0.0012	0.0001	0.0001	4.3302	
	$\mu$	1.4439	$0.9218 \times 10^{-4}$				
Normal	$\sigma$	0.1361	$0.4643 \times 10^{-4}$				
	$B$	1.0255	0.0013				
Rayleigh	$s$	1.4375	$0.9298 \times 10^{-4}$				
	$\sigma$	0.1361	$0.4650 \times 10^{-4}$				
Rician	$\mu$	1.3913	$4.1786 \times 10^{-5}$				
	$\sigma$	0.0919	$2.1721 \times 10^{-5}$				
	$\gamma$	-0.9839	$4.0060 \times 10^{-5}$				
Skew-normal	$A$	1.4675	0.0001				
	$B$	32.6186	4.3302				
Weibull	$A$	1.4675	0.0001	257.5174	-511.0349	-510.4285	-509.3639
	$B$	32.6186	4.3302				

Table 34: MLE results of the statistical distribution fitting of the CT (ms) for *long-path channel* (SE is the estimated standard error).

Distribution	Parameter	Estimate	SE	Log-likelihood	AIC	BIC	EDC
Exponential	$\mu$	0.5672	0.0077	-18.1859	38.3717	37.9950	37.6679
	$a$	1.3282	0.0683	-17.2225	38.4449	37.6914	37.0372
	$b$	0.4271	0.0103				
Inverse Gaussian	$\mu$	0.5672	0.0111	-17.0727	38.1453	37.3918	36.7376
	$\lambda$	0.3904	0.0073				
Logistic	$\mu$	0.5138	0.0058	-29.0187	62.0375	61.2840	60.6298
	$\sigma$	0.2772	0.0012				
Log-logistic	$\mu$	-0.9617	0.0273	-19.4324	42.8649	42.1114	41.4572
	$\sigma$	0.5993	0.0056				
Log-normal	$\mu$	-0.9885	0.0238	-17.5970	39.1939	38.4404	37.7862
	$\sigma$	1.1004	0.0124				
Nakagami	$\mu$	0.4716	0.0071	-17.4573	38.9146	38.1611	37.5069
	$\omega$	0.5392	0.0147				
Normal	$\mu$	0.5672	0.0053	-27.5591	59.1183	58.3648	57.7106
	$\sigma$	0.4719	0.0027				
Rayleigh	$B$	0.5192	0.0016	-28.4616	58.9233	58.5465	58.2194
Rician	$s$	0.0228	5.7623	-28.4616	60.9233	60.1698	59.5156
	$\sigma$	0.5190	0.0044				
	$\mu$	0.6079	0.0007	-14.8528	35.7058	34.5755	33.5942
Skew-normal	$\sigma$	0.4130	0.0042				
	$\gamma$	0.9951	$0.0003 \times 10^{-2}$				
	$\mu$	0.5672	0.0049	-27.5531	61.1062	59.9759	58.9946
t-Student	$\sigma$	0.4663	0.0025				
	$\nu$	$4.9391 \times 10^6$	$2.0371 \times 10^{11}$				
Weibull	$A$	0.6022	0.0068	-17.2795	38.5589	37.8054	37.1512
	$B$	1.1873	0.0213				